MODELING, ANALYSIS, AND DESIGN OF SUBCARRIER MULTIPLEXING ON MULTIMODE FIBER

Surachet Kanprachar

Dissertation submitted to the Faculty of the
Virginia Polytechnic Instituted and State University
in partial fulfillment of the requirements for the degree of

DOCTOR OF PHILOSOPHY

in

Electrical Engineering

Ira Jacobs, Chairman
Timothy T. Pratt
John K. Shaw
Rogers H. Stolen
Anbo Wang

March, 2003
Blacksburg, Virginia

Keywords: Subcarrier Multiplexing (SCM), Diversity coding, Training process, Multimode fibers, Optical fiber transmission

MODELING, ANALYSIS, AND DESIGN OF SUBCARRIER MULTIPLEXING ON MULTIMODE FIBER

by

Surachet Kanprachar

Ira Jacobs, Chairman

Electrical Engineering

(ABSTRACT)

This dissertation focuses on the use of subcarrier multiplexing (SCM) in multimode fibers, utilizing carrier frequencies above what is generally utilized for multimode fiber transmission, to achieve high bit rates. In the high frequency region (i.e., frequencies larger than the intermodal bandwidth), the magnitude response of multimode fiber does not decrease monotonically as a function of the frequency but is shown to become relatively flat (but with several deep nulls) with an amplitude below that at DC. The statistical properties of this frequency response at high frequencies are analyzed. The probability density function of the magnitude response at high frequencies is found to be a Rayleigh density function. The average amplitude in this high frequency region does not depend on the frequency but depends on the number of modes supported by the fiber. To transmit a high bit rate signal over the multimode fiber, subcarrier multiplexing is adopted. The performance of the SCM multimode fiber system is presented. The performance of the SCM system is significantly degraded if there are some subcarriers located at the deep nulls of the fiber. Equalization and spread spectrum techniques are

investigated but are shown to be not effective in combating the effects of these nulls. To cancel the effects of these deep nulls, training process and diversity coding are considered. The basic theory of diversity coding is given. It is found that the performances of the system with training process and the system with diversity coding are almost identical. However, diversity coding is more appropriate since it requires less system complexity. Finally, the practical limits and capacity of the SCM multimode fiber system are investigated. It is shown that a signal with a bit rate of 1.45 Gbps can be transmitted over a distance up to 5 km.

ACKNOWLEDGMENTS

I would like to express my deeply felt gratitude to Dr. Ira Jacobs, my advisor and mentor, who provided generous advice and subject area expertise throughout this entire process. I am also especially thankful for his continual support, understanding, and encouragement throughout my education at Virginia Tech. I dedicate this dissertation to him with great affection and respect.

My heartfelt appreciation is also extended to all members of my advisory committee, Dr. Timothy T. Pratt, Dr. John K. Shaw, Dr. Rogers Stolen and Dr. Anbo Wang, for their valuable comments and suggestions, especially during the final stage of the dissertation process.

My sincere gratitude goes to Dr. Sujin Jinayon, Dr. Karnjana Ngoarangsri, and Dr. Visharn Poopath for giving me an opportunity to further my study in the United States. I also wish to thank the Royal Thai Government in particular for financial support they provided during my study at Virginia Tech.

Special thanks are due to my friends at Virginia Tech, especially Dr. Virach Wongpaibool for brilliant perspectives on issues relating to fiber optic communications, Songwut Hengprathanee for his delicious Thai food, Amnart Kanarat and Siriroj Sirisukprasert for being supportive during the dissertation process.

Finally, I would like to thank my family for their unceasing love, understanding, and encouragement throughout my life. Last but not least, my deepest, warmest thank belongs to my love, Dr. Narat Sakontawut, for her immeasurable support and encouragement throughout my graduate studies.

TABLE OF CONTENTS

ABSTRACT……... ii

ACKNOWLEDGEMENT…… iv

TABLE OF CONTENTS……... v

LIST OF FIGURES…….... viii

LIST OF TABLES……... xii

CHAPTER 1. INTRODUCTION…… 1

1.1 Multimode fiber in high bit-rate transmission…… 2
1.2 Bandpass transmission on multimode fiber…… 5
1.3 System modifications for improving the system performance……... 8
1.4 Objectives and organization of dissertation…….. 11

CHAPTER 2. ANALYSIS OF THE PASSBAND REGION OF MULTIMODE FIBER……14

2.1 Introduction……14
2.2 Model of the multimode fiber……... 15
2.3 Statistical properties of the multimode fiber at high frequency…….19
2.3.1 Probability density function of the magnitude response……..19
2.3.2 Correlation function of the frequency response……...23
2.3.3 Correlation function of the magnitude response……..25
2.4 Conclusions……...31

CHAPTER 3. ELECTRICAL EQUALIZATION AT THE RECEIVER……..33

3.1 Introduction……33
3.2 Signal-to-noise ratio and eye-diagram of the received signals: without and with ideal electrical……34
3.3 Signal-to-noise ratio and eye-diagram of the received signals: with limited-gain electrical equalization……44
3.4 Comparisons of Signal-to-noise ratio and eye-diagram from different cases…… 49
3.5 Conclusions……50

CHAPTER 4. SPREAD SPECTRUM WITH MULTIMODE FIBER SYSTEM……...52

4.1 Introduction…… 52
4.2 Signal-to-noise ratio and eye-diagram……53
4.3 Probability density function of signal-to-noise ratio……..59
4.4 Conclusions…….64

CHAPTER 5. SUBCARRIER MULTIPLEXING (SCM) WITH MULTIMODE FIBER SYSTEM……..66

5.1 Introduction……66
5.2 Bit-error-rate of the received signal for a 20-subcarrier SCM multimode fiber system……..68
5.3 Effects of the number of subcarriers on bit-error-rate in SCM multimode fiber system……..78
5.4 Conclusions……81

CHAPTER 6. TRAINING PROCESS WITH SUBCARRIER MULTIPLEXED MULTIMODE FIBER SYSTEM……83

6.1 Introduction……83
6.2 Bit-error-rate of the received signal with 2 channels dropped……...84
6.3 Effects of the number of channels dropped on the achieved bit-error-rate: for 10-subcarrier system……..88
6.4 Conclusions……90

CHAPTER 7. DIVERSITY CODING WITH SUBCARRIER MULTIPLEXED MULTIMODE FIBER SYSTEM……91

7.1 Introduction……91
7.2 Diversity Coding Theory……...93
7.3 Application of diversity coding to SCM multimode fiber system…….96
7.4 Analysis and simulation of bit-error-rate of SCM multimode fiber system with diversity coding……109
7.5 Conclusions……..122

CHAPTER 8. PRACTICAL PERFORMANCE LIMITS AND SYSTEM CAPACITY……124

8.1 Introduction……..124
8.2 Effect of chromatic dispersion on the available bandpass bandwidth of multimode fiber……127
8.3 Analysis of the number of subcarriers located at the nulls……...134
8.3.1 Probability of having *k* subcarriers (from an *N*-subcarrier system) located at the nulls……...134
8.3.2 Number of subcarriers located at deep nulls…….....140
8.3.3 Number of subcarriers located at deep nulls from Poisson distribution…….146
8.4 System Capacity……...151
8.5 Conclusions……..167

CHAPTER 9. SUMMARY AND CONCLUSIONS……170

9.1 Summary of Contributions……...173
9.2 Suggestions for Future Research……. 173

APPENDIX A. Effect of the Bandwidth of Bandpass Filter (or Electrical Equalizer) on the Received SNR…….175

APPENDIX B. Effect of ΔG on the Received SNR of the System with Limited-Gain Equalization……..180

LIST OF ACRONYMS……..183

REFERENCES……185

VITA……..……...189

LIST OF FIGURES

2.1 Magnitude response of the complex envelope of the multimode fiber modeled by (2-2): $t_{d,avg}$ = 5 μs and $t_{d,dev}$ = 5 ns. For each N_m, there are three curves (i.e.; upper, middle, and lower curves) corresponding to different sets of delays. The magnitude responses for middle and lower curves are displaced by 20 and 40 dB, respectively……..... 17

2.2 Plots of normalized $R_{H_{fiber}}(\nu)$ and $\left\langle \left| H_{fiber}(f) H_{fiber}(f+\nu) \right|^2 \right\rangle$ for N_m = 100 modes, $t_{d,avg}$ = 5 μs and $t_{d,dev}$ = 5 ns…… 30

2.3 Plots of normalized $R_{H_{fiber}}(\nu)$ and $\left\langle \left| H_{fiber}(f) H_{fiber}(f+\nu) \right|^2 \right\rangle$ for N_m = 150 modes, $t_{d,avg}$ = 5 μs and $t_{d,dev}$ = 5 ns…… 31

3.1 Diagram of the transmission system using three subcarriers on multimode fiber…….. 35

3.2 Magnitude responses of multimode fiber and subcarrier signals located at 0.5, 1.0, and 1.5 GHz..……... 39

3.3 Eye-diagrams of received subcarrier signals: without electrical equalization and $BW_{BP} = 4R_b$..……... 40

3.4 Eye-diagrams of received subcarrier signals: with electrical equalization and $BW_{Eq} = 4R_b$……..... 41

3.5 Eye-diagrams of the combined signal from three received subcarrier signals: without and with electrical equalization and $BW_{BP} = BW_{Eq} = 4R_b$…….…….…….... 41

3.6 Illustration of the magnitude response of the ideal and limited-gain equalizers…….…….. 45

3.7 Eye-diagrams of received subcarrier signals: with limited-gain electrical equalization (ΔG = 0 dB) and $BW_{Eq} = 4R_b$…… 46

3.8 Eye-diagrams of combined signal from three received subcarrier signals: for different cases, $BW_{BP} = BW_{Eq} = 4R_b$…… 46

4.1 Diagram of the transmission system using subcarrier frequency and direct sequence spread spectrum with the passband region of the multimode fiber…….…….. 54

4.2 Magnitude responses of the multimode fiber, the input signal, and the input spread spectrum (code length = 7) signal: First simulation……. 55

4.3 Eye-diagrams of the received signal in the first simulation: without and with spread spectrum (code length = 7) ……... 55

4.4 Magnitude responses of the multimode fiber, the input signal, and the input spread spectrum (code length = 7) signal: Second simulation……. 56

4.5 Eye-diagrams of the received signal in the second simulation: without and with spread spectrum (code length = 7) ……... 56

4.6 Histogram of the signal-to-noise ratio from 300 simulations: without and with spread spectrum (code length of 7 and 15) …….. 60

4.7 Histogram of the signal-to-noise ratio from 300 simulations: without and with spread spectrum (code length of 7 and 15) …….. 63

5.1 Diagram of the multimode fiber transmission using subcarrier multiplexing (SCM) …….…… 68

5.2 Magnitude responses of 5 different sets ((a) to (e)) of frequency responses of multimode fiber; transmission bandwidth (Tx BW) is from 4.25 GHz to 7.5 GHz…….…… 72

5.3 Bit-error-rate (*BER*) as a function of input optical power to the photodetector for fives fibers [(a) to (e)] for the number of subcarriers = 20…….…….…. 76

5.4 Bit-error-rate (*BER*) as a function of input optical power to the photodetector for fiber (a) to (e): for number of subcarriers = 10, 20, 30, 40, and 50…….……. 79

6.1 Bit-error-rate (*BER*) as a function of input optical power to the photodetector for fiber(a) to fiber(e): without and with training sequence (2 channels dropped), and number of subcarriers = 10 and 40……. 87

6.2 Bit-error-rate (*BER*) as a function of input optical power to the photodetector of 10-subcarrier SCM multimode fiber system for 5 different sets of multimode fiber: without and with training sequence (dropping 1, 2, and 3 channels) ……..……... 89

7.1 Diagram of subcarrier multiplexed multimode fiber system with diversity coding…….……... 118

7.2 Comparison of performance of (1) no training sequence or diversity coding (No TS, No DC), (2) training sequence with two dropped channels, and (3) diversity coding with 2 parity channels. The five plots (a)-(e) correspond to the five different sets of multimode fiber from Figure 5.2……..……. 120

7.3 Performance of the three system configurations indicating sensitivity to fiber frequency response…….…….. 121

8.1 Illustration of frequency response of multimode fiber due to modal and material dispersion…….……... 132

8.2 Probability of having *k* subcarriers (from an *N*-subcarrier system) located at the nulls: for different values of *N* and ε.……... 138

8.3 Probability of having *k* subcarriers (from an *N*-subcarrier system) located at the deep nulls (at least 10 dB below the average amplitude)…… 142

8.4 The number (*k*) of subcarriers located at deep nulls as a function of the total number (*N*) subcarriers: for different values of probabilities…… 143

8.5 Probability of having *k* subcarriers (from an *N*-subcarrier system) located at the deep nulls (at least 10 dB below the average amplitude) determined from Poisson distribution in (8-19).…….……. 148

8.6 The number (*k*) of subcarriers located at deep nulls as a function of the total number (*N*) subcarriers: from Binomial and Poisson distributions, $p = 10^{-3}$…….…… 149

8.7 The ratio between the number (k) of subcarriers located at deep nulls and the total number (N) of subcarriers as a function of the total number subcarriers: from Binomial and Poisson distributions, $p = 10^{-3}$…… 150

8.8 Total received optical power, received optical DC power, and received optical AC power as a function of the fiber length……... 159

8.9 The signal-to-noise ratio of the received subcarrier signal as a function of the fiber length……. 160

8.10 The number of subcarriers as a function of the fiber length……. 161

8.11 The total bit rate as a function of the fiber length…… 163

A.1 Signal-to-noise ratio as a function of the bandwidth of bandpass filter: for different subcarriers……... 175

A.2 Signal-to-noise ratio as a function of the bandwidth of bandpass filter (or the bandwidth of electrical equalizer): without and with electrical equalization……... 176

B.1 Output signal-to-noise ratio as a function of ΔG: for limited-gain equalization with $BW_{Eq} = 4R_b$……... 180

B.2 Output signal-to-noise ratio (in dB) as a function of ΔG: for different subcarriers, $BW_{Eq} = 4R_b$…… 181

LIST OF TABLES

7.1 All possible cosets related to $p(x) = x^4 + x + 1$ ……. 97

7.2 Exponential, polynomial, and vector-space representations of GF(2^4)…..... 102

7.3 List of symbols at transmitter, receiver, and output of the decoder for example 1: one failure data channel……..... 105

7.4 List of symbols at transmitter, receiver, and output of the decoder for example 2: two failure data channels…… 108

8.1 List of the maximum fiber length, the maximum bit rate, and the number of subcarriers for different values of transmit optical power…… 169

Chapter 1

Introduction

The data rate required for local area networks has increased dramatically to over 1 Gbps. The only medium which can support such high data rate with small attenuation is the optical fiber. However, optical fibers that are available in many buildings or LAN links are multimode fibers, which normally have a baseband bandwidth-distance product less than 500 MHz-km. If the data rate is 2.5 Gbps, the data can only be transmitted over fiber lengths less than 200 m, which is too short for many applications. The bandwidth-distance product has to be increased. Increasing this by replacing the multimode fiber with a single mode fiber is generally too expensive. Moreover, the available multimode fibers will then be wasted. Hence, how to achieve a high data rate (in Gbps) transmission for a short distance (e.g., less than 10 km) on multimode fibers is a topic of considerable interest. This dissertation focuses on the use of subcarrier multiplexing, utilizing carrier frequencies above what is generally utilized for multimode fiber transmission, to achieve high bit rates.

In this Chapter, a brief review of multimode fibers and previous research on multimode fiber in high bit-rate transmission are given. This is followed by a discussion of subcarrier multiplexing (SCM) and types of system modifications for improving the

performance of high bit-rate transmission on multimode fiber. Finally, the dissertation objectives and organization of the dissertation are given.

1.1 Multimode Fiber in High Bit-Rate Transmission

Optical fibers can be categorized by the number of guided modes supported by the fiber. There are two types of optical fibers; that is, single-mode fiber and multimode fiber. For single-mode fibers, there is only one guided mode* supported by the fiber; whereas for multimode fibers, more than one mode is supported by the fiber. The number of guided modes in multimode fiber can be up to many hundreds of modes [1] and depends on many factors, including operating frequency, the core diameter, type of refractive index of the core (graded or step), and so on. The optical power from an optical pulse launched into a multimode fiber is generally distributed over all of the guided modes. These modes then propagate along the fiber to the receiving end, and in practical systems there is often interchange of power between the modes (mode coupling). The problem with multimode fiber is that the propagation velocity of each of the guided modes is different. This means that at the receiving end, the received optical pulse is spread out in time resulting in pulse dispersion. The pulse spread becomes larger if the fiber length increases. This type of dispersion is called intermodal dispersion. This dispersion is the main limitation of data transmission on multimode fiber. If the bit rate of the transmit signal is high, the bit period is small. When a received pulse is spread out in

* Note that there are actually two modes corresponding to two orthogonal polarizations. If the group velocities for these two modes are different, a potential source of pulse broadening called the polarization-mode dispersion (PMD) can become a problem. Although PMD is of concern in high bit rate long distance systems, it is negligible for the systems considered in this dissertation.

time caused by intermodal dispersion, the neighboring pulses may overlap. This may lead to a wrong decision in the decision circuit in the receiver; thus, a high bit-error-rate (*BER*). This effect becomes more significant both as the bit rate and distance increase. In practice, the intermodal bandwidth-distance product of a multimode fiber is specified. The unit of this parameter is normally in MHz-km. The intermodal bandwidth ($BW_{\text{intermodal}}$) of a multimode fiber can be estimated from the full width at half maximum of the received pulse (σ_τ) [41] when the transmitted pulse is very narrow; that is, $BW_{\text{intermodal}} = 0.44/\sigma_\tau$ .The typical value of the intermodal bandwidth-distance product for a multimode fiber is between 300 to 500 MHz-km. For binary transmission the maximum bit rate is of the order of the bandwidth, so that only about a 500-Mbps signal can be sent over a transmission distance of 1 km. To achieve a higher bit rate, the transmission distance has to be decreased. This is not a satisfactory situation since a high bit rate signal can only be transmitted for a short distance.

To increase the bandwidth-distance product of multimode fibers, many approaches have been suggested; for example, using an offset launch condition instead of over-filled launch [2-9], using multi-level coding [7, 8], and using parallel optics with multimode ribbon cable [8]. The offset launch is done by offsetting the launching spot from the core center of the fiber. By doing this, the number of guided modes excited by the launch is reduced and becomes smaller than the number of guided modes excited by the over-filled launch. Hence, the pulse spreading from an offset launch is smaller and the bandwidth of the fiber is increased. For multi-level coding, an *m*-ary modulation scheme with $m>2$ is adopted. The bit rate of the signal to be sent over the fiber is increased since one

transmitted symbol contains more than 2 bits. For the technique using parallel optics with multimode ribbon cable, a high bit rate signal is divided into many low bit rate signals and these signals are transmitted simultaneously over the multimode ribbon cable. However, in all of these three techniques, only the frequencies below the modal bandwidth of the fiber are used. The frequencies higher than the modal bandwidth of the fiber are not exploited. It has been shown in many papers [10-17] that the frequency response of the multimode fiber does not monotonically decrease as the frequency increases. The frequency response of the multimode fiber at low frequencies decreases monotonically with frequency and can be modeled as a Gaussian shape. However, in the high frequency range, the frequency response does not fall off but becomes relatively flat with an amplitude of 6 to 10 dB below the amplitude at zero frequency. One interesting approach to utilize this high frequency region is to use subcarrier multiplexing with the multimode fiber. It has been shown that using subcarrier multiplexing within this high frequency region, a high data rate can be successfully transmitted over a fiber length larger than 400 meters. For example, in [7], a 1.25-Gbps signal is divided into two 625-Mbps signals. One of these two signals is modulated onto a subcarrier frequency of 1 GHz and the other is modulated onto a subcarrier frequency of 3 GHz. These two subcarrier signals are combined and sent to a laser to convert the subcarrier electrical signal into an output optical signal. This optical signal is then transmitted over the high frequency region of the multimode fiber. It has been shown that the total 1.25 Gbps signal can be successfully transmitted over a fiber length of 500 m. The origin of the passband region of the multimode fiber has been explained roughly as resulting from an impulse response that is a series of delta functions with different delays corresponding to

different guided modes in the fiber when the mode coupling and chromatic dispersion are ignored [11, 13]. The detailed explanation and analysis of this passband region is treated in Chapter 2, and was reported in [18].

1.2 Subcarrier multiplexing (SCM) transmission on multimode fiber

Although the bandpass region of the multimode fiber is relatively flat with amplitude of 6 to 10 dB below the amplitude at zero frequency, it may not be possible to use this passband region to transmit a signal with bit rate large compared to 3-dB modal bandwidth. The deep nulls and variation of the amplitude of the frequency response of the multimode fiber within the transmission frequency can significantly degrade the output signal of the multimode fiber; thus, leading to high *BER* at the receiver. It is seen from [18] that the probability density function of the amplitude response of the multimode fiber in the high frequency range is Rayleigh distributed and does not depend on the frequency. This property of the bandpass region of the multimode fiber is similar to the property of the channel in a wireless communications system; that is, the fiber is a wideband frequency-selective channel. The effect of having a wideband frequency-selective channel for data transmission can be overcome by using orthogonal frequency division multiplexing (OFDM). This technique has been proposed and analyzed by many groups of researchers [19-25]. In OFDM, the high data rate signal is divided into many small data rate signals. These small data rate signals are then transmitted via different

subcarrier frequencies. By doing this the wideband frequency-selective channel is separated into a series of many narrowband frequency-nonselective channels. The main requirement of doing OFDM is the orthogonality between all OFDM signals in the frequency domain. That is, the spectrum of each OFDM signal should not interfere with the spectra of neighboring OFDM signals. To have completely non-overlapping spectra, the required bandwidth of the system will then be large; that is, less spectral efficiency. To increase the spectral efficiency of the system, the signal spectra must be packed tightly. By doing this, very sharp filtering (which is very difficult to implement) is needed; thus, more system complexity is required [19]. It is seen that using sharp filtering is not a good way to increase the spectral efficiency of an OFDM system. Other approaches are given in [19] to [25]. In [19], it is shown that using Staggered Quadrature Amplitude Modulation (SQAM) can increase the spectral efficiency of the OFDM system. The subcarriers are located exactly at the nulls of the immediate neighboring spectra. Each spectrum overlaps only its immediate neighbors. Orthogonality of spectra is achieved by staggering the data on alternate in-phase and quadrature channels. However, the amount of the filtering used in this technique is still considerable so it is not widely used. Another technique is to make the individual spectra to be sinc functions. The subcarriers are put at the nulls of the neighboring spectra. It is seen that the OFDM spectra are not bandlimited but they can be separated by the baseband processing using discrete-Fourier transform (DFT) techniques [19-23]. The detailed analysis of using DFT for OFDM system is given in [22] and [23]. The applications of using OFDM with fiber-optic transmission have been shown in [24] and [25]. OFDM was used in the subcarrier multiplexed fiber-optic video transmission as a digital transmission scheme of the hybrid

AM/OFDM system [24]. The performance of the OFDM system was given and compared to the performance of a conventional QAM system. It has been shown that the OFDM technique provides much better performance. This is because the period of an OFDM symbol is much longer than the period of a QAM symbol. The clipping impulse noise only affects a small fraction of an OFDM symbol. Another example of using OFDM with a fiber-optic system is shown in [25]. The multimode fiber is used as an inexpensive cell feed in broad-band 60-GHz indoor picocellular systems. To overcome the effect of multipath fading in a wireless environment, OFDM is chosen to be the modulation scheme for the wireless transmission. However, to reduce the complexity required by the remote site, the signal modulation should be done at the central office and sent from the central office to the remote site via an optical fiber system. Using multimode fiber as the medium instead of singlemode fiber can reduce the cost of implementing the optical fiber system. However, the problem of using multimode fiber as the medium is the effect of the dispersion in multimode fiber. Since the multipath problems in wireless system can be overcome by the use of OFDM, OFDM might also be able to reduce the effect of frequency selectivity in the dispersive multimode fiber. It was shown in [25] that OFDM can offer good protection against the frequency selectivity of the dispersive multimode fiber. Thus, the seamless transition between the fiber and radio parts of the system with an inexpensive cost for the fiber part is possible.

It is seen that the key point for combating a wideband frequency-selective channel, such as occurs for high frequencies in multimode fiber, is to divide a high bit rate signal

into many small bit rate signals and transmit these signals with different subcarriers. By doing this, the wideband frequency-selective channel is transformed into a series of narrowband non-selective channels. Applying this idea to the multimode fiber transmission in the high frequency region, OFDM is a good approach. However, since the available bandpass bandwidth of multimode fiber is very large, the orthogonality between subcarriers is easily achieved by increasing the frequency separation between two consecutive subcarriers. There is no need to tightly put subcarriers in a specific bandwidth. The sharp filtering is then not required. Consequently, it is seen that it may be possible to use subcarrier multiplexing (SCM) to transmit a high bit rate signal over the high frequency region of multimode fiber, but there are many open questions concerning the design of such systems, e.g., the frequency response at frequencies above the intermodal bandwidth limit, the total available bandwidth, the bit rate that may be transmitted on each subcarrier, the number of subcarriers that may be used, the coding across multiple subcarriers to improve performance, and the total bit rates and distances that may be achieved. This dissertation will be devoted mainly to answering these questions.

1.3 System modifications for improving the system performance

Even though using OFDM and/or SCM, the wideband frequency-selective channel can be transformed into a series of narrowband frequency-nonselective channels, this does not guarantee that the subcarriers will not be placed at the nulls of the frequency

response. If this happens, the signal performance at the receiver end will be degraded significantly. There are many techniques to improve the signal performance. A good approach is using channel encoding. With this approach, errors in the received signal can be corrected at the receiver. Many types of channel encodings have been applied to OFDM systems; for example, block code [26], convolutional code [27, 28], Trellis-code modulation [29], Reed-Solomon code with Trellis-code modulation [30]. The received signal is surely improved since there is some redundancy systematically added to the signal. However, with these coding techniques, the effect of having subcarriers located near the deep nulls of the frequency response of the multimode fiber may not be totally canceled.

Another approach might be using electrical equalization at the receiving end. With this approach, the property of each subcarrier channel has to be determined so that an electrical equalizer for each such channel can be constructed. The equalizer will undo what the channel has done to the signal. The attenuated pulse can be retrieved completely even if the subcarrier is at a deep null. However, noise can become a main problem since the gain of the equalizer will be very high, if the subcarrier is located at a deep null. The effects of adding electrical equalization at the receiver are studied in Chapter 3.

Spreading the spectrum of the transmitted signal by using direct sequence spread spectrum might be a good technique to improve the system performance since there will be more passband regions covered by the signal spectrum; that is, obtaining the effect of frequency diversity. The amplitude of each frequency component is small and if there is a

frequency component located at a null, the degradation from such null to the overall received signal should be small. The effects of using direct sequence spread spectrum with multimode fiber system are studied in Chapter 4.

It is shown in Chapters 3 and 4 that adding electrical equalization to the receiver and/or using the direct sequence spread spectrum do not really eliminate the effect of having some subcarriers located at deep nulls. A better way to completely remove the effects of these nulls might be the use of a training sequence to determine the properties of subcarrier channels. With the training sequence, the subcarrier channels to be used for signal transmission will be determined during the training process. With this technique, any bad channels (which are normally located near the deep nulls) will not be used for transmission; thus, the effect of the nulls is completely removed. However, using training sequence requires more system complexity. It requires more channels during the training process since some of channels will be dropped out after the training process. And, if the channels are time-varying, the training process must be done frequently to update the channels' properties. This is not good for real-time communications. Also, the transmitter must be able to re-locate the subcarriers for data transmission if the channels are time-varying.

To reduce the system complexity and eliminate the effect of the nulls in the frequency response of the multimode fiber, another technique has to be used. It is shown in [31] that diversity coding is very useful for self-healing communication networks. This technique is accomplished by adding parity symbols and parity channels; that is, more channels are

needed. The parity symbols are generated from the data symbols from all data channels. By doing this, at the receiver, the data received from the poorest channels (decided by the signal-to-noise ratios of all received subcarrier signals) will be totally disregarded. The lost data from these poorest channels will be recovered by the data received from other good channels at the decoder. Applying this technique to the SCM multimode fiber system, it is seen that if there are some channels located near the nulls of the multimode fiber, the data received from those channels will not be taken into account as a part of the received signal. Thus, the effect of the deep nulls in the multimode fiber is totally removed. Using this diversity coding, there is no need to update the channels' properties and there is no need to have the ability to re-locate the subcarriers for data transmission since any lost data can be recovered instantaneously at the receiver; that is, less system complexity compared to that required by using training sequence with SCM multimode fiber system.

1.4 Objectives and Organization of Dissertation

From the previous discussion, it is seen that the frequency response of multimode fiber, which seems to decrease as the frequency increases, becomes relatively flat as the frequency increases beyond the intermodal bandwidth. It is important then to study analytically the frequency response of multimode fiber at high frequencies and determine how a high bit rate signal can be transmitted efficiently using this frequency region. Another important topic is the limitations on the performance that may be achieved with

bandpass transmission on multimode fiber. Based on this discussion, the following major research objectives are established.

(1) Study of the statistical properties of frequency response of multimode fiber at high frequencies,

(2) Study of different transmission approaches for transmitting a signal using the bandpass region of multimode fiber,

(3) Study of the system modifications for improving the performance of subcarrier multiplexed system on multimode fiber, and

(4) Study of the practical performance limits and system capacity of subcarrier multiplexed system on multimode fiber.

The organization of the dissertation is as follows. In Chapter 1, a brief review of multimode fiber and the recent research on how to transmit the high bit rate signal are given. Also, the discussion about possible types of transmission and system modifications are given. In Chapter 2, the frequency response of multimode fiber at high frequencies is analyzed and modeled. The statistical properties of multimode fiber in the high frequency region are given. Chapter 3 presents the simulation results of having electrical equalization added to the receiver for a three-subcarrier system. The simulation results for the multimode fiber using spread spectrum are given in Chapter 4. It is found that using electrical equalization or using spread spectrum with bandpass transmission on

multimode fiber does not give good system performance. The main focus of the dissertation is in Chapters 5 to 8. In Chapter 5, the subcarrier multiplexing (SCM) is applied to the multimode fiber system. The simulation results of bit-error-rate (*BER*) for different numbers of subcarriers are shown. The improvements of using training sequence and diversity coding with SCM multimode fiber system are presented in Chapters 6 and 7, respectively. The practical performance limits and system capacity of SCM multimode fiber system is discussed in Chapter 8. And, finally, the summary and conclusions of the dissertation are given in Chapter 9.

Chapter 2

Analysis of the Passband Region of Multimode Fiber

2.1 Introduction

It has been shown in many papers [10-17] that the frequency response of the multimode fiber does not monotonically decrease as the frequency increases. At high frequency region, the frequency response of multimode fiber is relatively flat with an amplitude 6 to 10 dB below the amplitude at zero frequency. There are many passbands available at high frequencies. These passbands can be used as transmission channels for sending the data. To make use of these passbands effectively, it is useful to understand the characteristics of these passbands. The origin of these passbands has been explained roughly as resulting from a series of delta functions with different delays corresponding to different guided modes in the fiber when the mode coupling and chromatic dispersion are ignored [11, 13]. However, this does not give any insight into the detail about these passbands. To understand clearly about such passbands, a detailed analysis of the frequency response of multimode fiber at high frequencies has to be done. In the following sections in this chapter, the frequency response of multimode fiber at high frequencies is modeled and analyzed [18]. Statistical properties of the bandpass regions are also determined.

2.2 Model of the Multimode Fiber

Using the suggestion in [11] and [13], the impulse response of the complex envelope of the multimode fiber with N_m guided modes is just the combination of the delta functions corresponding to different delays; that is,

$$h_{fiber}(t) = \sum_{n=1}^{N_m} \delta\left(t - t_{d,n}\right) \tag{2-1}$$

Taking the Fourier transform of the impulse response in (2-1), the frequency response of the complex envelope of the multimode fiber with N_m guided modes is given by

$$H_{fiber}(f) = \sum_{n=1}^{N_m} e^{-j2\pi f \cdot t_{d,n}} \tag{2-2}$$

To find the delay for a particular guided mode, the normalized propagation constant (b) or the propagation constant (β) or the modal index ($\overline{n}$) for that mode have to be determined by solving the eigenvalue equation for that mode. The time delay is given by

$$t_d = \frac{L}{\left(c/\overline{n}\right)} \tag{2-3}$$

and

$$b = \frac{\beta/k_0 - n_2}{n_1 - n_2} = \frac{\overline{n} - n_2}{n_1 - n_2} \tag{2-4}$$

where L is the fiber length

c is the speed of light in free-space

k_0 is the free-space wave number defined as $k_0 = \dfrac{2\pi}{\lambda}$ (2-5)

From (2-2), it is seen that to get the frequency response of the multimode fiber, the delays for all N_m guided modes have to be found; that is, the modal index of each guided mode has to be found. However, for practical multimode fibers the number of guided modes has to be large to avoid modal noise; thus, many time delays have to be determined in order to construct the frequency response. In the following analysis, the time delays are modeled to be independent realizations of a random variable, which is uniformly distributed about $t_{d,avg}$ with the maximum deviation of $t_{d,dev}$; the probability density function of $t_{d,n}$ is given by

$$f_{t_{d,n}}\left(t_{d,n}\right)=\begin{cases} \dfrac{1}{2t_{d,dev}} & ;\ \text{for}\ \ t_{d,avg}-t_{d,dev}\le t_{d,n}\le t_{d,avg}+t_{d,dev} \\ 0 & ;\ \text{elsewhere} \end{cases} \tag{2-6}$$

Note that $t_{d,avg}$ and $t_{d,dev}$ depend on the fiber length, the number of guided modes, and the refractive index profile of the fiber.

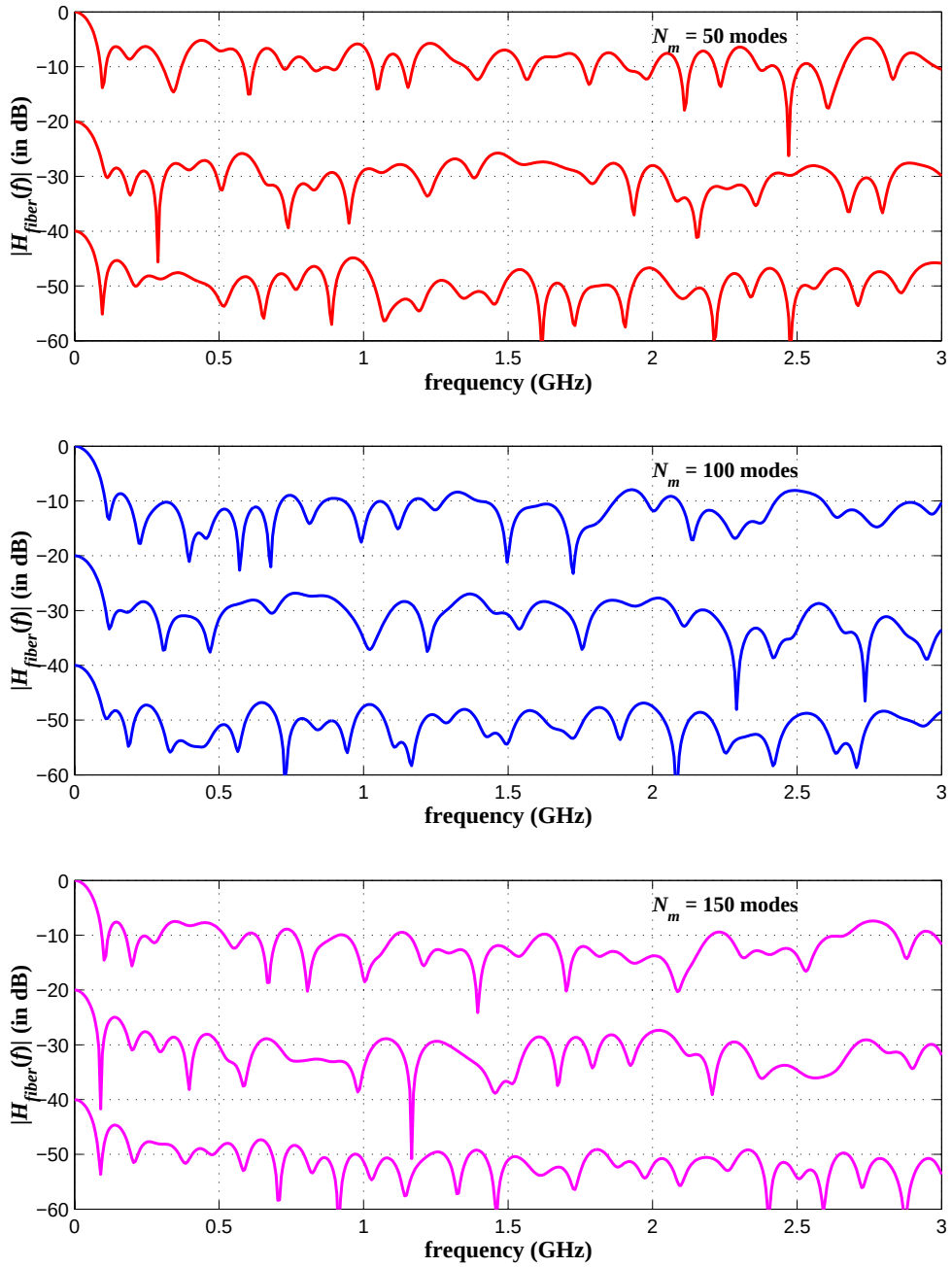

Figure 2.1 Magnitude response of the complex envelope of the multimode fiber modeled by (2-2): $t_{d,avg}$ = 5 μs and $t_{d,dev}$ = 5 ns. For each N_m, there are three curves (i.e.; upper, middle, and lower curves) corresponding to different sets of delays. The magnitude responses for middle and lower curves are displaced by 20 and 40 dB, respectively.

Using (2-2) and (2-6) with N_m = 50, 100, and 150, the plots of the magnitude of the complex envelope of the frequency response of the multimode fiber are shown in Figure 2.1. The values of $t_{d,avg}$ and $t_{d,dev}$ are 5 μs and 5 ns, respectively. The unit of the amplitude response is in dB, which is defined by $10\log_{10}\{|H_{fiber}(f)|\}$*. Randomly choosing the delays corresponding to the number of modes (N_m) and applying these delays to (2-2), the magnitude of the complex envelope of the multimode fiber is determined. The probability density function of the delays used in this figure is uniformly distributed about $t_{d,avg}$, as given in (2-6). For each N_m, there are three curves (that is; upper, middle, and lower curves) corresponding to different sets of delays. The magnitude responses shown by middle and lower curves are displaced by 20 and 40 dB, respectively, to more easily see and compare these curves with the upper one. From these three plots for different N_m in Figure 2.1, it is seen that the frequency response of the multimode fiber does not monotonically decrease as a function of frequency. For low frequencies, the frequency response of the multimode fiber is dominated by the lower-order guided modes, which have large delays. Thus, for this frequency range, the frequency response of the fiber monotonically decreases with an approximate Gaussian shape as a function of frequency. However, when the frequency increases, the effect of the higher-order guided modes, which have smaller delays, becomes stronger and leads to a relatively flat response. The amplitude of this relatively flat region is below the DC level. From these three plots, it is seen that the amplitude in this region depends on the number of guided modes in the fiber. If the number of guided modes increases, the loss in this region becomes larger. The average amplitudes of this relatively flat region are –8.5, –10.2, and –11.2 dB for

* Note that $10\log_{10}\{|H_{fiber}(f)|\}$ is used consistent with the assumption that the optical modulation index is small resulting in an approximate linear relation between the time-varying portion of the field amplitude and the time-varying portion of the optical intensity.

N_m = 50, 100, and 150, respectively. Considering the passband bandwidth in each case, it is seen that there are many bandpass regions that have in total a much larger bandwidth than the 3-dB baseband bandwidth. For example, for N_m = 50 (upper curve), the bandpass regions, which have large passband, are at 0.24, 0.5, 0.8, 1.25, 1.5, 1.7, 2.3, and 2.8 GHz. The bandwidth from these passbands is approximately 1.5 GHz (estimated from the regions where the response is greater than –10 dB). It is seen that just from these eight passbands, the available bandwidth is much larger than the baseband bandwidth, which is approximately 100 MHz. Thus, the data rate can be increased significantly if these passband regions of the multimode fiber are used. It should be noted that comparing the magnitude responses from different sets of delays for each N_m, it is seen that the shapes of the responses at low frequencies (baseband region) are almost identical. At high frequencies, although the locations of the passband regions are not identical for these three sets of delays, the structure of these passband regions are the same; that is, they are relatively flat with the same average value.

2.3 Analysis of statistical properties of the multimode fiber at high frequency

2.3.1 Probability density function of the magnitude response of the multimode fiber

From (2-2), we get

$$\left|H_{fiber}(f)\right| = \sqrt{\left[\sum_{n=1}^{N_m}\cos\left(2\pi f t_{d,n}\right)\right]^2 + \left[\sum_{n=1}^{N_m}\sin\left(2\pi f t_{d,n}\right)\right]^2} = \sqrt{\left[\sum_{n=1}^{N_m} x_n\right]^2 + \left[\sum_{n=1}^{N_m} y_n\right]^2} \qquad (2\text{-}7)$$

where $x_n = \cos\left(2\pi f t_{d,n}\right)$ and $y_n = \sin\left(2\pi f t_{d,n}\right)$

Letting $\varphi = 2\pi f t_{d,n}$, it follows that

$$f_{\varphi}(\varphi) = \begin{cases} \dfrac{1}{4\pi f t_{d,dev}} & ;\ \text{for } 2\pi f\left(t_{d,avg} - t_{d,dev}\right) \le \varphi \le 2\pi f\left(t_{d,avg} + t_{d,dev}\right) \\ 0 & ;\ \text{elsewhere} \end{cases} \tag{2-8}$$

Thus, we get $$x_n = \cos(\varphi) = g(\varphi) \ ;\ -1 \le x_{n,\min} \le x_n \le x_{n,\max} \le 1 \tag{2-9}$$

where $x_{n,\min}$ and $x_{n,\max}$ depend on $2\pi f t_{d,avg}$ and $2\pi f(2t_{d,dev})$. If $2\pi f(2t_{d,dev}) \ge 2\pi$, $-1 \le x_n \le 1$.

Considering $n = 1$, we get

$$g'(\varphi) = -\sin(\varphi) = -\sqrt{1 - x_1^2} \tag{2-10}$$

and, $$\varphi_m = \cos^{-1}(x_1) \ ;\ m = 1, 2, 3, ..., M_s \tag{2-11}$$

where M_s is the total number of φ_m satisfying (2-11).

Note that M_s depends on the value of x_1 and $2\pi f(2t_{d,dev})$; that is,

$0 < 2\pi f(2t_{d,dev}) \le \pi$ or $0 < f \le \dfrac{1}{4t_{d,dev}}$ $\Rightarrow$ $M_s = 1$ or 2 (depending on f and x_1)

$\pi < 2\pi f(2t_{d,dev}) \le 2\pi$ or $\dfrac{1}{4t_{d,dev}} < f \le \dfrac{1}{2t_{d,dev}}$ $\Rightarrow$ $M_s = 2$ or 3 (depending on f and x_1)

$2\pi < 2\pi f(2t_{d,dev}) \le 3\pi$ or $\dfrac{1}{2t_{d,dev}} < f \le \dfrac{1}{t_{d,dev}}$ $\Rightarrow$ $M_s = 3$ or 4 (depending on f and x_1)

and so on.

Given $t_{d,avg}$ and $t_{d,dev}$, it is seen that M_s depends on x_1 and f. The probability density function of x_1 is given by

$$f_{x_1}(x_1) = \sum_{m=1}^{M_s} \frac{f_{\varphi}(\varphi_m)}{\left|g'(\varphi_m)\right|} \tag{2-12}$$

Using (2-8) and (2-10) with (2-12), we get

$$f_{x_1}(x_1) = \frac{1}{\sqrt{1-x_1^2}} \cdot \frac{M_s}{4\pi f t_{d,dev}} \tag{2-13}$$

Considering the case where the frequency is very large (passband region); i.e.,

$f >> \frac{1}{2t_{d,dev}}$; we get that

$$M_s \cong 2\left[f \cdot 2t_{d,dev} \right] = 4 f t_{d,dev} \tag{2-14}$$

Substituting (2-14) into (2-13), the probability density function of x_1 at high frequency is given by

$$f_{x_1}(x_1) = \frac{1}{\pi\sqrt{1-x_1^2}} \quad ; \quad -1 \le x_1 \le 1 \tag{2-15}$$

The mean and variance of x_1, obtained from the probability density function given in (2-15) are 0 and 0.5, respectively.

Note that the probability density function of each x_n is also given by (2-15).

Let $$X = \sum_{n=1}^{N_m} x_n \tag{2-16}$$

With large N_m, the probability density function of X can be determined by using the central limit theorem; that is, we get

$$f_X(X) \cong \frac{1}{\sigma_X\sqrt{2\pi}} e^{\frac{-(X-m_X)^2}{2\sigma_X^2}} \tag{2-17}$$

where $$m_X = \sum_{n=1}^{N_m} m_{x_n} = \sum_{n=1}^{N_m} 0 = 0\,. \tag{2-18}$$

and, $$\sigma_X^2 = \sum_{n=1}^{N_m} \sigma_{x_n}^2 = \sum_{n=1}^{N_m} 0.5 = \frac{N_m}{2} \tag{2-19}$$

Similarly, for the sine terms in (2-7) or y_n, we get that for a high frequency, the probability density function of y_n is approximated by

$$f_{y_n}(y_n) = \frac{1}{\pi\sqrt{1-y_n^2}} \quad ; \quad -1 \le y_n \le 1 \tag{2-20}$$

The mean and variance of y_n given in (2-20) are 0 and 0.5, respectively.

Let $$Y = \sum_{n=1}^{N_m} y_n \tag{2-21}$$

With large N_m, the probability density function of Y can similarly be determined by using the central limit theorem; that is, we get

$$f_Y(Y) \cong \frac{1}{\sigma_Y\sqrt{2\pi}} e^{\frac{-(Y-m_Y)^2}{2\sigma_Y^2}} \tag{2-22}$$

where $$m_Y = \sum_{n=1}^{N_m} m_{y_n} = \sum_{n=1}^{N_m} 0 = 0\,. \tag{2-23}$$

and, $$\sigma_Y^2 = \sum_{n=1}^{N_m} \sigma_{y_n}^2 = \sum_{n=1}^{N_m} 0.5 = \frac{N_m}{2} \tag{2-24}$$

From (2-17) to (2-24), the probability density functions of X and Y are normal distributions with zero mean and variance of $N_m/2$. Also, X and Y are independent since X is from the cosine terms of $t_{d,n}$ and Y is from the sine terms of $t_{d,n}$. Thus, using these properties with (2-7), the probability density function of $\left|H_{fiber}(f)\right|$ at the high frequency range is given by

$$\begin{aligned} f_{|H_{fiber}(f)|}\left(\left|H_{fiber}(f)\right|\right) &= \frac{\left|H_{fiber}(f)\right|}{\sigma_X^2}\exp\left\{\frac{-\left|H_{fiber}(f)\right|^2}{2\sigma_X^2}\right\}U\left(\left|H_{fiber}(f)\right|\right) \\ &= \frac{2\left|H_{fiber}(f)\right|}{N_m}\exp\left\{\frac{-\left|H_{fiber}(f)\right|^2}{N_m}\right\}U\left(\left|H_{fiber}(f)\right|\right) \end{aligned} \tag{2-25}$$

where U is the unit step function.

Note that the density function given in (2-25) is the Rayleigh density function.

From (2-25), the mean and the variance of $\left|H_{fiber}\left(f\right)\right|$ are given by

$$m_{|H_{fiber}(f)|} = \sqrt{\frac{\pi}{2}}\sigma_X = \sqrt{\frac{\pi}{2}}\sqrt{\frac{N_m}{2}} = \sqrt{\frac{\pi N_m}{4}} \tag{2-26}$$

$$\sigma^2_{|H_{fiber}(f)|} = \left[2-\frac{\pi}{2}\right]\sigma_X^2 = \left[2-\frac{\pi}{2}\right]\frac{N_m}{2} = \left[1-\frac{\pi}{4}\right]N_m \tag{2-27}$$

Using (2-26), the mean value of $\left|H_{fiber}\left(f\right)\right|$ compared to the maximum value of $\left|H_{fiber}\left(f\right)\right|$ at $f = 0$ is given by

$$m_{|H_{fiber}(f)|}\left(\text{in dB}\right) = 10\log_{10}\left\{\frac{m_{|H_{fiber}(f)|}}{N_m}\right\} = 10\log_{10}\left\{\frac{1}{N_m}\sqrt{\frac{\pi N_m}{4}}\right\} = 10\log_{10}\left\{\sqrt{\frac{\pi}{4N_m}}\right\} \tag{2-28}$$

which indicates that the mean value decreases as N_m increases, consistent with Figure 2.1. For example, (2-28) indicates that for N_m = 100, the mean value of $\left|H_{fiber}\left(f\right)\right|$ is –10.5 dB and for N_m = 150, the mean value of $\left|H_{fiber}\left(f\right)\right|$ is –11.4 dB.

2.3.2 Correlation function of the frequency response

Another important statistical parameter is the correlation function since this influences the bandwidth at high frequency. In this section, the correlation function of the frequency response of the multimode fiber ($R_{H_{fiber}}\left(\nu\right)$) is determined.

From (2-7), we get

$$H_{fiber}(f)=\sum_{n=1}^{N_m}\cos\left(2\pi f t_{d,n}\right)+j\sum_{n=1}^{N_m}\sin\left(2\pi f t_{d,n}\right)=X(f)+jY(f) \tag{2-29}$$

And, $R_{H_{fiber}}(\nu)=\left\langle H_{fiber}(f)H^{*}_{fiber}(f+\nu)\right\rangle=\left\langle\{X(f)+jY(f)\}\{X(f+\nu)-jY(f+\nu)\}\right\rangle$

$$=\left\langle X(f)X(f+\nu)+Y(f)Y(f+\nu)+j\left[Y(f)X(f+\nu)-X(f)Y(f+\nu)\right]\right\rangle \tag{2-30}$$

From (2-30), we get that $\left\langle Y(f)X(f+\nu)\right\rangle=\left\langle X(f)Y(f+\nu)\right\rangle=0$ since the averages of X and Y are zero and they are uncorrelated to one another. And,

$$\left\langle X(f)X(f+\nu)\right\rangle=\left\langle\left\{\sum_{n=1}^{N_m}\cos\left(2\pi f t_{d,n}\right)\right\}\left\{\sum_{m=1}^{N_m}\cos\left(2\pi(f+\nu)t_{d,m}\right)\right\}\right\rangle$$

$$=\left\langle\sum_{n=1}^{N_m}\sum_{m=1}^{N_m}\frac{1}{2}\left[\cos\left(2\pi\left(f\left[t_{d,n}+t_{d,m}\right]+\nu t_{d,m}\right)\right)+\cos\left(2\pi\left(f\left[t_{d,n}-t_{d,m}\right]-\nu t_{d,m}\right)\right)\right]\right\rangle$$

Since we are interested in the properties of the multimode fiber at high frequency, it is reasonable to assume that $f>>\frac{1}{2t_{d,dev}}$ (see the discussion in (2-10) to (2-14)). However, if ν is very large (i.e., ν is also much greater than $\frac{1}{2t_{d,dev}}$), the frequency response at frequency $f+\nu$ will be independent of the frequency response at frequency f. Consequently, we are concerned with $\nu<\frac{1}{2t_{d,dev}}$. Using these two inequalities, we get that

$$\left\langle X(f)X(f+\nu)\right\rangle=\left\langle\sum_{n=1}^{N_m}\sum_{m=1}^{N_m}\frac{1}{2}\cos\left(2\pi\left(f\left[t_{d,n}-t_{d,m}\right]-\nu t_{d,m}\right)\right)\right\rangle \tag{2-31}$$

Considering (2-31), it is seen that if $m\neq n$, $\left\langle\cos\left(2\pi\left(f\left[t_{d,n}-t_{d,m}\right]-\nu t_{d,m}\right)\right)\right\rangle=0$; thus,

$$\left\langle X(f)X(f+\nu)\right\rangle = \left\langle \sum_{n=1}^{N_m} \frac{1}{2}\cos\left(2\pi\nu t_{d,n}\right)\right\rangle = \frac{1}{2}\sum_{n=1}^{N_m}\left\langle \cos\left(2\pi\nu t_{d,n}\right)\right\rangle \quad (2\text{-}32)$$

Similarly, for the term $\left\langle Y(f)Y(f+\nu)\right\rangle$, we get that

$$\left\langle Y(f)Y(f+\nu)\right\rangle = \left\langle \left\{\sum_{n=1}^{N_m}\sin\left(2\pi f t_{d,n}\right)\right\}\left\{\sum_{m=1}^{N_m}\sin\left(2\pi(f+\nu)t_{d,m}\right)\right\}\right\rangle$$

$$= \left\langle \sum_{n=1}^{N_m}\sum_{m=1}^{N_m}\frac{1}{2}\left[\cos\left(2\pi\left(f\left[t_{d,n}-t_{d,m}\right]-\nu t_{d,m}\right)\right)-\cos\left(2\pi\left(f\left[t_{d,n}+t_{d,m}\right]+\nu t_{d,m}\right)\right)\right]\right\rangle$$

Assuming $f >> \frac{1}{2t_{d,dev}}$, and $\nu < \frac{1}{2t_{d,dev}}$, we get that

$$\left\langle Y(f)Y(f+\nu)\right\rangle = \left\langle \sum_{n=1}^{N_m}\sum_{m=1}^{N_m}\frac{1}{2}\cos\left(2\pi\left(f\left[t_{d,n}-t_{d,m}\right]-\nu t_{d,m}\right)\right)\right\rangle = \frac{1}{2}\sum_{n=1}^{N_m}\left\langle \cos\left(2\pi\nu t_{d,n}\right)\right\rangle \quad (2\text{-}33)$$

Therefore,

$$R_{H_{fiber}}(\nu) = \left\langle H_{fiber}(f)H^{*}_{fiber}(f+\nu)\right\rangle = \sum_{n=1}^{N_m}\left\langle \cos\left(2\pi\nu t_{d,n}\right)\right\rangle \quad (2\text{-}34)$$

2.3.3 Correlation function of the magnitude response

Although the correlation function of the frequency response is of interest, the correlation function of the magnitude of the frequency response is of greater interest. Using a similar approach to that in the previous section, we get that

$$\left\langle \left|H_{fiber}(f)H_{fiber}(f+\nu)\right|^2\right\rangle = \left\langle H_{fiber}(f)H^{*}_{fiber}(f)H_{fiber}(f+\nu)H^{*}_{fiber}(f+\nu)\right\rangle$$

$$= \left\langle \left[X_1+jY_1\right]\left[X_1-jY_1\right]\left[X_2+jY_2\right]\left[X_2-jY_2\right]\right\rangle$$

$$\left\langle \left|H_{fiber}(f)H_{fiber}(f+\nu)\right|^2\right\rangle = \left\langle X_1^2X_2^2+Y_1^2Y_2^2+X_1^2Y_2^2+X_2^2Y_1^2\right\rangle \quad (2\text{-}35)$$

where $$X_1 = \sum_{n=1}^{N_m} \cos\left(2\pi f t_{d,n}\right);\ Y_1 = \sum_{n=1}^{N_m} \sin\left(2\pi f t_{d,n}\right) \tag{2-36}$$

and $$X_2 = \sum_{n=1}^{N_m} \cos\left(2\pi (f+\nu) t_{d,n}\right);\ Y_2 = \sum_{n=1}^{N_m} \sin\left(2\pi (f+\nu) t_{d,n}\right) \tag{2-37}$$

Considering each term in (2-35), we get that

-For $\left\langle X_1^2 X_2^2 \right\rangle$;

$$\left\langle X_1^2 X_2^2 \right\rangle = \left\langle \left[\sum_{n=1}^{N_m} \cos\left(2\pi f t_{d,n}\right)\right]^2 \left[\sum_{m=1}^{N_m} \cos\left(2\pi (f+\nu) t_{d,m}\right)\right]^2 \right\rangle$$

$$= \left\langle \left[\sum_{n=1}^{N_m}\sum_{m=1}^{N_m} \cos\left(2\pi f t_{d,n}\right)\cos\left(2\pi (f+\nu) t_{d,m}\right)\right]^2 \right\rangle$$

$$= \left\langle \left[\sum_{n=1}^{N_m}\sum_{m=1}^{N_m} \cos\left(2\pi f t_{d,n}\right)\cos\left(2\pi (f+\nu) t_{d,m}\right)\right]\left[\sum_{q=1}^{N_m}\sum_{r=1}^{N_m} \cos\left(2\pi f t_{d,q}\right)\cos\left(2\pi (f+\nu) t_{d,r}\right)\right] \right\rangle$$

$$\left\langle X_1^2 X_2^2 \right\rangle = \frac{1}{4}\left\langle \left[\sum_{n=1}^{N_m}\sum_{m=1}^{N_m} \cos\left(2\pi\left[f\left(t_{d,n}+t_{d,m}\right)+\nu t_{d,m}\right]\right) + \cos\left(2\pi\left[f\left(t_{d,n}-t_{d,m}\right)-\nu t_{d,m}\right]\right)\right] \right.$$
$$\left. \times \left[\sum_{q=1}^{N_m}\sum_{r=1}^{N_m} \cos\left(2\pi\left[f\left(t_{d,q}+t_{d,r}\right)+\nu t_{d,r}\right]\right) + \cos\left(2\pi\left[f\left(t_{d,q}-t_{d,r}\right)-\nu t_{d,r}\right]\right)\right] \right\rangle \tag{2-38}$$

There are four terms in (2-38); that is,

$$\Rightarrow \left\langle \sum_{m,n,q,r=1}^{N_m} \cos\left(2\pi\left[f\left(t_{d,n}+t_{d,m}\right)+\nu t_{d,m}\right]\right)\cos\left(2\pi\left[f\left(t_{d,q}+t_{d,r}\right)+\nu t_{d,r}\right]\right) \right\rangle$$

$$= \frac{1}{2}\sum_{m,n,q,r=1}^{N_m} \left\langle \begin{array}{l} \cos\left(2\pi\left[f\left(t_{d,n}+t_{d,m}+t_{d,q}+t_{d,r}\right)+\nu\left(t_{d,m}+t_{d,r}\right)\right]\right) \\ +\cos\left(2\pi\left[f\left(t_{d,n}+t_{d,m}-t_{d,q}-t_{d,r}\right)+\nu\left(t_{d,m}-t_{d,r}\right)\right]\right) \end{array} \right\rangle$$

Assuming $f >> \dfrac{1}{2t_{d,dev}}$, and $\nu < \dfrac{1}{2t_{d,dev}}$; we get that

$$\left\langle \sum_{m,n,q,r=1}^{N_m} \cos\left(2\pi\left[f\left(t_{d,n}+t_{d,m}\right)+\nu t_{d,m}\right]\right)\cos\left(2\pi\left[f\left(t_{d,q}+t_{d,r}\right)+\nu t_{d,r}\right]\right)\right\rangle$$

$$= \frac{1}{2}\sum_{m,n,q,r=1}^{N_m}\left\langle \cos\left(2\pi\left[f\left(t_{d,n}+t_{d,m}-t_{d,q}-t_{d,r}\right)+\nu\left(t_{d,m}-t_{d,r}\right)\right]\right)\right\rangle$$

$$= \frac{1}{2}\left\{ {N_m}^2 + \sum_{m=1}^{N_m}\sum_{r=1}^{N_m}\left\langle \cos\left(2\pi\nu\left(t_{d,m}-t_{d,r}\right)\right)\right\rangle\right\} \tag{2-39}$$

$$\Rightarrow \left\langle \sum_{m,n,q,r=1}^{N_m} \cos\left(2\pi\left[f\left(t_{d,n}+t_{d,m}\right)+\nu t_{d,m}\right]\right)\cos\left(2\pi\left[f\left(t_{d,q}-t_{d,r}\right)-\nu t_{d,r}\right]\right)\right\rangle$$

$$= \frac{1}{2}\sum_{m,n,q,r=1}^{N_m}\left\langle \begin{array}{l} \cos\left(2\pi\left[f\left(t_{d,n}+t_{d,m}+t_{d,q}-t_{d,r}\right)+\nu\left(t_{d,m}-t_{d,r}\right)\right]\right) \\ +\cos\left(2\pi\left[f\left(t_{d,n}+t_{d,m}-t_{d,q}+t_{d,r}\right)+\nu\left(t_{d,m}+t_{d,r}\right)\right]\right) \end{array}\right\rangle$$

Assuming $f >> \frac{1}{2t_{d,dev}}$, and $\nu < \frac{1}{2t_{d,dev}}$; we get that

$$\left\langle \sum_{m,n,q,r=1}^{N_m} \cos\left(2\pi\left[f\left(t_{d,n}+t_{d,m}\right)+\nu t_{d,m}\right]\right)\cos\left(2\pi\left[f\left(t_{d,q}-t_{d,r}\right)-\nu t_{d,r}\right]\right)\right\rangle = 0 \tag{2-40}$$

$$\Rightarrow \left\langle \sum_{m,n,q,r=1}^{N_m} \cos\left(2\pi\left[f\left(t_{d,n}-t_{d,m}\right)-\nu t_{d,m}\right]\right)\cos\left(2\pi\left[f\left(t_{d,q}+t_{d,r}\right)+\nu t_{d,r}\right]\right)\right\rangle$$

$$= \frac{1}{2}\sum_{m,n,q,r=1}^{N_m}\left\langle \begin{array}{l} \cos\left(2\pi\left[f\left(t_{d,n}-t_{d,m}+t_{d,q}+t_{d,r}\right)-\nu\left(t_{d,m}-t_{d,r}\right)\right]\right) \\ +\cos\left(2\pi\left[f\left(t_{d,n}-t_{d,m}-t_{d,q}-t_{d,r}\right)-\nu\left(t_{d,m}+t_{d,r}\right)\right]\right) \end{array}\right\rangle$$

Assuming $f >> \frac{1}{2t_{d,dev}}$, and $\nu < \frac{1}{2t_{d,dev}}$; we get that

$$\left\langle \sum_{m,n,q,r=1}^{N_m} \cos\left(2\pi\left[f\left(t_{d,n}-t_{d,m}\right)-\nu t_{d,m}\right]\right)\cos\left(2\pi\left[f\left(t_{d,q}+t_{d,r}\right)+\nu t_{d,r}\right]\right)\right\rangle = 0 \tag{2-41}$$

$$\Rightarrow \left\langle \sum_{m,n,q,r=1}^{N_m} \cos\left(2\pi\left[f\left(t_{d,n}-t_{d,m}\right)-\nu t_{d,m}\right]\right)\cos\left(2\pi\left[f\left(t_{d,q}-t_{d,r}\right)-\nu t_{d,r}\right]\right)\right\rangle$$

$$= \frac{1}{2}\sum_{m,n,q,r=1}^{N_m}\left\langle \begin{array}{l} \cos\left(2\pi\left[f\left(t_{d,n}-t_{d,m}+t_{d,q}-t_{d,r}\right)-\nu\left(t_{d,m}+t_{d,r}\right)\right]\right) \\ +\cos\left(2\pi\left[f\left(t_{d,n}-t_{d,m}-t_{d,q}+t_{d,r}\right)-\nu\left(t_{d,m}-t_{d,r}\right)\right]\right) \end{array}\right\rangle$$

Assuming $f >> \frac{1}{2t_{d,dev}}$, and $\nu < \frac{1}{2t_{d,dev}}$; we get that

$$\left\langle \sum_{m,n,q,r=1}^{N_m} \cos\left(2\pi\left[f\left(t_{d,n}-t_{d,m}\right)-\nu t_{d,m}\right]\right)\cos\left(2\pi\left[f\left(t_{d,q}-t_{d,r}\right)-\nu t_{d,r}\right]\right)\right\rangle$$

$$= \frac{1}{2}\left\{2\left[\sum_{m=1}^{N_m}\sum_{r=1}^{N_m}\left\langle\cos\left(2\pi\nu\left(t_{d,m}+t_{d,r}\right)\right)\right\rangle\right] + {N_m}^2 + \left[\sum_{m=1}^{N_m}\sum_{r=1}^{N_m}\left\langle\cos\left(2\pi\nu\left(t_{d,m}-t_{d,r}\right)\right)\right\rangle\right]\right\} \quad (2\text{-}42)$$

Substituting (2-39) to (2-42) into (2-38), we get

$$\left\langle X_1^2 X_2^2\right\rangle = \frac{1}{4}\left\{\left[\sum_{m=1}^{N_m}\sum_{r=1}^{N_m}\left\langle\cos\left(2\pi\nu\left(t_{d,m}+t_{d,r}\right)\right)\right\rangle\right] + {N_m}^2 + \left[\sum_{m=1}^{N_m}\sum_{r=1}^{N_m}\left\langle\cos\left(2\pi\nu\left(t_{d,m}-t_{d,r}\right)\right)\right\rangle\right]\right\} \quad (2\text{-}43)$$

-For $\left\langle Y_1^2 Y_2^2\right\rangle$; using the same approach as we did for $\left\langle X_1^2 X_2^2\right\rangle$, we get

$$\left\langle Y_1^2 Y_2^2\right\rangle = \frac{1}{4}\left\{\left[\sum_{m=1}^{N_m}\sum_{r=1}^{N_m}\left\langle\cos\left(2\pi\nu\left(t_{d,m}+t_{d,r}\right)\right)\right\rangle\right] + {N_m}^2 + \left[\sum_{m=1}^{N_m}\sum_{r=1}^{N_m}\left\langle\cos\left(2\pi\nu\left(t_{d,m}-t_{d,r}\right)\right)\right\rangle\right]\right\} \quad (2\text{-}44)$$

-For $\left\langle X_1^2 Y_2^2\right\rangle$ and $\left\langle X_2^2 Y_1^2\right\rangle$; since X and Y are independent to one another, we get

$$\left\langle X_1^2 Y_2^2\right\rangle = \left\langle X_1^2\right\rangle\left\langle Y_2^2\right\rangle \text{ and } \left\langle X_2^2 Y_1^2\right\rangle = \left\langle X_2^2\right\rangle\left\langle Y_1^2\right\rangle \quad (2\text{-}45)$$

Using the results from (2-19) and (2-24); that is, $\langle X^2 \rangle = \langle Y^2 \rangle = \frac{N_m}{2}$; we get that

$$\langle X_1^2 Y_2^2 \rangle = \langle X_2^2 Y_1^2 \rangle = \frac{N_m}{2} \cdot \frac{N_m}{2} = \frac{{N_m}^2}{4} \tag{2-46}$$

Substituting (2-43), (2-44), and (2-46) into (2-35), we get

$$\left\langle \left| H_{fiber}(f) H_{fiber}(f+\nu) \right|^2 \right\rangle = {N_m}^2 + \frac{1}{2} \sum_{m=1}^{N_m} \sum_{r=1}^{N_m} \left\langle \cos\left(2\pi\nu\left(t_{d,m} + t_{d,r}\right)\right) + \cos\left(2\pi\nu\left(t_{d,m} - t_{d,r}\right)\right) \right\rangle \tag{2-47}$$

Using the results from (2-34) and (2-47) with $t_{d,avg}$ = 5 μs, $t_{d,dev}$ = 5 ns, the plots of $R_{H_{fiber}}(\nu)$ and $\left\langle \left| H_{fiber}(f) H_{fiber}(f+\nu) \right|^2 \right\rangle$ as a function of frequency ν for the number of guided modes (N_m), and normalized by N_m and $2{N_m}^2$, respectively, are shown in Figure 2.2 and 2.3. From the plots, the shapes of $R_{H_{fiber}}(\nu)$ and $\left\langle \left| H_{fiber}(f) H_{fiber}(f+\nu) \right|^2 \right\rangle$ for different number of guided modes (N_m) are almost identical. As the frequency (ν) increases, the values of normalized $R_{H_{fiber}}(\nu)$ and $\left\langle \left| H_{fiber}(f) H_{fiber}(f+\nu) \right|^2 \right\rangle$ approach 0 and 0.5, respectively. Considering the plot of $\left\langle \left| H_{fiber}(f) H_{fiber}(f+\nu) \right|^2 \right\rangle$, the available bandwidth is approximately 100 MHz (two times the width of the autocorrelation function), which is comparable to the 3-dB modal bandwidth found from Figure 2.1. Note that from (2-34) and (2-47) it is seen that to get larger bandwidth, the maximum delay deviation ($t_{d,dev}$) should be reduced. The value of the maximum delay deviation used in this chapter is for illustrative purposes only; actual values will depend on the fiber type and length.

From the results found in (2-25), (2-28), (2-34), and (2-47), it is seen that to get a high average value of $\left|H_{fiber}(f)\right|$ at high frequency and large available passband bandwidth, the number of guided modes and the maximum delay deviation should be decreased. However, if the number of guided modes is too small, another impairment namely modal noise becomes stronger and can degrade the system performance. In practice, the effective number of modes will be less than the actual number of modes since all modes are not equally excited, and modes near cut-off will have higher attenuation. In the model considered here, all modes are assumed to have equal amplitude. The effective number of modes in multimode fiber used for communications is of the order of 100.

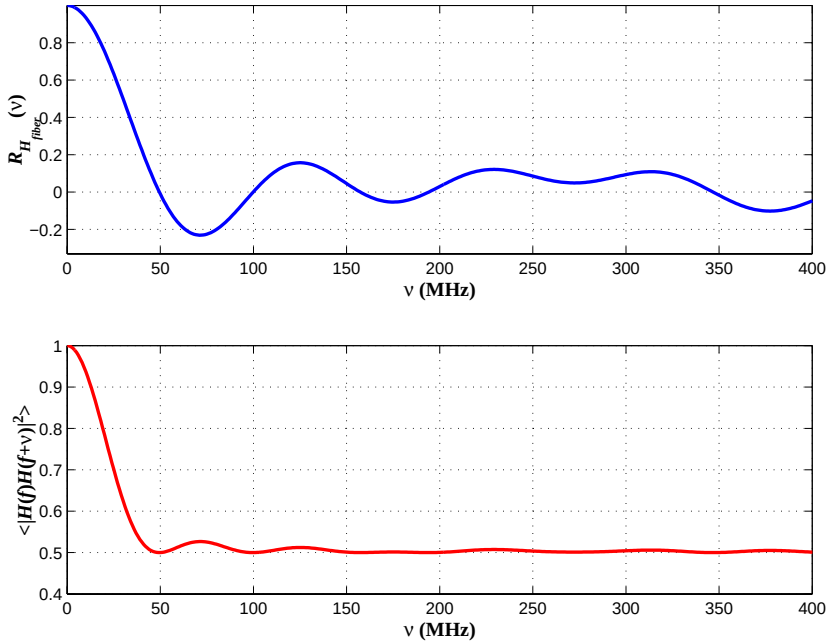

Figure 2.2 Plots of normalized $R_{H_{fiber}}(\nu)$ and $\left\langle \left|H_{fiber}(f)H_{fiber}(f+\nu)\right|^2 \right\rangle$ for N_m = 100 modes, $t_{d,avg}$ = 5 μs and $t_{d,dev}$ = 5 ns.

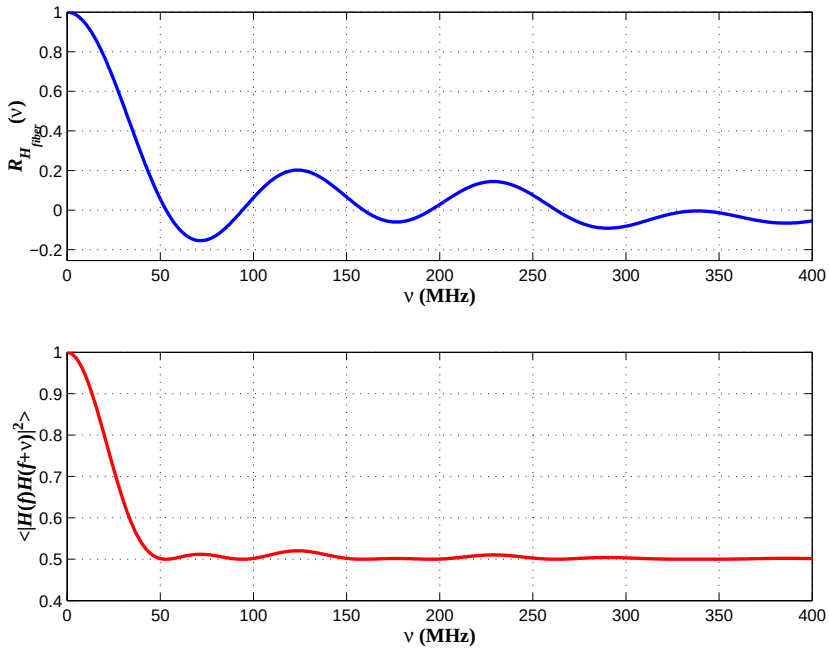

Figure 2.3 Plots of normalized $R_{H_{fiber}}(\nu)$ and $\left\langle \left| H_{fiber}(f) H_{fiber}(f+\nu) \right|^2 \right\rangle$ for $N_m = 150$ modes, $t_{d,avg} = 5$ μs and $t_{d,dev} = 5$ ns.

2.4 Conclusions

Assuming that the delay $t_{d,n}$ is a random variable, which is uniformly distributed about $t_{d,avg}$ with the maximum deviation of $t_{d,dev}$, the probability density function of the amplitude of the transfer function ($\left| H_{fiber}(f) \right|$) of the multimode fiber at high frequency range has been analyzed. The probability density function of $\left| H_{fiber}(f) \right|$ is a Rayleigh density function. The average value of $\left| H_{fiber}(f) \right|$ and the average value of $\left| H_{fiber}(f) \right|$ compared to the maximum (at $f = 0$) are given. It has been shown that the probability density function and the average value of $\left| H_{fiber}(f) \right|$ do not depend on frequency but

depend on the number of guided modes supported by the fiber. This analysis agrees with the experiments found by many groups of researchers; that is, at the high frequency, the amplitude response of the multimode fiber does not fall off as a function of frequency but becomes relatively flat at a particular level below the maximum. For example, it is shown in [13] that the response of a multimode fiber at high frequencies is relatively flat with an attenuation level of approximately 10 dB relative to the zero frequency level. Moreover, the correlation function ($R_{H_{fiber}}(\nu)$) of the frequency response of the multimode fiber and the correlation function ($\left\langle \left| H_{fiber}(f) H_{fiber}(f+\nu) \right|^2 \right\rangle$) of the amplitude response of the multimode fiber has been studied. It has been shown that the available bandwidth for one frequency band at the high frequency region determined from these correlation functions mainly depends on the delay spread introduced by the fiber and is approximately comparable to the 3-dB modal bandwidth. Using this high frequency region with subcarrier multiplexing, many high data rate signals can be simultaneously transmitted through the multimode fiber; thus, the total data rate can be increased significantly. The subcarrier frequencies should be at the peak of passband regions so that the maximum data rate can be obtained. However, the available passband regions vary from fiber to fiber as seen from Figure 2.1. Also, for a given fiber, these passband regions may also vary due to many factors; for example, temperature change, mechanical stress, and so on. Thus, appropriate transmission system and system modification are required in order to transmit signals over the bandpass region effectively. The system performance from different types of transmission systems and system modifications are presented in Chapters 3 to 8.

Chapter 3

Electrical Equalization at the Receiver

3.1 Introduction

It has been shown in Chapter 2 that there are many passbands available in the frequency response of multimode fiber at high frequencies. If these passbands are used as transmission channels, the total data rate will increase significantly. However, there are many nulls in this high frequency range. These nulls can degrade the system performance considerably and lead to unsuccessful bandpass transmission if the main frequency component of the signal is located at the null. To improve the quality of the received signal, an electrical equalizer may be added to the receiving end in order to compensate for the frequency variation of the channel response.

The effect of adding electrical equalization to subcarrier transmission on multimode fiber is studied in this chapter. To show the achieved performance from different amplitude variations caused by the multimode fiber at high frequencies, the same data is sent through three different subcarriers. At the receiver, two types of electrical equalization are used; that is, ideal electrical equalization and limited-gain equalization. The signal-to-noise ratio and eye-diagram of the received signals from different cases are

presented. The results of using these two types of equalization are discussed and compared to the case of not having equalization. Also, to study the effect of using frequency diversity, these three received signals are combined. The signal-to-noise ratios and the eye-diagrams from the combined signal for the cases of without and with electrical equalization are presented.

3.2 Signal-to-noise ratio and eye-diagram of the received signals: without and with ideal electrical equalization

The block diagram for digital transmission with three subcarriers in the passband region of the multimode fiber is shown in Figure 3.1. The input bit sequence from the bit generator is sent through the pulse generator to generate the input pulses. The input pulse is assumed to be a Gaussian shape with $T_0 = 0.25T_b$, where T_0 is the half-width at $1/e$ – intensity point and T_b is the bit period. The spectrum of the input pulses is shifted to be centered at the different subcarriers ($f_{\text{subcarier}}$). This signal is then passed through the laser to convert the electrical signal into an optical signal. The spectrum of the complex envelope of the optical signal contains the spectrum of the input pulses centered at $f_{\text{subcarier}}$ and an impulse with an amplitude of 1 located at $f = 0$ (this impulse is for the carrier component of the light source). Passing this optical signal through the multimode fiber (whose magnitude response is relatively flat at high frequencies), the spectrum of the signal at high frequencies is attenuated. To limit the input optical power to a required level, a variable attenuator (loss) is placed in front of the square-law detector. The optical signal at the output of this attenuator is converted back to an electrical signal at the

square-law detector. The electrical output signal of the detector is combined with thermal noise generated by the receiver (assuming that a PIN detector and transimpedance amplifier receiver are used).

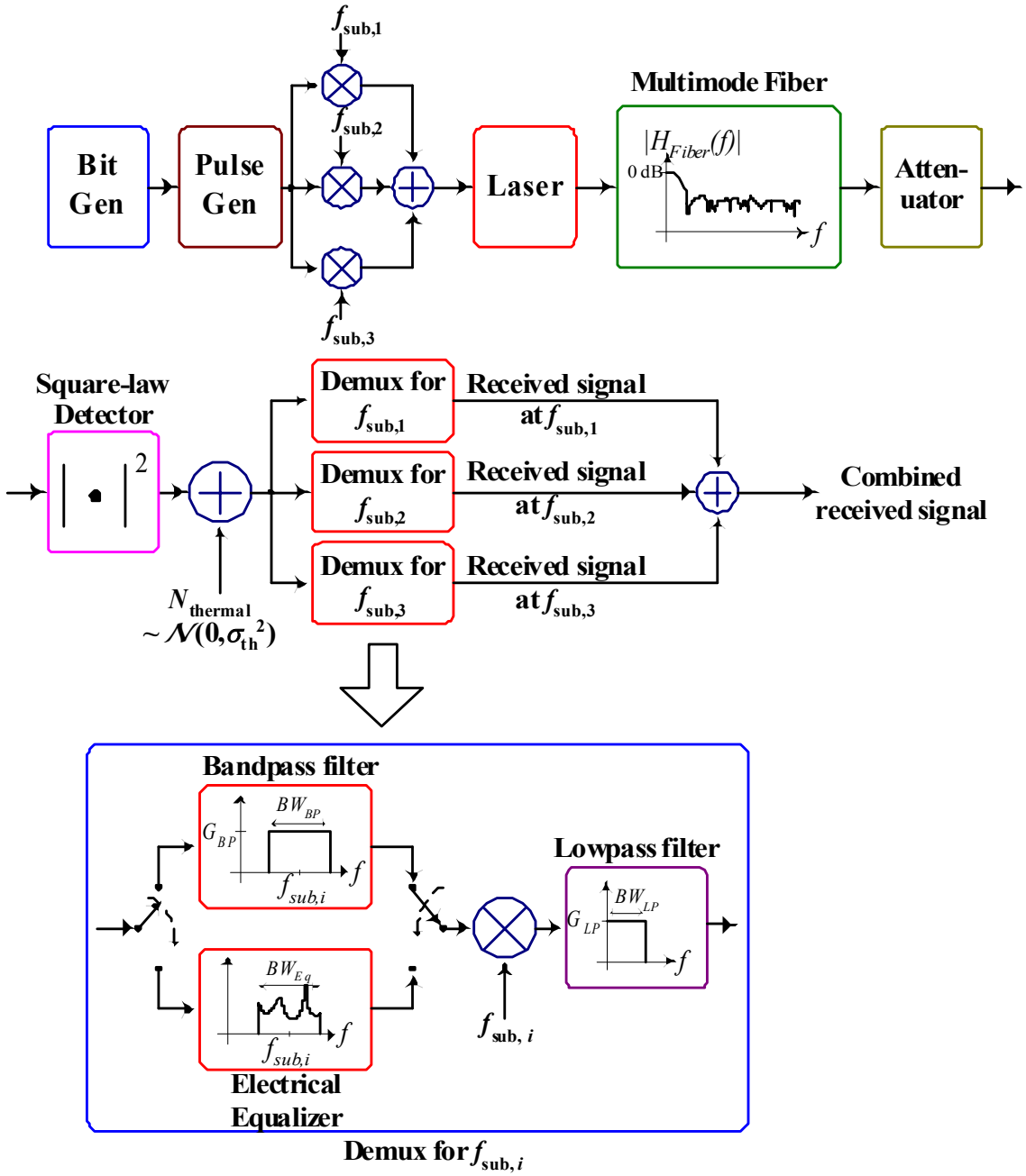

Figure 3.1 Diagram of the transmission system using three subcarriers on multimode fiber.

The probability density function of thermal noise is assumed to be zero-mean Gaussian with a variance of σ_{th}^2. The variance of thermal noise is given by [41]

$$\sigma_{th}^2 = 8\pi q V_T C_e B_e^2 \tag{3-1}$$

where q is the charge of an electron (= $1.6*10^{-19}$ C)

$$V_T = \frac{k_B T}{q} = 0.025 \text{ V} \text{ at } T = 290 \text{ K}$$

C_e is the effective noise capacitance of the transimpedance preamplifier

k_B is the Boltzmann constant (=$1.38*10^{-23}$ J/K)

T is the absolute temperature

B_e is the effective noise bandwidth of the receiver.

Note that the preamplifier is a component at the receiver placed after the photodetector in order to convert the photocurrent from the photodetector into voltage. There are three main types of preamplifier design; that is, low-impedance, high-impedance, and transimpedance preamplifiers [1]. The transimpedance preamplifier is the most common type since it has many advantages compared to the other two; for example, wider dynamic range, less susceptibility to crosstalk and electromagnetic interference, and so on.

The output of the summation is sent to the bandpass filter or the electrical equalizer as indicated in Figure 3.1. These two components have a center frequency at $f_{\text{subcarier}}$ and a bandwidth of BW_{BP} or BW_{Eq}.

Since the frequency response of the fiber is not known beforehand, it is necessary to measure this response to adjust the equalizer. The response of the electrical equalizer for each subcarrier channel is determined by sending narrowband noise as an input to the multimode fiber at each subcarrier channel. At the receiver, this narrowband noise is attenuated and shaped by the multimode fiber. To restore the narrowband noise to its spectral shape at the input, the frequency response of the electrical equalizer must be the inverse of the spectrum of the received narrowband noise. Hence, the frequency response of the electrical equalizer can be determined from the received narrowband noise spectrum. This process is done prior to transmitting the communication signal. The output of the bandpass filter (or the electrical equalizer) is then passed through a mixer and a lowpass filter. The output of the lowpass filter is the received signal, which is at baseband. At the end of the diagram in Figure 3.1, it is seen that all received signals are combined. This combination of the signals is done in order to study whether signal quality can be improved if frequency diversity is used.

The plots of frequency responses of the multimode fiber and the input optical signals at different $f_{\text{subcarier}}$, are shown in Figure 3.2. The frequency response of multimode fiber is generated by taking the Fourier transform of the complex envelope of the impulse response of multimode fiber, which is the combination of the delta functions corresponding to different delays (see equation (2-1)). Each delay corresponds to a particular guided mode supported by the multimode fiber. For this simulation, the number of modes supported by the multimode fiber is 100 modes and the total delay spread of the multimode fiber is 10 ns. Similarly, the frequency responses of three

subcarrier signals are generated by taking Fourier transform of the time responses of three subcarrier signals. A bit rate (R_b) of each subcarrier signal is 50 Mbps. The bit rate of 50 Mbps is used since it was found in Chapter 2 that the available bandwidth of each passband of multimode fiber is approximately comparable to the intermodal bandwidth. With a total delay spread of 10 ns, the intermodal bandwidth of the multimode fiber is 100 MHz. Consequently, the maximum bit rate for each subcarrier signal is then one-half of that number; that is, 50 Mbps, since amplitude modulation of the subcarrier results in a double sideband signal. The three subcarriers are taken to be at 0.5, 1.0, and 1.5 GHz to illustrate different aspects of the effect of the fiber frequency response (see figure 3.2).

The gains of the bandpass and lowpass filters are assumed to be unity. The noise equivalent bandwidth (prior to filtering) is assumed to be approximately equal to the maximum subcarrier frequency plus R_b. Also, if the maximum subcarrier frequency is very large compared to the bit rate (R_b), the noise equivalent bandwidth is then approximated by the maximum subcarrier frequency. The effective noise capacitance (C_e) of the receiver is taken to be 0.1 pF. Practical subcarrier receivers may have larger values of C_e (see Chapter 8), but we are concerned in this chapter with relative rather than absolute performance.

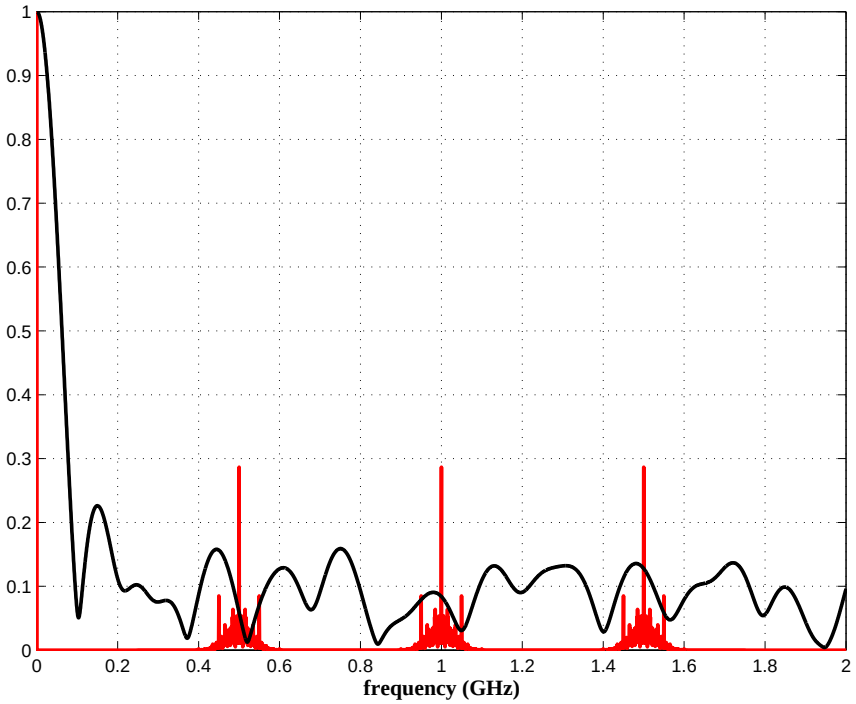

Figure 3.2 Magnitude responses of multimode fiber and subcarrier signals located at 0.5, 1.0, and 1.5 GHz.

Considering the magnitude responses of the multimode fiber and the signals at different subcarrier frequencies shown in Figure 3.2, it is seen that for the signal with $f_{\text{subcarier}}$ = 0.5 GHz, the magnitude response of the multimode fiber is very small (or a null) at frequencies near 0.5 GHz. Hence, the subcarrier signal at this $f_{\text{subcarier}}$ is strongly attenuated. The equalizer then needs to provide high gain at this subcarrier frequency. For the signals with $f_{\text{subcarier}}$ = 1.0 and 1.5 GHz, there are no deep nulls located near the main components (i.e., at $f_{\text{subcarier}}$ and $f_{\text{subcarrier}} \pm R_b$) of these subcarrier signals. The shapes of the magnitude response of the multimode fiber from these two subcarriers are almost

identical except the amplitude. The amplitude of the multimode fiber at $f_{\text{subcarier}}$ = 1.5 GHz is larger than at the amplitude of the multimode fiber at $f_{\text{subcarier}}$ = 1.0 GHz.

The plots of eye-diagrams for different subcarrier frequencies are shown in Figure 3.3 to Figure 3.5. Also, the signal-to-noise ratios for the different cases are indicated on the figures. The signal-to-noise ratio is determined by the ratio between the received signal power and the noise power at the output of the lowpass filter. To get good performance, the signal-to-noise ratio needs to be high since with this high signal-to-noise ratio, the effect of noise on the decision between bit "0" and bit "1" is negligible; thus, a low bit-error-rate is achieved. For a digital system, the signal-to-noise ratio is generally required to be greater than 15 dB. The bandwidth of the bandpass filter (or the bandwidth of the equalizer) is $4R_b$. To show the improvement of frequency diversity, the eye-diagram of the combined version of three received signals is given in Figure 3.5.

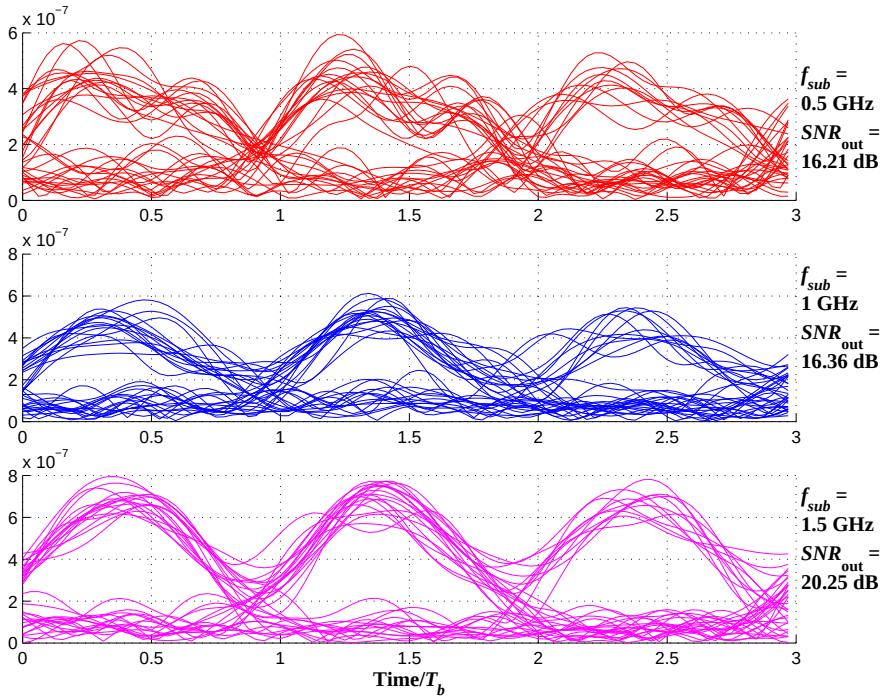

Figure 3.3 Eye-diagrams of received subcarrier signals: without electrical equalization and $BW_{BP} = 4R_b$.

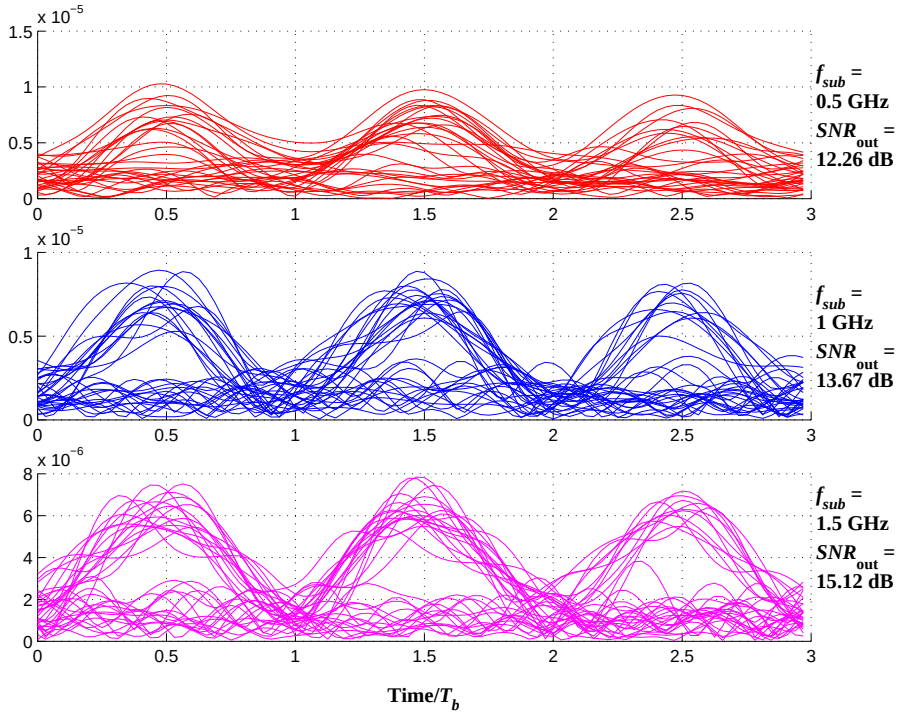

Figure 3.4 Eye-diagrams of received subcarrier signals: with electrical equalization and $BW_{Eq} = 4R_b$.

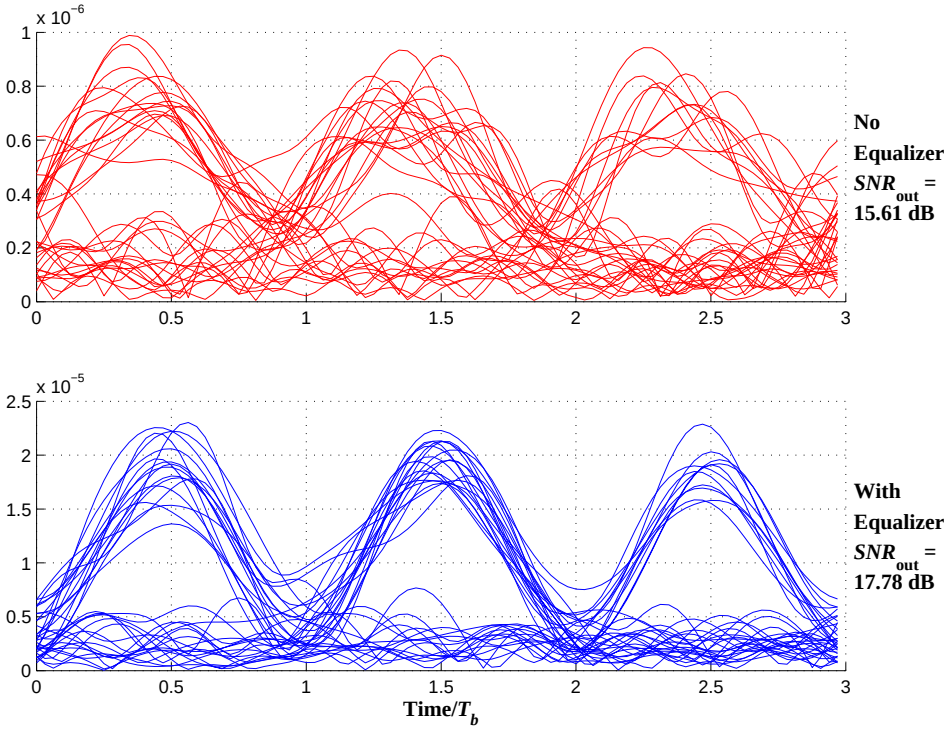

Figure 3.5 Eye-diagrams of the combined signal from three received subcarrier signals: without and with electrical equalization and $BW_{BP} = BW_{Eq} = 4R_b$.

From Figure 3.3 to Figure 3.5, it is seen that the output signal-to-noise ratio (SNR_{out}) depends mainly on the subcarrier frequency (i.e., the frequency response of the multimode fiber at the particular subcarrier) and the type of modification used at the receiver (i.e., without or with electrical equalization, frequency diversity).

Considering the effect of the subcarrier frequency, SNR_{out} at $f_{subcarrier}$ of 1.5 GHz is higher than SNR_{out} at $f_{subcarrier}$ of 0.5 GHz. For example, from Figure 3.3, the values of SNR_{out} at $f_{subcarrier}$ = 0.5, 1.0, and 1.5 GHz are 16.21, 16.36, and 20.25 dB, respectively. This is explained by considering the magnitude response of the multimode fiber; that is, the magnitude response of the multimode fiber in the vicinity of 0.5 GHz has a deep null at 0.52 GHz and this null strongly attenuates the signal power at $f_{subcarrier}$ = 0.5 GHz. On the other hand, the magnitude response of the multimode fiber in vicinity of 1.5 GHz has a good response and there is no deep null in this region. Thus, the output signal at this subcarrier frequency has a good signal strength and hence large SNR_{out}. Note that for the subcarrier signal at $f_{subcarrier}$ = 1.0 GHz even though there is no deep null at the frequency component at 1.0 GHz, the attenuation from the multimode fiber at the component at $f_{subcarrier} \pm R_b$ is larger than the attenuation from multimode fiber at the component at $f_{subcarrier} \pm R_b$ for the subcarrier signal at $f_{subcarrier}$ = 0.5 GHz. Hence, the SNR_{out} of the signal at $f_{subcarrier}$ of 1.0 GHz is slightly larger than the SNR_{out} of the signal at $f_{subcarrier}$ 0.5 GHz.

The main difference between the cases of with and without equalization is the response of the bandpass filter (used in the case of without equalization), which is flat,

and the response of the electrical equalizer, which depends on the frequency response of the multimode fiber at a particular subcarrier frequency. This then results in a difference between the signal-to-noise ratios from these two cases. It is seen from Figure 3.3 and 3.4 that the signal-to-noise ratio ($SNR_{out,Eq}$) from the system with equalization is smaller than the signal-to-noise ration (SNR_{out}) from the system without equalization. Since the gain profile of the electrical equalizer is not totally flat, the thermal noise at the frequency which has a large gain can also be strongly enhanced. This then results in a larger thermal noise power; thus, a small $SNR_{out,Eq}$ compared to SNR_{out}. Hence, from this point, it is seen that using an electrical equalizer does not significantly improve the system performance.

Combining three output signals from different subcarrier frequencies, that is, using frequency diversity, might be a good way to reduce the receiver complexity since with this diversity, the receiver does not need the ability to choose the best signal among different subcarrier signals. For the case of without equalization, from Figures 3.3 and 3.5, it is seen that SNR_{out} from the combined signal (i.e., 15.61 dB) is worse than SNR_{out} from the individual subcarrier frequency (i.e., 16.21, 16.36, and 20.25 dB from f_{sub} = 0.5, 1.0, and 1.5 GHz, respectively). Thus, for the case of without equalization, combining the output signals is not a good approach.

Considering the combined signal for the system with electrical equalization, a better $SNR_{out,Eq}$ (compared to $SNR_{out,Eq}$ from the individual subcarrier frequency) can be achieved. As given in Figure 3.4, $SNR_{out,Eq}$ from $f_{subcarrier}$ of 0.5, 1.0, and 1.5 GHz are 12.26, 13.67, and 15.12 dB, respectively, while $SNR_{out,Eq}$ from the combined version

(from Figure 3.5) of these three signals is 17.78 dB. Comparing the combined signal for the case of without equalization to the combined signal for the case of using equalization, it is seen that SNR_{out} for the case of without equalization is smaller. The reason for this is explained in Appendix A. Note that the effect of the bandwidth of the bandpass filter (or the bandwidth of the electrical equalizer) on the signal-to-noise ratio of the received signal is also presented in Appendix A.

3.3 Signal-to-noise ratio and eye-diagram of the received signals: with limited-gain electrical equalization

From the previous section, it is seen that using electrical equalization with three-subcarrier system is not a good way to improve the signal quality since the signal-to-noise ratio from such a system is small. This is the result of having large gain profile in the response of the electrical equalizer; thus, noise is strongly amplified. To reduce the noise amplification, the peak gain of the electrical equalizer has to be decreased. By doing this, the amplitude of each subcarrier signal is not completely equalized but it is interesting to determine whether the signal-to-noise ratio can be improved by limiting the peak gain of the electrical equalizer.

In this section, the electrical equalizer is modified. As discussed, because of the narrow-band high gain profile of the ideal electrical equalizer, noise is amplified

considerably. To limit this noise amplification, the gain of the electrical equalizer should be limited. The illustration of the magnitude response of the ideal and limiter-gain electrical equalizers is shown in Figure 3.6.

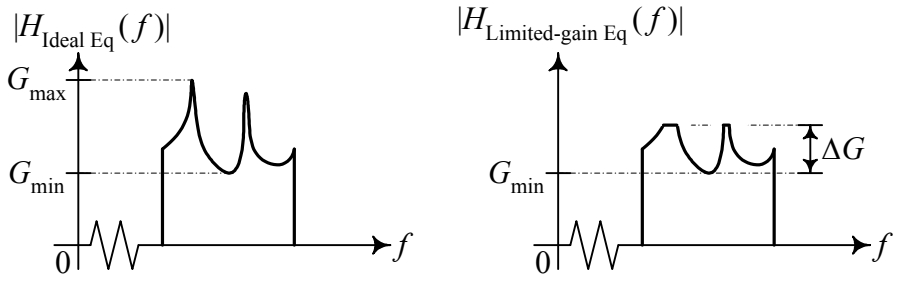

Figure 3.6 Illustration of the magnitude response of the ideal and limited-gain equalizers

From the sketch, it is seen that for the ideal equalizer, there are two peaks. These two peaks have large gain compared to the minimum gain of the ideal equalizer. Noise can be enhanced significantly if it is passed through these regions. Thus, to limit the amount of the noise amplification, the gain from these two peaks should be reduced. The maximum difference between the minimum and maximum gains is needed and is abbreviated by ΔG. Applying ΔG to the ideal equalizer, the limited-gain equalizer is achieved and is also shown in Figure 3.6. Note that the phase responses of these two equalizers are the same. Using this limited-gain equalizer with the received signal, the eye diagrams and output *SNR*s are shown in Figure 3.7 and 3.8.

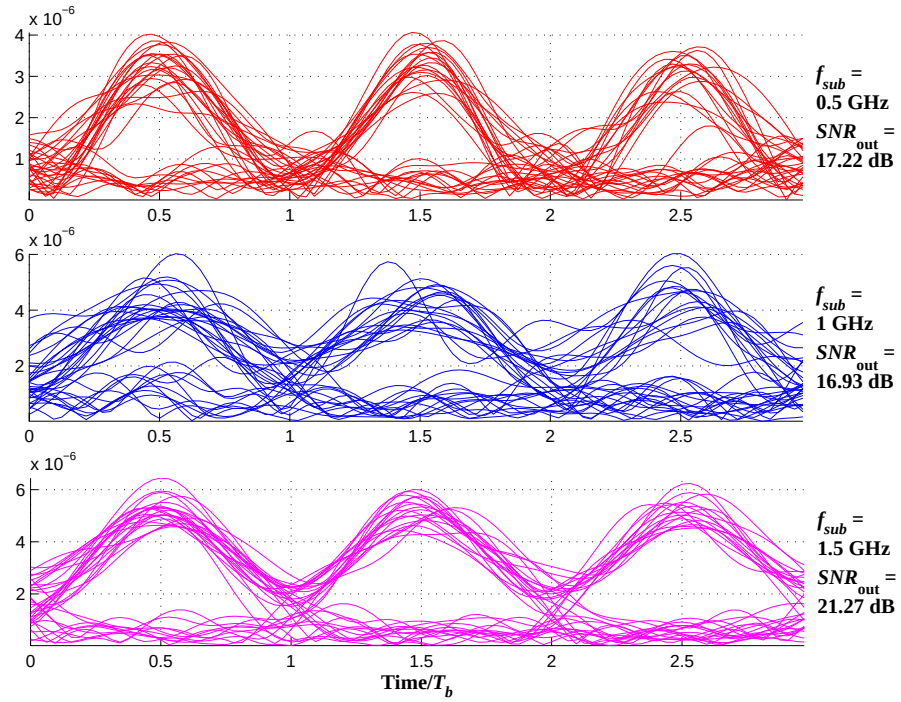

Figure 3.7 Eye-diagrams of received subcarrier signals: with limited-gain electrical equalization ($\Delta G = 0$ dB) and $BW_{Eq} = 4R_b$.

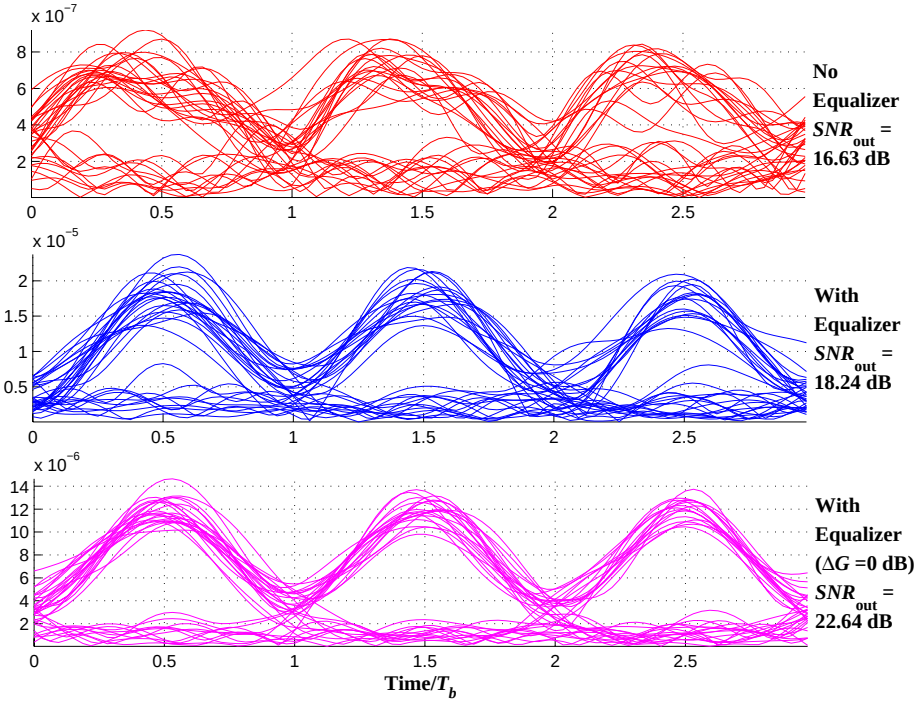

Figure 3.8 Eye-diagrams of combined signal from three received subcarrier signals: for different cases, $BW_{BP} = BW_{Eq} = 4R_b$.

Eye diagrams of the received signal with BW_{Eq} of $4R_b$ are shown in Figure 3.7. The bandwidth of $4R_b$ is used since, as indicated in Appendix A, it results in less signal distortion, although the signal-to-noise ratio from this large bandwidth is less than that for smaller bandwidth. ΔG for the limited-gain equalizer used in Figure 3.7 and 3.8 is 0 dB; that is, the gain profile of the limited-gain equalizer is flat, only phase equalization is performed. Considering the eye diagrams of individual subcarrier signals between the limited-gain equalization in Figure 3.7 and ideal equalization in Figure 3.4, it is seen that the eye opening of the limited-gain equalized signal is larger than the eye opening of the ideal equalized signal. Also, the output *SNR* from the limited-gain equalized signal is larger than the output *SNR* of the ideal equalized signal. This is the result of the gain limiting in the limited-gain equalizer.

Combining the received signals, the eye diagrams of different cases are shown in Figure 3.8. It is seen that the maximum eye opening and output *SNR* between three combined signals are from the case of using limited-gain equalizer. This can be explained as follows.

The reason of getting larger output *SNR* from the case of using ideal equalization compared to the case of without equalization was discussed in the previous section. Here, the reason of getting better output *SNR* from the case of using limited-gain equalization compared to the case of using ideal equalization will be discussed. Since there is a limitation on the gain profile of the limited-gain equalizer, noise from the case of using

limited-gain equalizer is then smaller than noise from the case of using ideal equalizer. However, the phase response of the limited-gain equalizer is the same as the phase response of the ideal gain equalizer. It means that the phases of the received subcarrier signals for the case of using limited-gain equalizer are almost the same. Thus, combining these signals will give an increase in signal power by approximately 9 dB, which is the same as the increase achieved from the case of using the ideal equalizer. The total noise power is just the linear summation of noises from different equalized signals. It is seen that the increase of the output *SNR* of the combined signal for the case of using limited-gain equalization is the same as that for the case of using ideal equalization. However, since the output *SNR* from individual limited-gain equalized signal is better than the output *SNR* from individual equalized signal, the output *SNR* of the combined signal from the case of using limited-gain equalizer is then larger than that from the case of using ideal equalizer as seen from Figure 3.8.

From this section, it is seen that limiting the maximum gain of the equalizer will improve the output *SNR* of individual subcarrier signal since thermal noise is not strongly amplified. Moreover, it is shown from Appendix B that the best output *SNR* is achieved from using phase equalization (ΔG = 0 dB). Combining the equalized signals can increase the output *SNR*. The achieved output *SNR* depends on many factors; that is, the magnitude response of the multimode fiber at particular subcarrier frequency, the bandwidth of the equalizer, the maximum difference between the minimum and maximum gains (ΔG), and the type of the signal (individual or combined).

3.4 Comparisons of Signal-to-noise ratio and eye-diagram from different cases

The simulation results of sending a signal using three subcarriers on multimode fiber have been presented. It has been seen that the quality of received subcarrier signal depends on many factors; the frequency response of the multimode fiber at a particular subcarrier channel, the bandwidth of the bandpass filter (or the bandwidth of the electrical equalizer), and type of equalization used in the system.

If the subcarrier is located at or near a deep null of the magnitude response of the multimode fiber, the received signal from that subcarrier will be significantly attenuated. Hence, the signal-to-noise ratio of the received signal will be very low. The bandwidth of the bandpass filter (or the bandwidth of the electrical equalizer) is also another factor determining the quality of the received signal. If this bandwidth is too small, the high frequency components of the signal are rejected and not included in the received signal. This then results in degradation on the shape and power of the received signal. However, with large bandwidth, more noise is included in the signal; thus, a lower signal-to-noise ratio is achieved.

Adding ideal electrical equalization to the receiver helps improve the shape of the received signal as seen from Figure 3.3 and 3.4. However, since it is not just the signal that passes through the ideal electrical equalizer, noise also passes through this component; the gain profile (which is not flat) of the equalizer can intensify the noise power significantly. This leads to strong noise at the output of the equalizer; thus, low

signal-to-noise ratio. If the maximum gain of the equalizer is limited, the noise intensification can be reduced. It is shown that using limited-gain electrical equalizer can increase the signal-to-noise ratio of the received signal, and the best result is obtained by using a phase equalizer.

Applying frequency diversity to the system by combining all three received signals might be a good way to reduce the system complexity at the receiver since there is no need to have a circuit to choose the best received signal. It is shown that for the case of combined signals without equalization the signal-to-noise ratio is actually lower than that of the individual received signals. On the other hand, the quality of the combined signal for the case with electrical equalization (both ideal and limited-gain equalization) is improved; especially, for the case with limited-gain equalization, the signal-to-noise ratio of the combined signal is at least 2 dB higher than the highest signal-to-noise ratio among the three received signals (see Appendix B).

3.5 Conclusions

It is shown that transmitting a signal using high frequency region of multimode fiber is possible. The quality of the received signal depends mainly on the magnitude response of the multimode fiber at the particular subcarrier channel. Using just ideal electrical equalization does not improve anything. It, moreover, can degrade the received signal by enhancing the noise power; thus, lowering the signal-to-noise ratio. On the other hand,

using a phase equalizer can improve the received signal quality since it does not increase the noise power. And, the received signal can be further improved if all received signals are combined.

The problem of using equalization is that the system needs to know the properties of all subcarrier channels in advance so that the frequency response of the equalizer can be constructed. These properties may need to be updated frequently if the properties of these subcarrier channels are time-varying. And, if, for higher bit rate transmission, the number of transmitted signals increases, the number of equalizers has to be increased; thus, more system complexity is added. Also, it is shown that the signal-to-noise ratio of the received signal from the system with phase equalization is not much different from the signal-to-noise ratio from the received signal from the system without equalization. Although combining the received signals with phase equalization will help improve the signal quality it is not bandwidth-efficient and cost-efficient since three bandpass regions and three subcarrier systems are used for transmitting just one signal. Therefore, adding electrical equalization to the receiving end is not a suitable choice for improving the signal transmission using the bandpass region of multimode fiber.

Chapter 4

Spread Spectrum with Multimode Fiber System

4.1 Introduction

Adding electrical equalization to the receiving end of bandpass transmission on a multimode fiber does not improve the received signal quality, as shown in Chapter 3. The signal-to-noise ratio of the received signal is degraded since the noise is significantly amplified by the equalizer. However, it was shown that combining all phase-equalized signals can improve the quality of the received signal. This means that to transmit a narrowband signal, frequency diversity and phase equalization are needed. Using equalization with a multimode fiber system may not be practical since if the channels are time-varying, the equalizers may need to be updated frequently to correctly equalize the received signals. This then adds more complexity to the system. However, it might be possible to improve performance by spreading the spectrum of the signal over a bandwidth larger than the correlation bandwidth of the channel thereby obtaining the effect of frequency diversity. Even if there is a frequency component located at a null, the degradation from such null to the overall received signal should be small.

In this chapter, we consider the case where the spectrum of the transmitted signal is spread out. This spread spectrum signal modulates a subcarrier and is then sent through the multimode fiber. The eye-diagram and signal-to-noise ratio of the received signal are determined and compared to the case of not using spread spectrum. The simulation of the probability density function and cumulative distribution of the signal-to-noise ratio of the received signal from the system without and with spread spectrum are presented.

4.2 Signal-to-noise ratio and eye-diagram

The block diagram of a transmission system using spread spectrum with a subcarrier signal is shown Figure 4.1. The spectrum of the input signal is spread by using the direct sequence (DS) technique. The input signal is multiplied by a code sequence, $c(t)$. The code sequence, $c(t)$, is generated by using pseudo-noise sequence generation. The code generator contains an N-stage shift register and mod-2 addition. The code length depends on the number (N) of stages in the shift register; that is, code length = $2^N - 1$. The pulse width (T_c) of the code sequence is much smaller than the bit period (T_b) of the input signal and the ratio between the bit period of the input signal and the pulse width of the code sequence equals the code length (or $2^N - 1$). Thus, multiplying the input signal with this code sequence, the bandwidth of the spread spectrum signal is equal to $(2^N - 1) \times R_b$. Detailed information about spread spectrum systems can be found in [37 – 39].

After multiplying the input signal with the code sequence, the center of the spread spectrum signal is shifted to a high frequency; that is, to the subcarrier frequency ($f_{subcarrier}$). This subcarrier spread spectrum signal is converted to an optical format by the

laser, and is transmitted through the bandpass region of the multimode fiber system. At the receiver, the received optical signal is detected and converted back to an electrical signal. Thermal noise is added to the signal at this point. The assumption for thermal noise is the same as used in Chapter 2. The signal is passed through a bandpass filter to filter out both the DC and high frequency components. The center frequency of this bandpass spread spectrum signal is shifted to zero frequency by multiplying with the subcarrier frequency. After that, the spread spectrum signal is decoded by multiplying with $c(t)$ and passed through a lowpass filter to filter out the unwanted high frequency components, thereby recovering the received baseband signal.

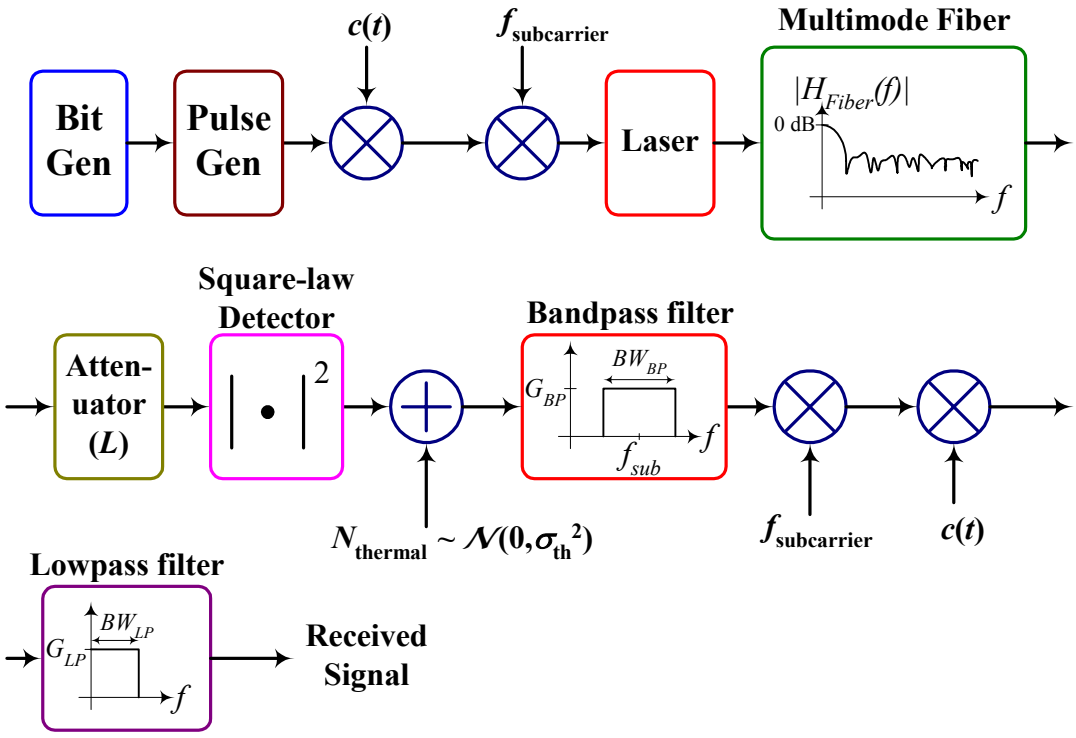

Figure 4.1 Diagram of the transmission system using subcarrier frequency and direct sequence spread spectrum within the passband region of the multimode fiber.

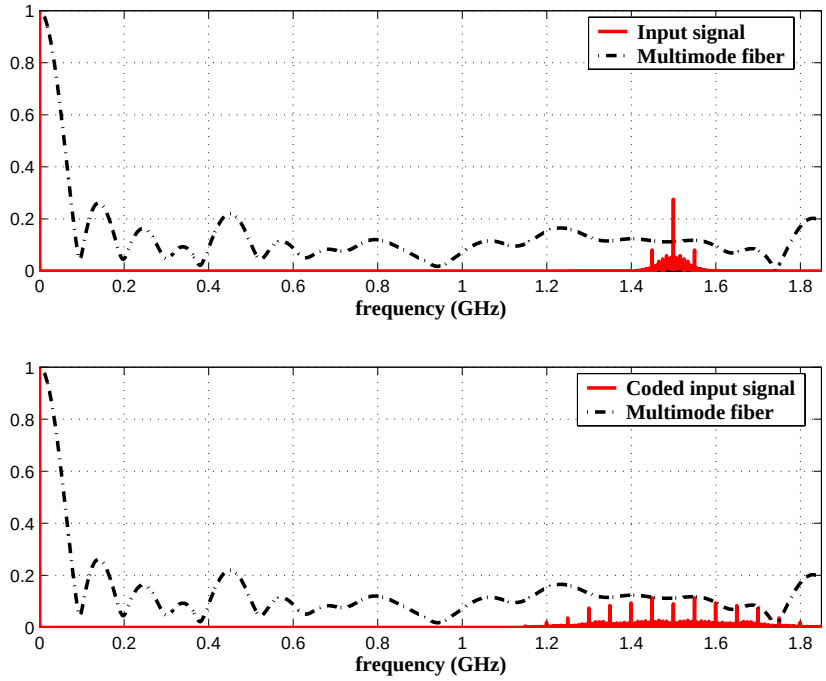

Figure 4.2 Magnitude responses of the multimode fiber, the input signal, and the input spread spectrum (code length = 7) signal: First simulation.

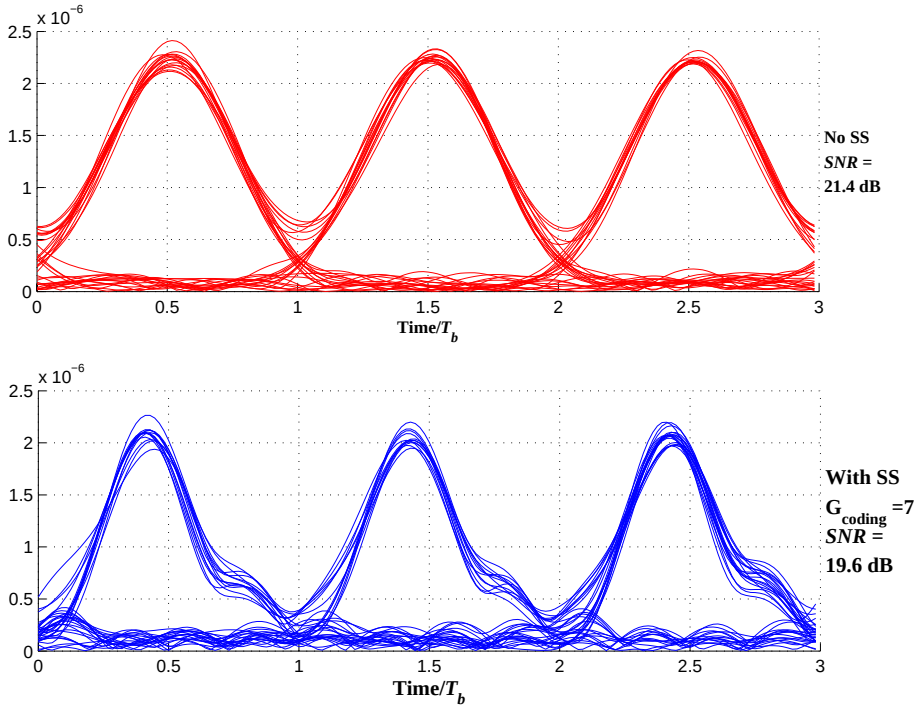

Figure 4.3 Eye-diagrams of the received signal in the first simulation: without and with spread spectrum (code length = 7).

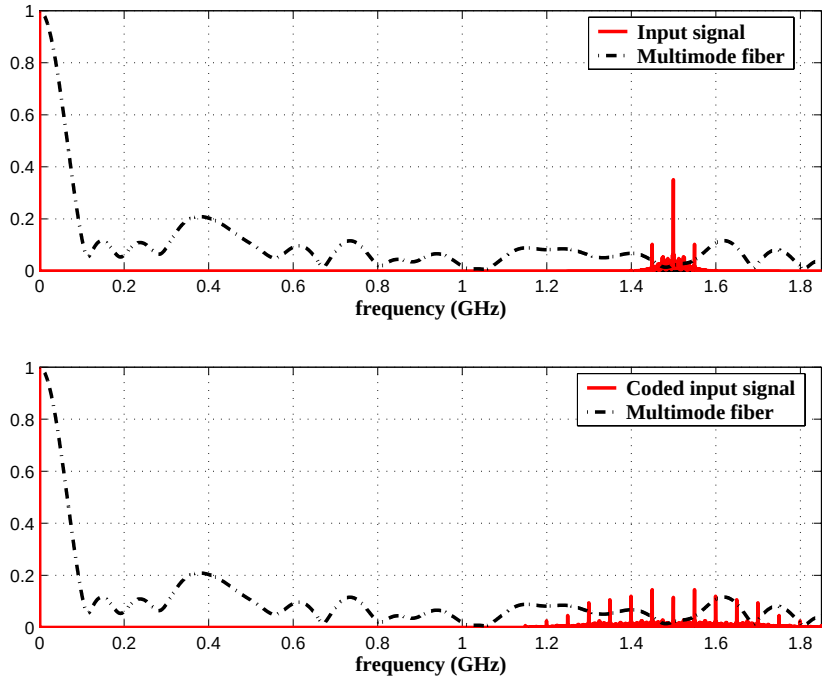

Figure 4.4 Magnitude responses of the multimode fiber, the input signal, and the input spread spectrum (code length = 7) signal: Second simulation.

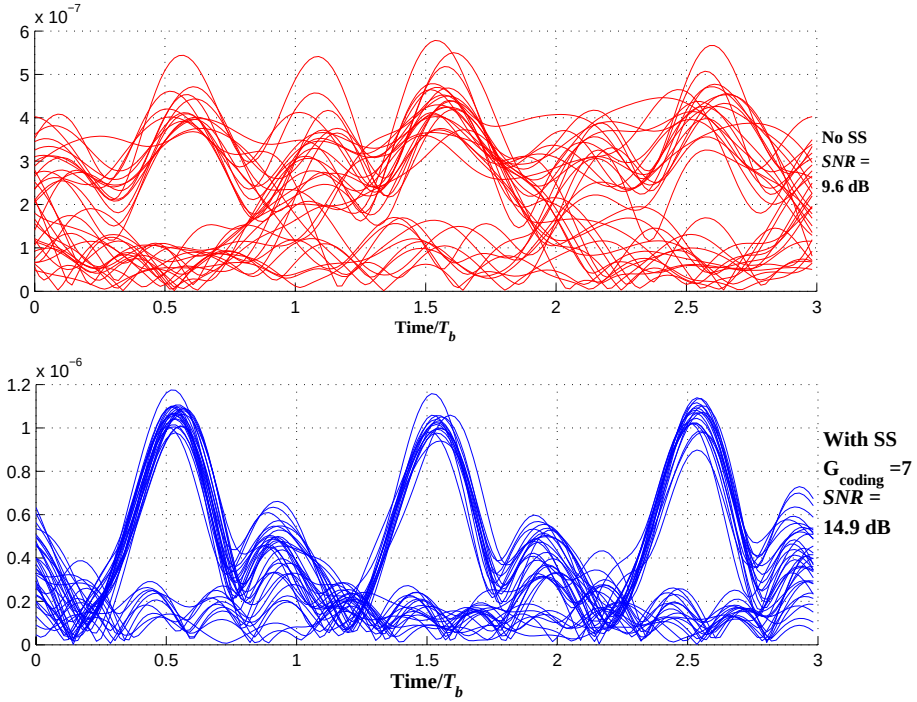

Figure 4.5 Eye-diagrams of the received signal in the second simulation: without and with spread spectrum (code length = 7).

Using the diagram shown in Figure 4.1, the simulation is done for two trials (i.e., two sets of multimode fiber) with the code length of 7. This code length is from a code generator containing 3 shift-registers. With an input bit rate (R_b) of 50 Mbps, the total bandwidth of the spread spectrum signal equals $7\times2\times R_b$ = 700 MHz. The total delay spread from different guided modes in the multimode fiber considered here is 10 ns; hence, the correlation bandwidth of the fiber is approximately 100 MHz. It is seen that the total bandwidth of the spread spectrum signal is 7 times larger than this correlation bandwidth. Other important parameters used in the simulation are given as follows: $BW_{BP} = 4R_b$, $BW_{LP} = 2R_b$, f_{sub} = 1.5 GHz. The magnitude response of the multimode fiber, the input signal, and the spread-spectrum signal are presented in Figures 4.2 and 4.4. Also, the eye-diagram of the received signal and the achieved signal-to-noise ratio are shown in Figures 4.3 and 4.5.

From Figure 4.2 to 4.5, it is seen that the performance of the received signal depends mainly on the magnitude response of the multimode fiber and the type of the signal (with or without spread spectrum). That is, if the subcarrier signal is located at the middle of the passband region, the achieved *SNR* will be large (as seen from the first simulation). However, if the subcarrier signal is at the null region of the response of the multimode fiber (not at the middle of the passband), the achieved *SNR* then becomes small (as seen from the second simulation). In the first simulation, the output *SNR* in the case of spread spectrum ($SNR_{\text{out,ss}}$) is slightly smaller than the corresponding quantity in the absence of spread spectrum (SNR_{out}) since the high frequency signal of the spread spectrum signal is attenuated by the multimode fiber response (~ 1.7 GHz). However, from the second

simulation, it is seen that SNR_{out} is smaller than $SNR_{out,ss}$ since the magnitude response of multimode fiber at the frequency of 1.5 GHz is very poor. Spreading the spectrum of the input signal can lessen the effect of the poor response at the frequency of 1.5 GHz. Comparing the two simulations, it is seen that as the magnitude response of the multimode fiber varies, the variation of achieved *SNR* for the case of using spread spectrum with the transmit signal is smaller than the variation of the *SNR* for the case of not using spread spectrum; that is, $\Delta SNR_{out,ss} = 4.7$ dB < 11.8 dB $= \Delta SNR_{out}$.

Considering the eye diagram from the first simulation in Figure 4.3, it is seen that the shape of the eye diagram for the case of not using spread spectrum is better than that when spread spectrum is used. This may be explained as follows. For the case when spread spectrum is used, the amplitude of the high frequency component (greater than R_b) of the received signal may be large (depending on the magnitude response of the fiber). And, if the bandwidth of the lowpass filter covers this high frequency range, the received signal amplitude spectrum is distorted which results in a distortion of the pulse shape. In this simulation the bandwidth of the lowpass filter equals $2R_b$. If the bandwidth of the lowpass filter is decreased to $1.5R_b$, the shape of the achieved eye diagram should be improved since the frequency component at $2R_b$, which can be large, is not included. For the second simulation in Figure 4.5, the same explanation can be used. However, since the magnitude response of the multimode fiber in this simulation is very poor in the vicinity of the frequency of 1.5 GHz, the eye-diagram of the received signal from the system without spread spectrum is degraded significantly as seen from the figure.

4.3 Probability density function of signal-to-noise ratio

The previous simulations suggest that the variation of *SNR* from the system with spread spectrum is smaller than the variation of *SNR* from the system without spread spectrum. However, this conjecture is only from two simulations. More simulations are required to understand this variation.

In this section, the probability density function of the received *SNR* is studied using computer simulation. Two types of systems are studied; that is, without and with spread spectrum. The received *SNR* of each system is collected. There are 300 simulations for each system. The histograms of the received *SNR* from both systems are shown. The average *SNR*, the standard deviation, and the difference between maximum and minimum *SNR* are determined. There are two cases for the system using spread spectrum; that is, with code lengths of 7 and 15. The bandwidths of the spread spectrum signal from these two cases are equal to $7BW_{corr}$ and $15BW_{corr}$, where BW_{corr} is the correlation bandwidth of multimode fiber at high frequencies. Other parameters used in Figure 3.2 to Figure 3.5 are also used in this section.

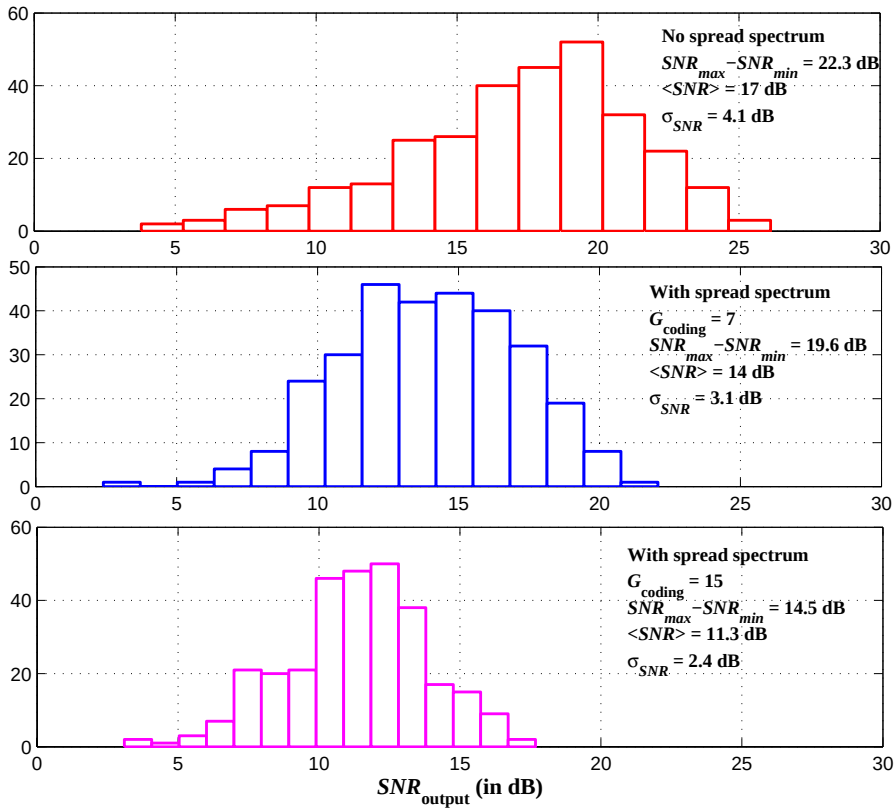

Figure 4.6 Histogram of the signal-to-noise ratio from 300 simulations: without and with spread spectrum (code length of 7 and 15).

In Figure 4.6, the histograms of the received *SNR*s from the case of not using spread spectrum and from the case of using spread spectrum with code length of 7 and 15 are shown. Considering these histograms, it is seen that the shapes of the histograms are similar to a Gaussian shape, especially for the cases using spread spectrum. The shape of the histogram of the system without spread spectrum is asymmetric with a long tail at low *SNR*. Considering the data given in these plots, it is seen that the difference between the maximum and the minimum *SNR*s for the case of using spread spectrum (i.e., 19.6 dB and 14.5 dB for the code length of 7 and 15, respectively) is smaller than that from the case of not using spread spectrum (i.e., 22.3 dB). The standard deviations of the case with spread spectrum with code length of 7 and 15 are 3.1 dB and 2.4 dB, respectively. These

standard deviations are smaller than the standard deviation of the case without spread spectrum, which is 4.1 dB. It is seen that the achieved *SNR* from the system with spread spectrum has a smaller variation. The reason for getting smaller variation of *SNR* from the system with spread spectrum may be explained as follows. Multiplying the transmitted signal with a pseudo-random sequence with a pulse width much smaller than the bit period, the spectrum of the transmitted signal is spread out and covers more passband regions of the multimode fiber. It has been shown that for this high frequency range, the average of the magnitude response of the multimode fiber depends mainly on the number of guided modes. However, if a narrowband signal is sent through this passband region, there is no guarantee that it will always be located at the middle of the passband region; thus, large variance of the achieved *SNR* results. To lower the risk of putting the signal spectrum at any possible null of the fiber magnitude response, the signal spectrum should be large enough to cover many passband regions. Although more nulls are included, on the average, there is less variation of the magnitude response, and consequently less variation of the achieved *SNR*. However, it is seen that the average *SNR* from the case with spread spectrum is smaller than the average *SNR* from the case without spread spectrum; for example, $<SNR_{avg,SS,CL=7}>$ = 14 dB < 17 dB = $<SNR_{avg,No\ SS}>$. This can be explained by considering the receiving end of the system. It is seen that at the receiver, the received optical signal is converted to an electrical signal by a square-law detector, as seen in Figure 4.1. The phase information of the received optical signal is not included in the electrical signal. Hence, when this spread spectrum electrical signal is decoded by multiplying with the code sequence, $c(t)$; the spectra of this signal from different frequencies are combined. However, since the phase information of the received

optical signal is not included, there is no guarantee that these spectra are in-phase. That is, combining these spectra does not necessarily increase, but may decrease, the power of the decoded signal. And, when these spectra are combined, the noise components from these spectra are also combined. The output noise power is just the linear sum of the noise powers from different spectra. And, if the number of spectra increases (i.e., the code length increases), the output noise power becomes larger. It is seen that the power of the decoded signal does not increase while the output noise power increases linearly as a function code length; hence, the average *SNR* of the received signal from the spread spectrum system decreases as the code length increases. Consequently, the average *SNR* of the received signal from the system with spread spectrum is smaller than the average *SNR* of the received signal from the system without spread spectrum.

Considering the histograms from the system with spread spectrum with code length of 7 and 15, it is seen that the received *SNR* from the case of code length of 15 is better that the received *SNR* from the case of code length of 7 in terms of the difference between the maximum and the minimum *SNR* and the standard deviation of the received *SNR*. However, there is a disadvantage of using large code length. That is, with the larger code length, the average *SNR* is smaller. Also, with larger code length, the spectrum of the spread spectrum signal is larger; that is, more bandpass bandwidth is needed.

From the histograms shown in Figure 4.6, it is interesting to determine the cumulative distribution of the *SNR* for different cases. Using the cumulative distribution, the probability that the received signal is higher than a particular required *SNR*, can be

determined. The data used in Figure 4.6 is used to generate three plots of the cumulative distribution for the case of without and with spread spectrum (code length of 7 and 15), as presented in Figure 4.7.

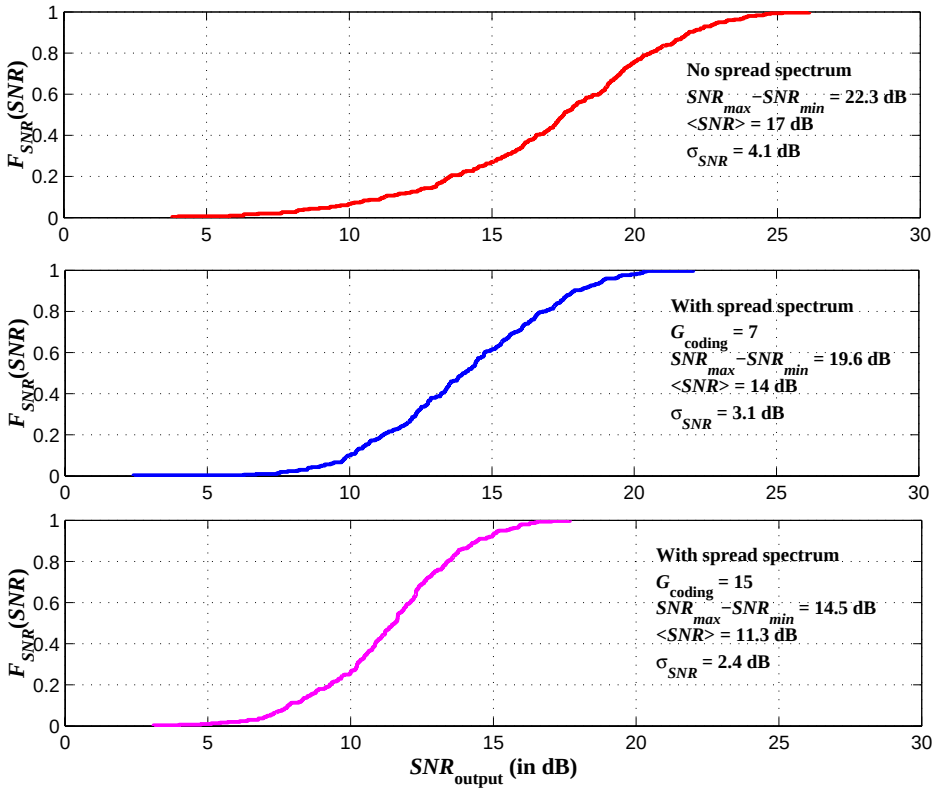

Figure 4.7 Cumulative distribution of signal-to-noise ratio from 300 simulations: without and with spread spectrum (code length of 7 and 15).

From Figure 4.7, it is clearly seen that the cumulative distribution function of the case without spread spectrum is better than that from the case of with spread spectrum. And, the cumulative distribution function from the spread spectrum system with small code length is better that from the spread spectrum system with large code length. For example, if the required *SNR* is 15 dB, it can be approximated from Figure 4.7 that

$$P\{SNR_{\text{No SS}} \leq 15 \text{ dB}\} = 0.25$$

$$P\{SNR_{\text{SS, code length = 7}} \leq 15 \text{ dB}\} = 0.62$$

$$P\{SNR_{\text{SS, code length = 15}} \leq 15 \text{ dB}\} = 0.95.$$

From these probabilities, it is seen that spread spectrum is not a good way to transmit a signal using the bandpass region of multimode fiber since the probability of having the achieved *SNR* less than a required *SNR* from the system with spread spectrum is larger than the probability from the system without spread spectrum. And, this probability increases as the code length increases.

4.4 Conclusions

The signal transmission using spread spectrum with multimode fiber system has been simulated, and the eye-diagrams and the *SNR* from the system without and with spread spectrum have been presented. It is seen that the received signal quality depends mainly on the magnitude response of the multimode fiber. Using direct sequence spread spectrum can improve the quality of the received signal if the subcarrier is located in vicinity of a null, as seen from Figure 4.5. However, if the subcarrier is not located in vicinity of a null, applying spread spectrum technique to the system may degrade the quality of the received signal since the spread spectrum signal will cover a larger bandwidth including more variation in the frequency response. The probability density function and the cumulative distribution of the received *SNR* for the systems without and

with spread spectrum are also determined numerically from 300 simulations. The *SNR* of the spread spectrum system is better than the *SNR* of the system without spread spectrum in terms of the variation in the *SNR* and the difference between the maximum and minimum *SNR*. However, the average *SNR* from the case with spread spectrum is smaller than the average *SNR* from the case without spread spectrum. For the system with spread spectrum, a larger code length system results in a smaller variation of the *SNR* and a smaller difference between the maximum and minimum *SNR*. But, with a large code length, the average *SNR* becomes smaller. This is because the square-law detector does not provide coherent addition of the different frequency components of the signal. Using the plots of cumulative distribution in Figure 4.7, it is clearly seen that spread spectrum is not a good approach to transmit the signal using the bandpass region of multimode fiber since the probability of having the received *SNR* less than a required *SNR* from the system with spread spectrum is much larger than that from the system without spread spectrum. In conclusion, direct sequence spread spectrum is not a good technique to improve the performance of the bandpass transmission on multimode fiber.

Chapter 5

Subcarrier Multiplexing with Multimode Fiber System

5.1 Introduction

The effects of using electrical equalization and spread spectrum with bandpass transmission on multimode fiber have been considered in Chapters 3 and 4, respectively. Adding electrical equalization to the receiving end does not improve the system performance since noise amplification is very strong and it results in a small signal-to-noise ratio (*SNR*). For the spread spectrum system, the variation of the received *SNR* has been shown to be smaller than that for a system without spread spectrum. However, spread spectrum reduces the average received *SNR* and the reduction is larger as the spread factor increases. Therefore, neither electrical equalization at the receiver nor direct sequence spread spectrum improves the performance of bandpass transmission on multimode fiber. Hence, another approach must be considered.

To transmit a high bit rate signal over the high frequency region of multimode fiber, where the magnitude response is relatively flat (as analyzed in Chapter 2), dividing the

high bit rate signal into many low bit rate signals and modulating these low bit rate signals onto different subcarriers might be a good technique. As discussed in Chapter 1, instead of sending a high bit rate signal through one subcarrier, transmitting many low data rate signals through different subcarriers, the wideband frequency-selective channel can be changed into a series of narrowband frequency-nonselective channels. Hence, the amplitude variation of each subcarrier channel is much less than the amplitude variation from one wideband subcarrier channel. This technique is similar to the Orthogonal Frequency Division Multiplexing (OFDM), which is now being widely considered in wireless communications systems in order to overcome the effects of having a wideband frequency-selective channel. However, in OFDM, all subcarriers are stacked tightly because of bandwidth limitations. This is of smaller concern in bandpass transmission on multimode fiber since the bandpass bandwidth of multimode fiber is very large; hence, there is no need to stack all subcarriers tightly as done in OFDM.

In this chapter, consideration is given to the transmission of a high bit rate signal through a multimode fiber system using subcarrier multiplexing (SCM). This high bit rate signal is divided into $N_{carrier}$ small bit rate signals, where $N_{carrier}$ is the number of subcarriers used in the SCM system. The bit-error-rate (*BER*) of the SCM system for different numbers of subcarriers and different sets of multimode fiber is determined, and the effect of the number of subcarriers on the achieved *BER* is discussed.

5.2 Bit-error-rate of the received signal for a 20-subcarrier SCM multimode fiber system

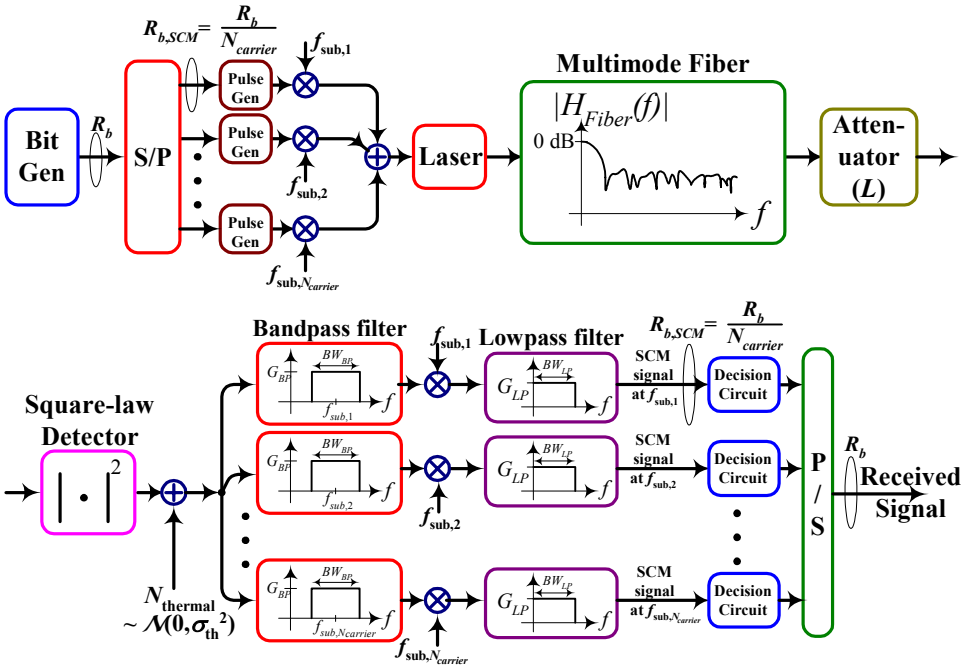

Figure 5.1 Diagram of the multimode fiber transmission using subcarrier multiplexing (SCM).

A block diagram of the system considered is given in Figure 5.1. The input bits from a high bit rate signal are divided into $N_{carrier}$ blocks at the serial-to-parallel block, where $N_{carrier}$ is the number of subcarriers in the system. The total bit rate is R_b and the bit rate of each subcarrier signal is $R_{b,SCM}$ (=$R_b/N_{carrier}$). Each SCM bit stream is passed through a pulse shaping block and then passed through a frequency mixer to modulate the signal with the desired subcarrier frequency. The subcarrier signals are combined and sent to the laser transmitter. The composite signal current, which intensity modulates the laser, is given by [34]

$$I(t) = I_{bias}\left[1 + \sum_{i=1}^{N_{carrier}} m_i \cos(\omega_i t)\right] \tag{5-1}$$

where I_{bias} is the bias current, which must be larger than the threshold current (I_{th}) of the laser in order to operate the laser in the stimulated emission region; m_i is the modulation index corresponding to the i^{th} subcarrier signal and is defined by the ratio of the amplitude of the i^{th} subcarrier signal to the difference between the bias current and the threshold current [1]; that is,

$$m_i = \frac{\Delta I_i}{I_{bias} - I_{th}} \tag{5-2}$$

ω_i is the angular subcarrier frequency corresponding to the i^{th} subcarrier signal

The output optical power of the laser is given by

$$P_{T,Optical}(t) = P_o\left[1 + \sum_{i=1}^{N_{carrier}} m_i \cos(\omega_i t)\right] \tag{5-3}$$

where P_o is the optical output power when there is no signal.

From (5-3), the average and variance of the output optical power are given by

$$\left\langle P_{T,Optical}(t)\right\rangle = P_o \tag{5-4}$$

and,

$$\sigma^2_{Optical} = \frac{P_o^2}{2}\sum_{i=1}^{N_{carrier}} m_i^2 \tag{5-5}$$

If the modulation index of each subcarrier signal is assumed to be the same; that is, $m_i = m$, the variance of the output optical power is then given by

$$\sigma_{Optical}^2 = \frac{P_o^2 m^2 N_{carrier}}{2} \tag{5-6}$$

From (5-4) and (5-6), the total rms modulation index, μ, of the optical signal is defined by

$$\mu = \sqrt{\frac{\sigma_{Optical}^2}{P_o^2}} = m\sqrt{\frac{N_{carrier}}{2}} \tag{5-7}$$

The total rms modulation index is the parameter that determines the nonlinear distortion. If the total rms modulation index is too large, there will be a significant probability that the drive current to the laser will fall below threshold which will result in clipping of the negative peaks of the input SCM signal. This, in turn, will lead to nonlinear distortion. As shown in [34 - 36], if the total rms modulation index is not greater than 0.5 then the carrier to nonlinear distortion ratio is greater than 25 dB which is sufficient for a digital system. Hence, in the simulation, $\mu = 0.5$ is used. A Gaussian pulse shape is used in the simulation with an rms width $T_0 = 0.25T_{b,\mathrm{SCM}}$. The subcarrier signals are combined and sent to the laser transmitter. The optical signal is passed through a multimode fiber and an attenuation block that controls the input optical power ($P_{r,opt}$) to the square-law photodetector having a responsivity of 0.9 mA/mW. Noise is added to the signal at the output of the photodetector, the power (i.e., the variance, σ_{th}^2) of which is proportional to the noise equivalent bandwidth of the receiver. For all simulations in this chapter and following chapters, the noise equivalent bandwidth is 8 GHz and the rms thermal noise current (referred to the output of the photodtector) is 0.8 μA, which is determined from (3-1) in Chapter 3 with C_e = 0.1 pF. It should be noted that the noise equivalent bandwidth is not critical since the receiver noise is limited by the electrical

filtering. The output of the square-law photodetector including noise is divided into $N_{carrier}$ paths. The signal in the i^{th} path is sent to a bandpass filter, whose center frequency is located at the i^{th} subcarrier frequency (where i = 1, 2, …, $N_{carrier}$) to filter out all other subcarrier signals. The filtered subcarrier signal is passed through a frequency mixer and a lowpass filter to demodulate the signal to baseband and to further reject out of band noise. Each subcarrier baseband signal is sent to a decision circuit to recover the output subcarrier bit stream. Then, all subcarrier bit streams are combined to obtain the received serial bit stream.

Simulations are done for 5 different sets of multimode fiber with 100 guided modes, whose magnitude responses are shown in Figure 5.2. The delay spread and average delay are 10 ns and 5 μs, respectively. The transmission bandwidth used in the simulation is from 4.25 GHz to 7.5 GHz.

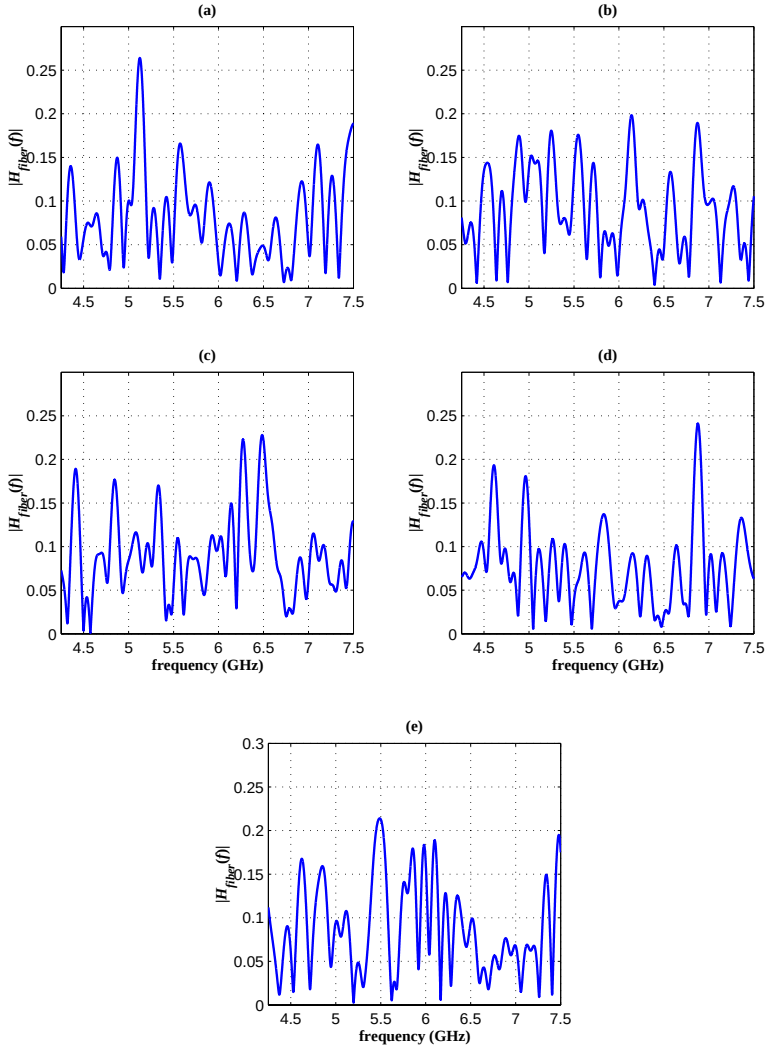

Figure 5.2 Magnitude responses of 5 different sets ((a) to (e)) of frequency responses of multimode fiber; transmission bandwidth (Tx BW) is from 4.25 GHz to 7.5 GHz.

It is seen from Figures 5.2(a) –5.2(e) that the magnitude responses differ dependent on the specific set of delays. In practice the response may indeed change dependent on launch conditions and bending of the fiber. Note that each of the responses shows deep nulls, but it is impractical to predict a priori the frequencies at which these nulls occur. Thus, from a systems standpoint we need either to measure the channel, or use a coding technique that is insensitive to these variations. Note also that these five magnitude

responses are chosen such that poor responses are included. The intent here is to consider "near worst case" conditions. The extent to which this is so will be analyzed in subsequent chapters

-BER calculation

In principle, the *BER* of each subcarrier signal could be determined by Monte Carlo simulation with random noise. However, for very low *BER*, this would take too much time since we have to generate many bits in order to get just one bit error. And, if more *BER* precision is required, only one bit error is not enough. Thus, a semi-analytic approach is adopted where the signal-to-noise ratio and a quantity called the *Q*-parameter are determined by simulation, and then analytic formulas relating the *Q*-parameter to error probability are used. This, in effect, assumes that the noise at the decision circuit is Gaussian distributed, which is a good assumption for the PIN receiver model considered here. The *Q*-parameter is calculated as follows [33].

The *BER* of each subcarrier signal is given by

$$BER_{SCM} = P[1]P[0\,|\,1] + P[0]P[1\,|\,0] \tag{5-8}$$

where $P[1]$ = probability of sending bit 1

$P[0]$ = probability of sending bit 0

$P[0|1]$ = probability of deciding bit 0 when bit 1 is sent

$P[1|0]$ = probability of deciding bit 1 when bit 0 is sent.

Assuming that bit 1 and bit 0 are equally likely to be sent, $P[1] = P[0] = 1/2$ and BER_{SCM} is given by

$$BER_{SCM} = \frac{1}{2}\left[P[0\,|\,1] + P[1\,|\,0]\right] \tag{5-9}$$

$P[0|1]$ and $P[1|0]$ depend on the probability density functions of bit 1 and bit 0 at the input of the decision circuit, respectively. It is assumed that thermal noise is described by Gaussian statistics with zero mean and variance (σ_{th}^2). Therefore, the probability density functions of bit 1 and bit 0 are also described by Gaussian statistics. And, $P[0|1]$ and $P[1|0]$ are given by

$$P[0\,|\,1] = \int_{-\infty}^{I_{threshold}} \frac{1}{\sigma_1\sqrt{2\pi}} e^{\frac{-(I-\mu_1)^2}{2\sigma_1^2}} dI = K\left(\frac{\mu_1 - I_{threshold}}{\sigma_1}\right) \tag{5-10}$$

and

$$P[1\,|\,0] = \int_{I_{threshold}}^{\infty} \frac{1}{\sigma_0\sqrt{2\pi}} e^{\frac{-(I-\mu_0)^2}{2\sigma_0^2}} dI = K\left(\frac{I_{threshold} - \mu_0}{\sigma_0}\right) \tag{5-11}$$

where

$$K(x) = \frac{1}{\sqrt{2\pi}} \int_x^{\infty} e^{-\frac{u^2}{2}} du \tag{5-12}$$

μ_1 = average value for bit 1

μ_0 = average value for bit 0

σ_1 = standard deviation for bit 1

σ_0 = standard deviation for bit 0

$I_{threshold}$ = threshold level for the decision circuit.

From (5-9), (5-10), and (5-11), we get that

$$BER_{SCM} = \frac{1}{2}\left[K\left(\frac{\mu_1 - I_{threshold}}{\sigma_1}\right) + K\left(\frac{I_{threshold} - \mu_0}{\sigma_0}\right)\right] \tag{5-13}$$

From (5-13), BER_{SCM} depends on $I_{threshold}$. The minimum BER_{SCM} is achieved when $I_{threshold}$ is optimized. Choosing $K\left(\frac{\mu_1 - I_{threshold}}{\sigma_1}\right) = K\left(\frac{I_{threshold} - \mu_0}{\sigma_0}\right)$ or $\frac{\mu_1 - I_{threshold}}{\sigma_1} = \frac{I_{threshold} - \mu_0}{\sigma_0}$, BER_{SCM} is approximately minimized and the optimum threshold level is given by

$$I_{threshold} = \frac{\sigma_0 \mu_1 + \sigma_1 \mu_0}{\sigma_0 + \sigma_1} \tag{5-14}$$

and, the minimum BER_{SCM} is given by

$$BER_{SCM} = K\left(\frac{\mu_1 - \mu_0}{\sigma_1 + \sigma_0}\right) = K\left(Q_{SCM}\right) \tag{5-15}$$

where

$$Q_{SCM} = \frac{\mu_1 - \mu_0}{\sigma_1 + \sigma_0} \tag{5-16}$$

From (5-15) and (5-16), it is seen that to evaluate BER_{SCM}, only four parameters (i.e., μ_1, μ_0, σ_1, and σ_0) have to be determined from the simulation. The advantage of using the *Q*-parameter to find *BER* is that the simulation time is considerably decreased.

The average *BER* of the received signal (from all subcarrier signals) is given by

$$BER = \frac{1}{N_{carrier}} \sum_{i=1}^{N_{carrier}} BER_{SCM,i} = \frac{1}{N_{carrier}} \sum_{i=1}^{N_{carrier}} K\left(Q_{SCM,i}\right) \tag{5-17}$$

- BER simulation for 20-subcarrier SCM system

The bit rate (R_b) of the input signal is taken to be 500 Mbps and this signal is divided into 20 subcarrier signals; that is, the bit rate for each subcarrier signal is 25 Mbps. The input optical power to the photodetector is varied from –20 to 0 dBm. The other parameters are the same as discussed in the beginning of this section. The *BER* of the received signal (from all subcarrier signals) for the five sets of $H_{fiber}(f)$ shown in Figure 5.2 is determined by calculating Q-parameter (using (5-8) to (5-10)). The resulting *BER* of the 20-subcarrier SCM system is plotted and shown in Figure 5.3.

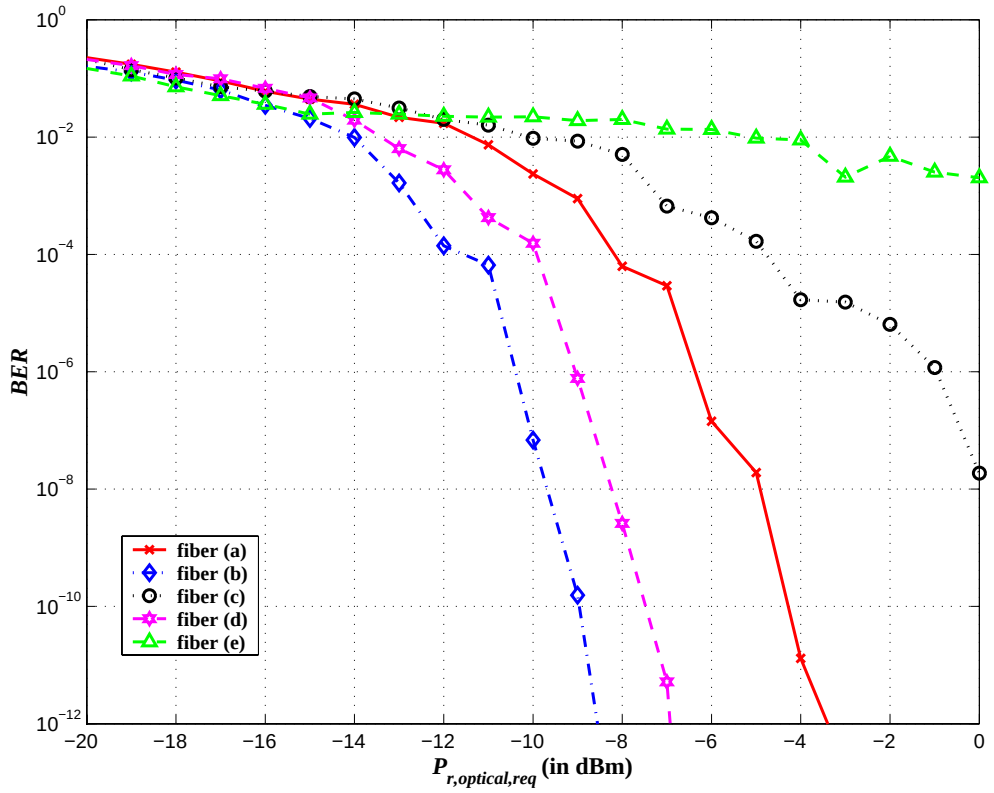

Figure 5.3 Bit-error-rate (*BER*) as a function of input optical power to the photodetector for fives fibers [(a) to (e)] for the number of subcarriers = 20.

From Figure 5.3, it is seen that the *BER*s of the received signal differs considerably from fiber to fiber. The *BER*s from fiber (c) and fiber (e) are very high and seem to have a lower bound to the *BER*. The *BER*s from fiber (a), (b), and (d) are very much better than those from fiber (c) and (e). To explain these results, the magnitude response of the multimode fibers at the frequencies of the 20 subcarriers needs to be considered. As seen from Figures 5.2(a) – 5.2(e), the magnitude responses of the fibers are indeed different. If any subcarriers are located at the nulls of the magnitude response of the fiber, the *BER*s for those subcarriers will be very high, and these high *BER*s will dominate the *BER* for the received signal; thus, high *BER* will result. The subcarrier frequencies (in GHz) in this 20-subcarrier system are given by

$$f_{sub,i} = 4.5 + 0.125 \times (i - 1) \;\; ; \;\; 1 \le i \le 20 \qquad (5\text{-}18)$$

From (5-18), the 20 subcarrier frequencies are at 4.5, 4.625, 4.75, …, 6.875 GHz. Using these 20 subcarrier frequencies with Figure 5.2(a) to 5.2(e), the results in Figure 5.3 can then be explained. For example, considering Figure 5.2(e), there is a deep null where a subcarrier frequency is located; that is, at f_{sub} = 5.625 GHz. The value of the magnitude response at this frequency is approximately 0.005 (or -23 dB below the magnitude response at DC), which is very small. The BER_{SCM} from this subcarrier signal is very high and leads to a high *BER* of the total system. Note that for fiber (a), (b), and (d), the values of the magnitude response of these fibers at the subcarrier frequencies given in (5-18) are all higher than 0.02.

5.3 Effects of the number of subcarriers on bit-error-rate in SCM multimode fiber system

It is shown in the previous section that the achieved *BER* of the SCM multimode fiber system depends on the locations of the subcarrier frequencies relative to the deep nulls of the magnitude response of the multimode fiber. However, the simulation done previously is only for a 20-subcarrier system. It is interesting to study whether the *BER* can be improved if the number of subcarriers is changed. In this section, the simulation similar to the previous simulation is done for 10, 20, 30, 40, and 50 subcarriers for the same five multimode fibers whose magnitude frequency response is shown in Figure 5.2. For all cases, the total bandpass bandwidths in all cases are the same; that is, 3.25 GHz. As the number of subcarriers increases, the bit rate per subcarrier (in Gbps) decreases and is given by

$$R_{b,sub} = \frac{0.5}{N_{carrier}} \tag{5-19}$$

And, the subcarrier frequencies (in GHz) for each case are defined by

$$f_{sub,i} = 4.5 + \frac{2.5}{N_{carrier}} \times (i-1) \;\; ; \;\; 1 \le i \le N_{carrier} \tag{5-20}$$

The simulation results are presented in Figure 5.4. There are five curves in each simulation plot corresponding to the five choices of $N_{carrier}$, and there are five plots (a-e) corresponding to the five fiber frequency responses from Figure 5.2.

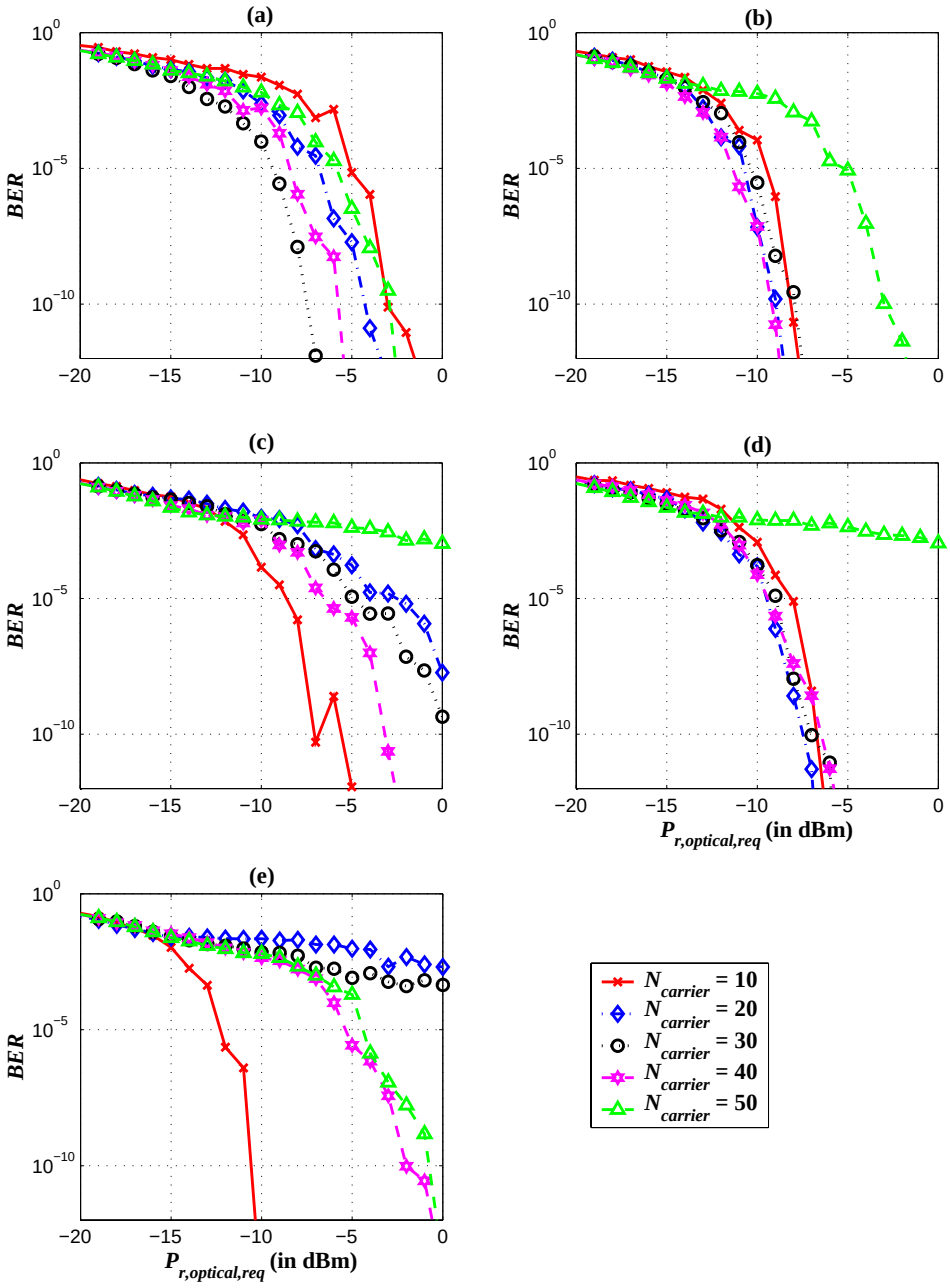

Figure 5.4 Bit-error-rate (*BER*) as a function of input optical power to the photodetector for fiber (a) to (e): for number of subcarriers = 10, 20, 30, 40, and 50.

Considering the *BER* from different sets of $H_{fiber}(f)$, it is seen that a good *BER* is obtained for fibers (a) and (b); and, poor *BER* for fibers (c) and (e). These results are consistent with the location of the nulls of the fiber frequency responses relative to the subcarrier frequencies. Note that there are approximately 10 nulls in each of magnitude responses shown in Figure 5.2, but the locations of these nulls are different.

Considering the number of subcarriers, it is seen from (5-19) that as $N_{carrier}$ is increased, the individual subchannel bandwidths are decreased, which results in less amplitude variation across a subchannel, and hence less intersymbol interference. This is the big advantage of using subcarrier multiplexing with a wideband frequency-selective channel. The *BER* of the system might then be expected to decrease as the number of subcarriers increase. However, this is not totally true since there are other factors affecting the achieved *BER*; that is, the relative locations of the subcarrier and null frequencies. The larger the number of subcarriers, the larger is the possibility that some of subcarriers are located at the nulls. For example, it is seen that from the simulation results in Figure 5.4 $N_{carrier} = 50$ never results in the best performance; indeed, in some simulations, it is the poorest. This is the result of having many subcarriers located at the nulls of the magnitude responses of the multimode fiber. To get small *BER*, the subcarriers should not be located near any nulls of the fiber frequency response. However, owing to changing environmental conditions this response may be time-varying, and it cannot be guaranteed that the same set of subcarriers will be good for sending the SCM signals all the time. Note that the probability of having k subcarriers (from N-subcarrier system) located at the nulls will be analyzed in Chapter 8.

5.4 Conclusions

The bit-error-rate (*BER*) from the transmission system using subcarrier multiplexing (SCM) on multimode fiber has been presented. The *BER* is determined using computer simulation for 5 different sets of multimode fiber. The numbers of subcarriers used in the simulation are 10, 20, 30, 40, and 50. It is shown that to get a good system performance (i.e., low *BER*), the locations of subcarriers used in the system are very important. If there are one or two subcarriers located at the deep nulls of the magnitude response, the *BER* from those subcarrier signals will be very high. And, these high-*BER* subcarrier signals will considerably degrade the total *BER* of the system; that is, a high *BER* results. The effect of the number of subcarriers on the system performance has been shown. It is seen that even though using a large number of subcarriers can reduce the amplitude variation cause by the magnitude response of the multimode fiber since the bit rate per subcarrier signal is small, the *BER* from the system with large number of subcarriers is not better than the *BER* from the system with small number of subcarriers. Furthermore, in some cases (for example, for $N_{carrier}$ = 50 in Figure 5.4(c)), the *BER* from the system with large number of subcarrier is much higher than the *BER* from the system with small number of subcarriers. The reason for this degradation, as noted previously, is the possibility of having some subcarriers located at the deep nulls of the fiber response increases if the number of subcarriers increases. The analysis of this probability will be given in Chapter 8. It is seen that even though the problem of having a wideband frequency-selective channel is overcome by dividing the high bit rate signal into many small bit rate signals and transmitting these signals via different subcarrier frequencies; the system

performance can still be degraded significantly if some subcarriers are at the deep nulls. Therefore, to improve the system performance, some technique is needed to prevent or cancel the effect of having some subcarriers located at deep nulls. In Chapters 6 and 7, two techniques for doing this (that is, training process and diversity coding, respectively) are studied.

Chapter 6

Training Process with Subcarrier Multiplexed Multimode Fiber System

6.1 Introduction

The bit-error-rate (*BER*) of the received signal for the multimode fiber system using subcarrier multiplexing (SCM) has been simulated, analyzed, and discussed in Chapter 5. It was seen that the *BER* of the received signal depends mainly on the locations of the subcarriers used in the system. If there are some subcarriers located at the deep nulls of the magnitude response of the multimode fiber, the *BER* of the received signal is degraded significantly; that is, *BER* is high. The effects of the number of subcarriers have also been studied in Chapter 5. It was seen that using a large number of subcarriers does not always give better system performance. The *BER* of the system with a large number of subcarriers can be higher than the *BER* of the system with a small number of subcarriers. This is explained by considering the likelihood of having subcarriers located at the deep nulls which increases as the number of subcarriers increases. Hence, using a smaller number of subcarriers is suggested. However, as the number of subcarriers is

reduced the achievable bit rate becomes smaller since the the bit rate per subcarrier signal ($R_{b,SCM}$) should not be larger than one-half of the intermodal fiber bandwidth as shown in Chapter 2.

The main problem with subcarrier multiplexing on multimode fiber is the deep nulls in the frequency response of the fiber. To avoid the effect of having subcarriers located at deep nulls, in this chapter, training sequences are used to determine the properties of all subcarrier channels before transmitting the signal. All bad subcarrier channels are dropped; and, only the good subcarriers channels are used in the signal transmission. It is of interest to see how much this technique can improve the system performance relative to that of the previous chapter. In the following sections, the *BER* of the received signal from the subcarrier multiplexed multimode fiber system with training sequence is presented. The effect on the *BER* of the number of channels dropped is studied.

6.2 Bit-error-rate of the received signal with 2 channels dropped

In this section, we consider the use of a training sequence to determine each channel's performance. This information is sent back to the transmitter so that only good channels are used to transmit the data. Again, the same five multimode fibers, the magnitude responses of which are shown in Figure 5.2, are used in the simulation. Only two values (10 and 40) of the number of subcarriers are used in these simulations since these values generally correspond to the best *BER*s in Chapter 5. Furthermore, it is assumed that

($N_{carrier}$ + 2) training sequences are first sent through the system via different subcarriers and the signal-to-noise ratios of these training signals are determined at the receiver. This information is sent back to the transmitter, and the two poorest channels (in terms of *SNR*) are dropped. Note that the effect of the number of channels dropped will be studied in the next section. Then, only $N_{carrier}$ subcarriers are used for signal transmission. The achieved *BER*s from the systems with and without training sequence for $N_{carrier}$ of 10 and 40 are shown in Figure 6.1. Other parameters are the same as used in Chapter 5. Note that, for these 2 systems, the total bit rate is fixed at 500 Mbps. Therefore, the bit rates per subcarrier are 50 and 12.5 Mbps, for the 10-subcarrier and 40-subcarrier systems, respectively.

It is seen from Figure 6.1 that, as expected, the use of training improves performance. For example, from Figure 6.1(a), at *BER* of 10^{-9}, the required input optical power to the photodetector for $N_{carrier}$ of 10 is decreased from -3 to -11 dBm, an 8 dB improvement. Similarly, for $N_{carrier}$ of 40, the required input optical power to the photodetector is decreased from -6 to -8.5 dBm, a 2.5 dB improvement. In general, it is seen that with the use of training sequences the performance of the 10-subcarrier case is better than that of the 40-subcarrier case. This can be explained by considering the number of subcarriers possibly located at the deep nulls from these two subcarrier multiplexing systems and the number of channels dropped out after the training. As discussed in Chapter 5, the number of subcarriers located at the deep nulls for the 40-subcarrier case should be larger than that for the 10-subcarrier case. In this section, for both cases, only the 2 poorest channels are dropped after the training. For the 40-subcarrier case this number of channels dropped

may not be high enough to assure that no subcarriers will be located at the deep nulls. In other words, the number of subcarriers located at the deep nulls from the 40-subcarrier case may be larger than 2. Dropping only the 2 poorest channels still leaves some subcarriers located at deep nulls, and these poor subcarrier channels can degrade the performance of the system. However, as will be shown later in Section 6.3 for the 10-subcarrier case it is highly unlikely that there are more than two subcarriers located at a deep null.

It is seen in this section that the system performance is improved if the training is used. The performance of the 10-subcarrier system is better than the performance of the 40-subcarrier system when 2 channels are dropped. Therefore with use of a training sequence, it is unnecessary to use a large number of subcarriers. That is, for this study, a 10-subcarrier system with training sequence can offer good system performance. However, in this section, only the 2 poorest channels are dropped after the training. It is of interest to determine the system performance when the number of channels dropped is varied. In the following section, the effect of the number of channels dropped on the 10-subcarrier system is studied. The 10-subcarrier system is chosen since from this section the performance of this system is better than the performance of the 40-subcarrier system; thus, there is no need to consider a more complex system when we can get a better performance from a system with less complexity.

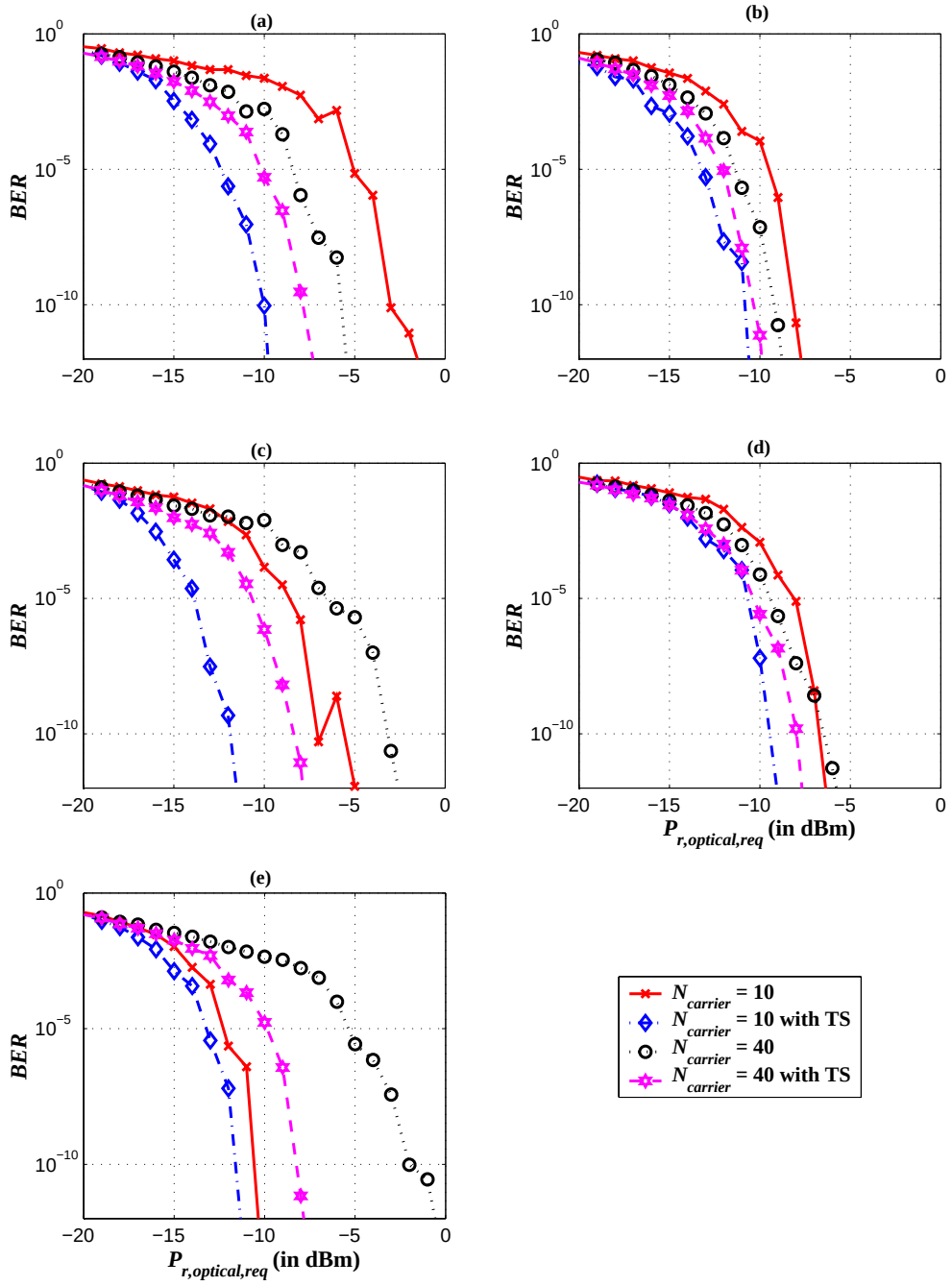

Figure 6.1 Bit-error-rate (*BER*) as a function of input optical power to the photodetector for fiber(a) to fiber(e): without and with training sequence (2 channels dropped), and number of subcarriers = 10 and 40.

6.3 Effects of the number of channels dropped on the achieved bit-error-rate: for 10-subcarrier system

From the results of the previous section it is seen that good system performance is achieved with $N_{carrier}$ = 10 and with two channels dropped (i.e., initially doing measurements on 12 channels.) Now we consider varying the number of channels that are dropped. The frequency gap (Δf_{sub}) between two consecutive subcarrier frequencies is set to be five times the bit rate per subcarrier; that is, 5×50 = 250 MHz. During the training process, (10 + N_{drop}) training sequences are sent through the system via different subcarriers to determine the *SNR* of each channel, and the N_{drop} poorest channels (in terms of *SNR*) are dropped out. In all cases 10 subcarrier frequencies are used for signal transmission. The achieved *BER*s from the systems with N_{drop} = 1, 2, 3 are shown in Figure 6.2. Also, the achieved *BER* of the 10-subcarrier system without training is given as a reference.

As expected, as N_{drop} is increased performance is improved. The difference between the required received optical power ($P_{r,optical,req}$) at *BER* of 10^{-9} from N_{drop} of 1 and 2, and from N_{drop} of 2 and 3 is generally not significant; that is, approximately 1-dB difference in most simulations. This may then suggest that using only 1 channel dropped is sufficient. However, if there is more than 1 subcarrier located at the nulls, the difference between the required received optical power ($P_{r,optical,req}$) at *BER* of 10^{-9} from N_{drop} of 1 and 2 is quite large; approximately 5 dB as seen from the third simulation (Figure 6.2(c)), but the additional improvement in going to N_{drop} of 3 is insignificant; less than 0.5 dB. This then suggests that for the 10-subcarrier SCM multimode fiber system in this study, using training sequence with 2 channels dropped is the most suitable.

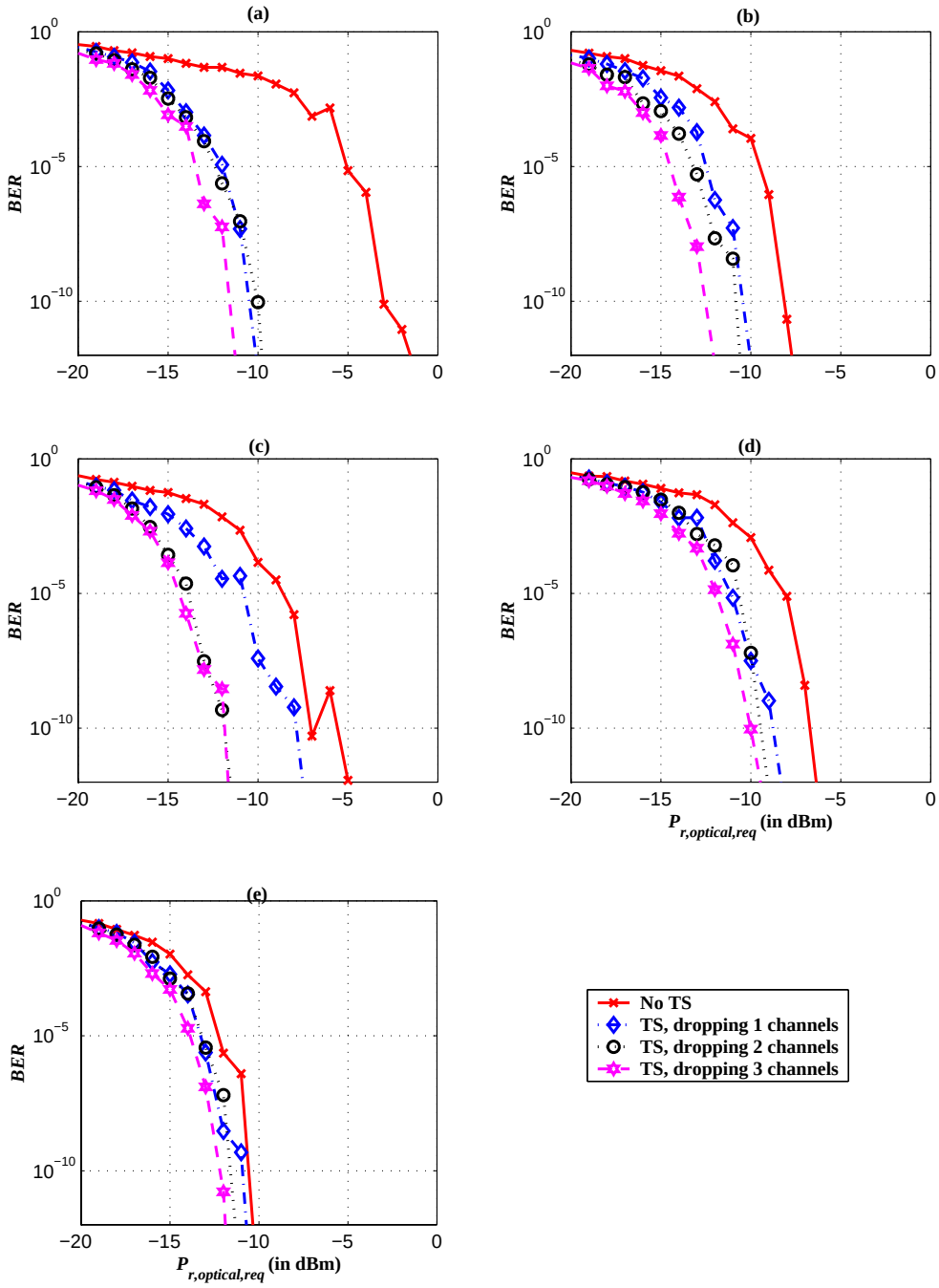

Figure 6.2: Bit-error-rate (*BER*) as a function of input optical power to the photodetector of 10-subcarrier SCM multimode fiber system for 5 different sets of multimode fiber: without and with training sequence (dropping 1, 2, and 3 channels).

6.4 Conclusions

The performance of subcarrier multiplexed multimode fiber system with training process has been presented. The bit-error-rate (*BER*) has been determined for 10-subcarrier and 40-subcarrier systems. It is seen that dropping only the 2 poorest channels after the training can significantly improve the system performance in terms of *BER*, especially for the 10-subcarrier system. And, the performance of the 10-subcarrier system with training (dropping 2 channels) is better than the performance of the 40-subcarrier system with training (dropping 2 channels). Hence, it is concluded that using a small number of subcarriers system is preferred since it requires less system complexity and gives better performance. Note that the number of subcarriers located at deep nulls for different total number of subcarriers will be discussed in Chapter 8. The effect of number of channels dropped after the training is also studied. It is shown that for the 10-subcarrier system, 2 channels dropped after the training is the most suitable. Increasing the number of channels dropped to 3, the additional improvement is insignificant.

Chapter 7

Diversity Coding with Subcarrier Multiplexed Multimode Fiber System

7.1 Introduction

Using training sequences with subcarrier multiplexed multimode fiber system, the effect of having some subcarriers located at the deep nulls of the magnitude response of the fiber is partially canceled since the properties of all subcarrier channels are determined and only good channels are assigned to be the medium for signal transmission.

Although the use of training sequences results in improved performance, it has several disadvantages. The information at the receiver during the training process has to be sent back to the transmitter for deciding which of the channels will be dropped. Also, in the training process, $N_{carrier}+N_{drop}$ subcarriers have to be used. This means that a feedback circuit and extra subcarriers are needed. Also, the transmitter has to have the ability to re-locate the data into the good subcarriers by using the information fed back

from the receiver. There is also the further question of how rapidly the channels will change, and consequently how frequently the training sequences will need to be sent.

To reduce this added complexity, instead of using training sequences, one may turn to channel coding techniques; for example, convolutional codes and block codes [26- 30]. However, if coding is simply applied to each channel individually, the coding gain may be insufficient for those channels located in a deep null of the frequency response. In this chapter, we consider another technique called *diversity coding*, which is normally used in network and data storage applications [31]. In this technique, some additional parity subcarriers are added to the system. If there are any subcarriers located in deep nulls, the data received from these subcarriers (called bad subcarriers) will be disregarded. The data from these bad subcarriers will be recovered by the data received from good subcarriers. This technique is very powerful since it can recover the lost data in bad subcarriers almost instantaneously and there is no need to do the training process before transmission.

In this chapter, the theory of diversity coding is first given [31]. The application of diversity coding to the subcarrier multiplexed multimode fiber system is then studied. Finally, the system performance in terms of bit-error-rate (*BER*) is analyzed and simulated. It is shown that diversity coding results in performance comparable to that achieved with training sequences, with however, considerably less complexity.

7.2 Diversity coding theory [31]

The case in which there are N data channels and M parity channels is considered, and the objective is to be able to recover the data in the presence of the loss of *any* M channels. The input serial bits are divided into N data channels; thus, the data is sent in parallel. In each symbol period (depending on the number of bits per symbol in the diversity coding), the data symbols in all data channels are multiplied by the parity generator matrix (P) to generate the parity symbols, which will be transmitted via parity channels. The parity generator matrix P is given by

$$P = [\beta_{ij}]_{N\times M} = [\alpha^{(i-1)(j-1)}]_{N\times M} = \begin{bmatrix} 1 & 1 & 1 & \cdots & 1 \\ 1 & \alpha & \alpha^2 & \cdots & \alpha^{(M-1)} \\ 1 & \alpha^2 & \alpha^4 & \cdots & \alpha^{2(M-1)} \\ \vdots & \vdots & \vdots & \ddots & \vdots \\ 1 & \alpha^{(N-1)} & \alpha^{2(N-1)} & \cdots & \alpha^{(N-1)(M-1)} \end{bmatrix} \tag{7-1}$$

The parity symbols (c) are given by

$$c = [c_1, c_2, ..., c_M] = [d_1, d_2, ..., d_N]P \tag{7-2}$$

or

$$c_j = \sum_{i=1}^{N} \beta_{ij} d_i \ , \qquad 1 \le j \le M. \tag{7-3}$$

where α is a primitive element in GF(2^m)

c_j is the data symbol in the j^{th} parity channel; $1 \le j \le M$

d_i is the data symbol in the i^{th} data channel; $1 \le i \le N$.

To recover any M failure channels from N+M channels, M parity channels are required. The total number of channels transmitted is N+M channels. The number of bits per data (and/or parity) symbol is given by $m = \log_2 \lceil N+1 \rceil$ for $M \le 3$ (as will be discussed later).

At the receiver, assume that $N_{failure}$ channels from N+M channels are failure channels, where $1 \le N_{failure} \le M$, and assume that n channels out of $N_{failure}$ failure channels are data channels, and $N_{failure}$-n out of $N_{failure}$ failure channels are parity channels. Since there are $N_{failure}$-n parity channels and $N_{failure} \le M$, there are at least n good parity channels. To recover n data failure channels, only n good parity channels are needed. Assume that, $c_{l_1}, c_{l_2}, \ldots, c_{l_n}$ where $1 \le l_1 \le l_2 \le \ldots \le l_n \le M$ are available. The modified parity symbol $\tilde{c}_j$ are generated by

$$\tilde{c}_j = c_{l_j} + \sum_{\substack{i=1 \\ i \neq k_1, k_2, \ldots, k_n}}^{N} \beta_{il_j} d_i \; ; \quad 1 \le j \le n \tag{7-4}$$

Since $[\beta_{ij}]$ or P are known at the transmitter and receiver, $\tilde{c}_j$ can be evaluated. To be able to recover all lost data symbols ($d_{k_1}, d_{k_2}, ..., d_{k_n}$) from $\tilde{c}_1, \tilde{c}_2, ..., \tilde{c}_n$, the parameter β_{il_j} has to be chosen such that the following relationship can be inverted.

$$\tilde{c}_j = \sum_{i=k_1, k_2, \ldots, k_n}^{N} \beta_{il_j} d_i \; , \qquad 1 \le j \le n. \tag{7-5}$$

It follows then that to recover $d_{k_1}, d_{k_2}, ..., d_{k_n}$, the matrix B, which is given by

$$B = \left[\beta_{il_j} \right]_{n \times n} = \begin{bmatrix} \beta_{k_1 l_1} & \beta_{k_1 l_2} & \cdots & \beta_{k_1 l_n} \\ \beta_{k_2 l_1} & \beta_{k_2 l_2} & \cdots & \beta_{k_2 l_n} \\ \vdots & \vdots & \ddots & \vdots \\ \beta_{k_n l_1} & \beta_{k_n l_2} & \cdots & \beta_{k_n l_n} \end{bmatrix}, \tag{7-6}$$

has to have an inverse.

Applying $\beta_{il_j} = \alpha^{(i-1)(l_j-1)}$ to (7-6), we get that

$$B = \begin{bmatrix} \alpha^{(k_1-1)(l_1-1)} & \alpha^{(k_1-1)(l_2-1)} & \cdots & \alpha^{(k_1-1)(l_n-1)} \\ \alpha^{(k_2-1)(l_1-1)} & \alpha^{(k_2-1)(l_2-1)} & \cdots & \alpha^{(k_2-1)(l_n-1)} \\ \vdots & \vdots & \ddots & \vdots \\ \alpha^{(k_n-1)(l_1-1)} & \alpha^{(k_n-1)(l_2-1)} & \cdots & \alpha^{(k_n-1)(l_n-1)} \end{bmatrix} \tag{7-7}$$

Even though α is a primitive element in GF(2^m), it does not follow in general that B is nonsingular and has an inverse. However, it has been shown in [31] that if the field GF(2^m) is chosen to be large enough, this matrix will be nonsingular. For $M \leq 3$, the minimum required m is given by $m = \log_2 \lceil N+1 \rceil$. If m satisfies this requirement, the matrix B will have an inverse, and the failure data symbols $d_{k_1}, d_{k_2}, ..., d_{k_n}$ can be recovered by

$$\left(d_{k_1}, d_{k_2}, ..., d_{k_n}\right) = \left(\tilde{c}_1, \tilde{c}_2, ..., \tilde{c}_n\right) B^{-1} \tag{7-8}$$

7.3 Application of diversity coding to subcarrier multiplexed multimode fiber system

Based on the results from Chapter 6, it is seen that good system performance can be achieved from a 10-subcarrier system using a training sequence with 2 channels dropped. Hence, in this chapter, diversity coding is applied to a 10-subcarrier SCM system with N = 8 and M =2. To recover 2 failure channels, the parameter "m" has to be 4 (i.e., $m = \log_2 \lceil N+1 \rceil$, with N = 8). Thus, GF(2^4) is used in the coding process. A primitive element, α, in GF(2^4) has to be used to construct the parity generator matrix, P.

To find a primitive element in GF(2^4), a 4th-degree primitive polynomial in GF(2) is needed. Using this 4th-degree primitive polynomial to construct a table of cosets, the roots of the 4th-degree primitive polynomial in GF(2^4) can be found. Since the roots of an m^{th}-degree primitive polynomial in GF(q)[x] are primitive elements in GF(q^m), a primitive element in GF(2^4) is also found.

From [32], a 4th-degree primitive polynomial in GF(2) is given by $p(x) = x^4 + x + 1$. Using this polynomial, a table for all possible cosets related to this polynomial is shown below. Note that there are 16 elements in GF(2^4), and 15 of these are non-zero elements.

Table 7.1 All possible cosets related to $p(x) = x^4 + x + 1$

	$0\times p(x)$	$1\times p(x)$	$x\times p(x)$	$(x+1)\times p(x)$	$x^2\times p(x)$	$(x^2+1)\times p(x)$	$(x^2+x)\times p(x)$	…
0	0	x^4+x+1	x^5+x^2+x	$x^5+x^4+x^2+1$	$x^6+x^3+x^2$	$x^6+x^4+x^3+x^2+x+1$	$x^6+x^5+x^3+x$	…
1	1	x^4+x	x^5+x^2+x+1	$x^5+x^4+x^2$	$x^6+x^3+x^2+1$	$x^6+x^4+x^3+x^2+x$	$x^6+x^5+x^3+x+1$	…
S	x	x^4+1	x^5+x^2	$x^5+x^4+x^2+x+1$	$x^6+x^3+x^2+x$	$x^6+x^4+x^3+x^2+1$	$x^6+x^5+x^3$	…
S+1	$x+1$	x^4	x^5+x^2+1	$x^5+x^4+x^2+x$	$x^6+x^3+x^2+x+1$	$x^6+x^4+x^3+x^2$	$x^6+x^5+x^3+1$	…
S^2	x^2	x^4+x^2+x+1	x^5+x	x^5+x^4+1	x^6+x^3	$x^6+x^4+x^3+x+1$	$x^6+x^5+x^3+x^2+x$	…
S^2+1	x^2+1	x^4+x^2+x	x^5+x+1	x^5+x^4	x^6+x^3+1	$x^6+x^4+x^3+x$	$x^6+x^5+x^3+x^2+x+1$	…
S^2+S	x^2+x	x^4+x^2+1	x^5	x^5+x^4+x+1	x^6+x^3+x	$x^6+x^4+x^3+1$	$x^6+x^5+x^3+x^2$	…
S^2+S+1	x^2+x+1	x^4+x^2	x^5+1	x^5+x^4+x	x^6+x^3+x+1	$x^6+x^4+x^3$	$x^6+x^5+x^3+x^2+1$	…
S^3	x^3	x^4+x^3+x+1	$x^5+x^3+x^2+x$	$x^5+x^4+x^3+x^2+1$	x^6+x^2	$x^6+x^4+x^2+x+1$	x^6+x^5+x	…
S^3+1	x^3+1	x^4+x^3+x	$x^5+x^3+x^2+x+1$	$x^5+x^4+x^3+x^2$	x^6+x^2+1	$x^6+x^4+x^2+x$	x^6+x^5+x+1	…
S^3+S	x^3+x	x^4+x^3+1	$x^5+x^3+x^2$	$x^5+x^4+x^3+x^2+x+1$	x^6+x^2+x+1	$x^6+x^4+x^2+1$	x^6+x^5	…
S^3+S+1	x^3+x+1	x^4+x^3	$x^5+x^3+x^2+1$	$x^5+x^4+x^3+x^2+x$	x^6+x^2+x+1	$x^6+x^4+x^2$	x^6+x^5+1	…
S^3+S^2	x^3+x^2	$x^4+x^3+x^2+x+1$	x^5+x^3+x	$x^5+x^4+x^3+1$	x^6	x^6+x^4+x+1	$x^6+x^5+x^2+x$	…

S^3+S^2+1	x^3+x^2+1	$x^4+x^3+x^2+x$	x^5+x^3+x+1	$x^5+x^4+x^3$	x^6+1	x^6+x^4+x	$x^6+x^5+x^2+x+1$	…
S^3+S^2+S	x^3+x^2+x	$x^4+x^3+x^2+1$	x^5+x^3	$x^5+x^4+x^3+x+1$	x^6+x	x^6+x^4+1	$x^6+x^5+x^2$	…
S^3+S^2+S+1	x^3+x^2+x+1	$x^4+x^3+x^2$	x^5+x^3+1	$x^5+x^4+x^3+x$	x^6+x+1	x^6+x^4	$x^6+x^5+x^2+1$	…

Using Table 7.1, the roots of $p(x)$ in GF(2^4) can be found as follows. There should be 4 roots for $p(x)$ since the degree of $p(x)$ is 4. Substituting all non-zero elements of GF(2^4) into $p(x)$, we obtain

For x=1, $p(1) = 1^4 + 1 + 1 = \mathbf{1}$. ($\neq 0$) (7-9)

For x=S, $p(S) = S^4 + S + 1 = (S+1) + S + 1 = \mathbf{0}$. (7-10)

For x=S+1, $p(S+1) = (S+1)^4 + (S+1) + 1$

$= S^4 + 1 + (S+1) + 1$

$= (S+1) + 1 + (S+1) + 1$ {from Table 7.1, $S^4 = S + 1$}

$= \mathbf{0}$. (7-11)

For x=S^2, $p(S^2) = (S^2)^4 + S^2 + 1$

$= (S^4)^2 + S^2 + 1$

$= (S+1)^2 + S^2 + 1$ {from Table 7.1, $S^4 = S + 1$}

$= S^2 + 1 + S^2 + 1 = \mathbf{0}$. (7-12)

For x=S^2+1, $p(S^2+1)= (S^2+1)^4 + (S^2+1) + 1$

$= (S^4+1)^2 + (S^2+1) + 1$

$= ((S+1)+1)^2 + (S^2+1) + 1$ {from Table 7.1, $S^4 = S + 1$}

$= S^2 + (S^2+1) + 1 = \mathbf{0}$. (7-13)

For $x=S^2+S$, $p(S^2+S)= (S^2+S)^4 + (S^2+S) + 1$

$= (S^4+S^2)^2 + (S^2+S) + 1$

$= ((S+1)+ S^2)^2 + (S^2+S) + 1$ {from Table 7.1, $S^4 = S + 1$}

$= (S^4+S^2+1) + (S^2+S) + 1$

$= ((S+1) + S^2+1) + (S^2+S) + 1 = \mathbf{1}. (\neq 0)$ (7-14)

For $x=S^2+S+1$, $p(S^2+S+1)= (S^2+S+1)^4 + (S^2+S+1) + 1$

$= (S^4+S^2+1)^2 + (S^2+S+1) + 1$

$= (S^2+S)^2 + (S^2+S+1) + 1$ {from Table 7.1, $S^4 = S + 1$}

$= (S^4+S^2) + (S^2+S+1) + 1$

$= ((S+1) + S^2) + (S^2+S+1) + 1 = \mathbf{1}. (\neq 0)$ (7-15)

For $x=S^3$, $p(S^3) = (S^3)^4 + S^3 + 1$

$= (S^4)^3 + S^3 + 1$

$= (S+1)^3 + S^3 + 1$ {from Table 7.1, $S^4 = S + 1$}

$= S^3 + S^2 + S + 1 + S^3 + 1 = \mathbf{S^2 + S}. (\neq 0)$ (7-16)

For $x=S^3+1$, $p(S^3+1)= (S^3+1)^4 + (S^3+1) + 1$

$= (S^6+1)^2 + (S^3+1) + 1$

$= ((S^3+S^2)+1)^2 + (S^3+1) + 1$ {from Table 7.1, $S^6 = S^3+ S^2$}

$= (S^6+S^4+1) + (S^3+1) + 1$

$= ((S^3+S^2) + (S+1)+1) + (S^3+1) + 1$

$= \mathbf{S^2 + S}. (\neq 0)$ (7-17)

For $x=S^3+S$, $p(S^3+S)= (S^3+S)^4 + (S^3+S) + 1$

$= (S^6+S^2)^2 + (S^3+S) + 1$

$= ((S^3+S^2)+ S^2)^2 + (S^3+S) + 1$ {from Table 7.1, $S^6 =S^3+ S^2$}

$= S^6 + (S^3+S) + 1$

$= (S^3+S^2)+ (S^3+S) + 1$

$= \mathbf{S^2+S+1}. (\neq 0)$ (7-18)

For $x=S^3+S+1$, $p(S^3+S+1)= (S^3+S+1)^4 + (S^3+S+1) + 1$

$= (S^6+S^2+1)^2 + (S^3+S+1) + 1$

$= ((S^3+S^2) + S^2 + 1)^2 + (S^3+S+1) + 1$

$= (S^3+1)^2 + (S^3+S+1) + 1$

$= (S^6+1) + (S^3+S+1) + 1$

$= ((S^3+S^2) + 1) + (S^3+S+1) + 1$

$= \mathbf{S^2+S+1}. (\neq 0)$ (7-19)

For $x=S^3+S^2$, $p(S^3+S^2)= (S^3+S^2)^4 + (S^3+S^2) + 1$

$= (S^6+S^4)^2 + (S^3+S^2) + 1$

$= ((S^3+S^2) + (S+1))^2 + (S^3+S^2) + 1$

$= (S^6+S^4+S^2+1) + (S^3+S^2) + 1$

$= ((S^3+S^2) + (S+1) +S^2+1) + (S^3+S^2) + 1$

$= \mathbf{S^2+S+1}. (\neq 0)$ (7-20)

For $x=S^3+S^2+1$, $p(S^3+S^2+1) = (S^3+S^2+1)^4 + (S^3+S^2+1) + 1$

$= (S^6+S^4+1)^2 + (S^3+S^2+1) + 1$

$= ((S^3+S^2) + (S+1) + 1)^2 + (S^3+S^2+1) + 1$

$= (S^3+S^2+S)^2 + (S^3+S^2+1) + 1$

$= (S^6+S^4+S^2) + (S^3+S^2+1) + 1$

$= ((S^3+S^2) + (S+1) + S^2) + (S^3+S^2+1) + 1$

$= \mathbf{S^2+S+1}. (\neq 0)$ (7-21)

For $x=S^3+S^2+S$, $p(S^3+S^2+S) = (S^3+S^2+S)^4 + (S^3+S^2+S) + 1$

$= (S^6+S^4+S^2)^2 + (S^3+S^2+S) + 1$

$= ((S^3+S^2) + (S+1) + S^2)^2 + (S^3+S^2+S) + 1$

$= (S^3+S+1)^2 + (S^3+S^2+S) + 1$

$= (S^6+S^2+1) + (S^3+S^2+S) + 1$

$= ((S^3+S^2) + S^2 +1) + (S^3+S^2+S) + 1$

$= \mathbf{S^2+S}. (\neq 0)$ (7-22)

For $x=S^3+S^2+S+1$, $p(S^3+S^2+S+1) = (S^3+S^2+S+1)^4 + (S^3+S^2+S+1) + 1$

$= (S^6+S^4+S^2+1)^2 + (S^3+S^2+S)$

$= ((S^3+S^2) + (S+1) + S^2 +1)^2 + (S^3+S^2+S)$

$= (S^3+S)^2 + (S^3+S^2+S)$

$= (S^6+S^2) + (S^3+S^2+S)$

$= ((S^3+S^2) + S^2) + (S^3+S^2+S)$

$= \mathbf{S^2+S}. (\neq 0)$ (7-23)

From (7-9) to (7-23), it is seen that there are four roots of $p(x)$ in GF(2^4); that is, S, S+1, S^2, and S^2+1. Since the roots of an mth-degree primitive polynomial in GF(q)[x] are primitive elements in GF(q^m), then S, S+1, S^2, and S^2+1 are primitive elements in GF(2^4).

Let S be the chosen primitive element in GF(2^4); thus, α = S and α^0, α^1, α^2, …,α^{14} will generate all non-zero elements in GF(2^4). Using this property with the table of all cosets, the exponential, polynomial, and vector-space representations of GF(2^4) are shown in Table 7.2.

Table 7.2 Exponential, polynomial, and vector-space representations of GF(2^4).

Exponential representation	Polynomial representation	Vector-space representation
0	0	[0 0 0 0]
α^0	1	[1 0 0 0]
α^1	α	[0 1 0 0]
α^2	α^2	[0 0 1 0]
α^3	α^3	[0 0 0 1]
α^4	$1+\alpha$	[1 1 0 0]
α^5	$\alpha+\alpha^2$	[0 1 1 0]
α^6	$\alpha^2+\alpha^3$	[0 0 1 1]
α^7	$1+\alpha+\alpha^3$	[1 1 0 1]
α^8	$1+\alpha^2$	[1 0 1 0]
α^9	$\alpha+\alpha^3$	[0 1 0 1]
α^{10}	$1+\alpha+\alpha^2$	[1 1 1 0]
α^{11}	$\alpha+\alpha^2+\alpha^3$	[0 1 1 1]
α^{12}	$1+\alpha+\alpha^2+\alpha^3$	[1 1 1 1]
α^{13}	$1+\alpha^2+\alpha^3$	[1 0 1 1]
α^{14}	$1+\alpha^3$	[1 0 0 1]

From Table 7.2, it is seen that 4 input data bits in each data line (or subcarrier) can be grouped to form a data symbol, which can be represented by the exponential format of the primitive element α. Also, the parity generator matrix, P, and the parity symbols (i.e., c_1 and c_2) can then be constructed. The parity generator matrix, P, for this case ($M = 2$, $N = 8$) is given by

$$P = \begin{bmatrix} 1 & 1 \\ 1 & \alpha^1 \\ 1 & \alpha^2 \\ \vdots & \vdots \\ 1 & \alpha^7 \end{bmatrix} \tag{7-24}$$

Using the above information, the data symbols from any two failure data channels can be recovered at the receiver. To understand more clearly how the symbols from the failure data channels can be recovered by using diversity coding, two examples are given next. The first example is for the case that there is only one failure data channel and the second example is for the case that there are two failure data channels in the system.

Example 1: one failure data channel.

The input serial bits to the SCM modulator are generated randomly and are given by

$$\begin{aligned} \text{bit\_in} = \quad & [1 \quad 0 \quad 1 \quad 0 \quad 1 \quad 1 \quad 0 \quad 0 \\ & 1 \quad 0 \quad 1 \quad 1 \quad 1 \quad 1 \quad 0 \quad 0 \\ & 1 \quad 1 \quad 0 \quad 1 \quad 0 \quad 0 \quad 1 \quad 0 \\ & 0 \quad 0 \quad 0 \quad 1 \quad 0 \quad 0 \quad 0 \quad 1] \end{aligned} \tag{7-25}$$

There are a total of 32 bits. These input bits are divided into 8 groups; thus, there are 4 bits in each group. The data bits in each group are sent to a particular data channel.

Since there are 4 data bits in each data channel, these 4 bits can be represented by the exponential representation as shown in Table 7.2; that is, we get

For data channel#1, bit_SCM= [1 1 1 0] ➔ $d_1 = \alpha^{10}$

For data channel #2, bit_SCM= [0 0 1 0] ➔ $d_2 = \alpha^{2}$

For data channel #3, bit_SCM= [1 1 0 0] ➔ $d_3 = \alpha^{4}$

For data channel #4, bit_SCM= [0 1 1 1] ➔ $d_4 = \alpha^{11}$

For data channel #5, bit_SCM= [1 1 0 0] ➔ $d_5 = \alpha^{4}$

For data channel #6, bit_SCM= [1 1 0 0] ➔ $d_6 = \alpha^{4}$

For data channel #7, bit_SCM= [0 0 1 0] ➔ $d_7 = \alpha^{2}$

For data channel #8, bit_SCM= [0 0 0 1] ➔ $d_8 = \alpha^{3}$

Thus, $(d_1, d_2, d_3, d_4, d_5, d_6, d_7, d_8) = (\alpha^{10}, \alpha^{2}, \alpha^{4}, \alpha^{11}, \alpha^{4}, \alpha^{4}, \alpha^{2}, \alpha^{3})$ (7-26)

Substituting (7-24) and (7-26) into (7-2), the parity symbols for the two parity channels, channel#9 and channel#10, are given by

$$c = [c_1, c_2] = [d_1, d_2, ..., d_8]P$$

$$= [\alpha^{10}\ \alpha^{2}\ \alpha^{4}\ \alpha^{11}\ \alpha^{4}\ \alpha^{4}\ \alpha^{2}\ \alpha^{3}] \begin{bmatrix} 1 & 1 \\ 1 & \alpha^{1} \\ 1 & \alpha^{2} \\ \vdots & \vdots \\ 1 & \alpha^{7} \end{bmatrix}$$

$$= [\alpha^{1}, \alpha^{10}] \quad (7\text{-}27)$$

Thus, at the transmitter, the channel symbols are

$$\begin{aligned} e &= [e_1, e_2, ..., e_{10}] \\ &= [d_1, d_2, ..., d_8, c_1, c_2] \\ &= [\alpha^{10}\ \alpha^2\ \alpha^4\ \alpha^{11}\ \alpha^4\ \alpha^4\ \alpha^2\ \alpha^3\ \alpha^1\ \alpha^{10}\ ] \end{aligned} \quad (7\text{-}28)$$

Assuming that data channel#2 fails (i.e., $k_1 = 2$), at the receiver, the received symbols from data channel#2 will be ignored. And, since there is one failure channel (i.e., $n = 1$), from (7-6), matrix B and its inverse are easy to find and are given by

$$B = [1] \text{ and } B^{-1} = [1] \quad (7\text{-}29)$$

From (7-4), the parameter $\tilde{c}_j$ will have only one element; that is, $\tilde{c}_1$, which is given by

$$\tilde{c}_1 = c_1 + \sum_{\substack{i=1 \\ i\neq 2}}^{8} \alpha^{(i-1)(1-1)} d_i = c_1 + \sum_{\substack{i=1 \\ i\neq 2}}^{8} d_i$$

$$= \alpha^1 + \alpha^{10} + \alpha^4 + \alpha^{11} + \alpha^4 + \alpha^4 + \alpha^2 + \alpha^3 = \alpha^2 \quad (7\text{-}30)$$

Substituting (7-29) and (7-30) into (7-8), the data symbol from channel#2 is recovered and is given by

$$d_{k_1} = d_2 = \tilde{c}_1 B^{-1} = \alpha^2 \alpha^0 = \alpha^2 \quad (7\text{-}31)$$

Table 7.3 List of symbols at transmitter, receiver, and output of the decoder for example 1: one failure data channel.

	d_1	d_2	d_3	d_4	d_5	d_6	d_7	d_8	c_1	c_2
Transmitted symbols	α^{10}	α^2	α^4	α^{11}	α^4	α^4	α^2	α^3	α^1	α^{10}
Received symbols	α^{10}	NA	α^4	α^{11}	α^4	α^4	α^2	α^3	α^1	α^{10}
Decoded symbols	α^{10}	α^2	α^4	α^{11}	α^4	α^4	α^2	α^3	α^2	α^{10}

where NA = not available since the channel fails.

The data from the second channel, d_2 , is not directly available at the receiver because of the failure of this channel. However, with diversity decoding, this lost d_2 can be recovered and is identical to the transmitted one, as seen from Table 7.3.

Example 2: two failure data channels.

The input serial bits to the SCM modulator are again generated randomly and are now given by

$$\begin{aligned}\text{bit\_in} = \quad & [0 \;\; 1 \;\; 0 \;\; 0 \;\; 1 \;\; 1 \;\; 0 \;\; 1 \\ & 1 \;\; 0 \;\; 1 \;\; 0 \;\; 1 \;\; 1 \;\; 1 \;\; 0 \\ & 0 \;\; 0 \;\; 0 \;\; 1 \;\; 0 \;\; 1 \;\; 0 \;\; 1 \\ & 0 \;\; 1 \;\; 1 \;\; 1 \;\; 0 \;\; 1 \;\; 1 \;\; 1]\end{aligned} \tag{7-32}$$

Similar to the first example, there are a total of 32 bits. As before, these input bits are divided into 8 groups; thus, there are 4 bits in each group. The data bits in each group are sent to a particular data channel. Since there are 4 data bits in each data channel, these 4 bits can be represented by the exponential representation as shown in Table 7.2; that is,

For data channel#1, bit_SCM= [0 1 0 0] ➔ $d_1 = \alpha^1$

For data channel #2, bit_SCM= [1 0 0 1] ➔ $d_2 = \alpha^{14}$

For data channel #3, bit_SCM= [0 1 0 1] ➔ $d_3 = \alpha^9$

For data channel #4, bit_SCM= [0 0 1 1] ➔ $d_4 = \alpha^6$

For data channel #5, bit_SCM= [1 1 0 0] ➔ $d_5 = \alpha^4$

For data channel #6, bit_SCM= [1 1 1 1] ➔ $d_6 = \alpha^{12}$

For data channel #7, bit_SCM= [0 1 0 1] ➔ $d_7 = \alpha^9$

For data channel #8, bit_SCM= [1 0 1 1] ➔ $d_8 = \alpha^{13}$

Thus, $(d_1, d_2, d_3, d_4, d_5, d_6, d_7, d_8) = (\alpha^1, \alpha^{14}, \alpha^9, \alpha^6, \alpha^4, \alpha^{12}, \alpha^9, \alpha^{13})$ (7-33)

Substituting (7-24) and (7-33) into (7-2), the parity symbols for channel#9 and channel#10 are now given by

$$\begin{aligned} c &= [c_1, c_2] = [d_1, d_2, ..., d_8]P \\ &= [\alpha^1 \ \alpha^{14} \ \alpha^9 \ \alpha^6 \ \alpha^4 \ \alpha^{12} \ \alpha^9 \ \alpha^{13}] \begin{bmatrix} 1 & 1 \\ 1 & \alpha^1 \\ 1 & \alpha^2 \\ \vdots & \vdots \\ 1 & \alpha^7 \end{bmatrix} \\ &= [\alpha^5, \alpha^0] \end{aligned} \tag{7-34}$$

Thus, at the transmitter, the channel symbols are

$$\begin{aligned} e &= [e_1, e_2, ..., e_{10}] \\ &= [d_1, d_2, ..., d_8, c_1, c_2] \\ &= [\alpha^1 \ \alpha^{14} \ \alpha^9 \ \alpha^6 \ \alpha^4 \ \alpha^{12} \ \alpha^9 \ \alpha^{13} \ \alpha^5 \ \alpha^0] \end{aligned} \tag{7-35}$$

Assuming that data channel#3 and channel #7 fail (i.e., $k_1 = 3$ and $k_2 = 7$), at the receiver, the received symbols from these two data channels will be ignored. And, since there are two failure channels (i.e., $n = 2$), from (7-6), matrix B is given by

$$B = [\beta_{ij}]_{2\times 2} = \begin{bmatrix} \alpha^{(k_1-1)(1-1)} & \alpha^{(k_1-1)(2-1)} \\ \alpha^{(k_2-1)(1-1)} & \alpha^{(k_2-1)(2-1)} \end{bmatrix} = \begin{bmatrix} 1 & \alpha^2 \\ 1 & \alpha^6 \end{bmatrix} \tag{7-36}$$

And, the inverse of matrix B is given by

$$\begin{aligned} B^{-1} &= \frac{1}{\det \begin{bmatrix} 1 & \alpha^2 \\ 1 & \alpha^6 \end{bmatrix}} \begin{bmatrix} \alpha^6 & \alpha^2 \\ 1 & 1 \end{bmatrix} = \frac{1}{\alpha^6 - \alpha^2} \begin{bmatrix} \alpha^6 & \alpha^2 \\ 1 & 1 \end{bmatrix} = \frac{1}{\alpha^3} \begin{bmatrix} \alpha^6 & \alpha^2 \\ 1 & 1 \end{bmatrix} \\ &= \begin{bmatrix} \alpha^3 & \alpha^{14} \\ \alpha^{12} & \alpha^{12} \end{bmatrix} \end{aligned} \tag{7-37}$$

From (7-4), the parameter $\tilde{c}_j$ will have two elements; that is, $\tilde{c}_1$ and $\tilde{c}_2$, which are given by

$$\tilde{c}_1 = c_1 + \sum_{\substack{i=1 \\ i\neq 3,7}}^{8} \alpha^{(i-1)(1-1)} d_i = c_1 + \sum_{\substack{i=1 \\ i\neq 3,7}}^{8} d_i$$

$$= \alpha^5 + \alpha^1 + \alpha^{14} + \alpha^6 + \alpha^4 + \alpha^{12} + \alpha^{13} = 0 \qquad (7\text{-}38)$$

and

$$\tilde{c}_2 = c_2 + \sum_{\substack{i=1 \\ i\neq 3,7}}^{8} \alpha^{(i-1)(2-1)} d_i = c_2 + \sum_{\substack{i=1 \\ i\neq 3,7}}^{8} \alpha^{(i-1)} d_i$$

$$= \alpha^0 + \alpha^1 + \alpha^0 + \alpha^9 + \alpha^8 + \alpha^2 + \alpha^5 = \alpha^{12} \qquad (7\text{-}39)$$

Substituting (7-37) to (7-39) into (7-8), the data symbols from channel#3 and channel #7 are recovered and are given by

$$\left(d_{k_1}, d_{k_2}\right) = \left(d_3, d_7\right) = \left(\tilde{c}_1, \tilde{c}_2\right) B^{-1} = \begin{bmatrix} 0 & \alpha^{12} \end{bmatrix} \begin{bmatrix} \alpha^3 & \alpha^{14} \\ \alpha^{12} & \alpha^{12} \end{bmatrix} = \begin{bmatrix} \alpha^9 & \alpha^9 \end{bmatrix} \qquad (7\text{-}40)$$

Table 7.4 List of symbols at transmitter, receiver, and output of the decoder for example 2: two failure data channels.

	d_1	d_2	d_3	d_4	d_5	d_6	d_7	d_8	c_1	c_2
Transmitted symbols	α^1	α^{14}	α^9	α^6	α^4	α^{12}	α^9	α^{13}	α^5	α^0
Received symbols	α^1	α^{14}	NA	α^6	α^4	α^{12}	NA	α^{13}	α^5	α^0
Decoded symbols	α^1	α^{14}	α^9	α^6	α^4	α^{12}	α^9	α^{13}	0	α^{12}

where NA = not available since the channel fails.

Now d_3 and d_7 at the receiver are ignored because of the line failures. However, with diversity decoding, these lost d_3 and d_7 can be recovered and are identical to the transmitted d_3 and d_7, as seen from Table 7.4.

So far in this chapter the application of diversity coding to a 10-subcarrier SCM multimode fiber system has been discussed. Some examples on how the data from the failure data channels can be recovered using diversity coding have also been given. Attention has been restricted to the case of 10 subcarriers, where 8 are for data channels and 2 are for parity channels. It is seen from these examples that the data from failure data channels can be recovered completely. Note that if the two failure channels are parity channels, there is no need to do the decoding since all data from the data channels are received correctly. Since the received data from the poorest and next poorest channels are disregarded, it seems plausible that this is similar to the case of using training sequences (with 12 subcarriers) and dropping the 2 poorest subcarriers. However, it is necessary to verify that this is indeed the case. It should be noted that since 10 subcarriers are needed during the actual transmission; for the system with training sequences, 12 subcarriers are used during the training and the 2 poorest subcarriers are dropped.

7.4 Analysis and simulation of bit-error-rate of subcarrier multiplexed multimode fiber system with diversity coding

It is shown in the previous section that using diversity coding with a SCM multimode fiber system, the data symbols from failure data channels can be recovered instantaneously if the number of good parity channels is greater than or equal to the number of failure data channels. There is no need of a training process to determine the

channel's properties; thus, the system is less complex. However, even though the data from failure channels can be recovered, it does not mean that there is no error in the recovered data. This error can happen since the lost data is recovered from the data from good channels. But the word "good" does not mean that those data are completely error free. The error from the data received from good channels will certainly affect the recovered data; thus, increase the total bit-error-rate (*BER*) of the system. In the remainder of this chapter a combined analysis and simulation of the *BER* is provided.

- *BER analysis for the SCM multimode fiber system with diversity coding*

Consider the general case of diversity coding in which there are N data channels, and M parity channels, and the symbols consist of m bits. It is assumed that there are $N_{failure}$ failure channels. Note that the maximum number of failure channels for which the data in these failure channels can be recovered by using M for N diversity coding is M. Among these $N_{failure}$ channels, assume as before that n channels are data channels and $N_{failure} - n$ are parity channels. At the receiver, $N+M-N_{failure}$ channels are good channels and N channels (N-n data channels and n parity channels) are used for the decoding process. Note that if there are more than n good parity channels, the best n parity channels will be used for decoding. Within these N channels, there certainly is a poorest channel, which is taken to be the channel having the lowest signal-to-noise ratio (*SNR*). The recovered data will be strongly affected by this poorest channel; that is, if the *BER* from this channel is high, the probability that the recovered data will be wrong is also high; thus, the total system *BER* will be high. It will be assumed that the *BER* from the worst subcarrier

(among the N good channels) dominate the *BER* calculation of the recovered data. To calculate the *BER* of the recovered data, the symbol-error-rate of this worst channel has to be evaluated since now the data is represented in symbols (i.e., m bits per symbol).

Let $BER_{SCM,worst}$ be the *BER* of the worst channel (among N-n good data channels and n good parity channels); that is,

$$BER_{SCM,worst} = BER\Big[\min\left\{SNR_{SCM,i}\right\} \;\Big|\; \text{for } 1 \le i \le N,\ i \ne k_1, k_2, ..., k_n; \quad \text{for } N+1 \le i \le N+M,\ i = N+l_1, N+l_2, ..., N+l_n\Big] \tag{7-41}$$

where $k_1, k_2, \ldots, k_n$ are the indices of the failure data channels, and

$l_1, l_2, \ldots, l_n$ are the indices of the good parity channels.

To determine the probability of symbol error for this worst channel, the probabilities of 1-bit error, 2-bit errors, …, m-bit errors in an m-bit symbol have to be determined. The summation of these probabilities is the symbol-error-rate of the worst channel; that is,

$$SER_{SCM,worst} = \sum_{j=1}^{m} \Pr_{SCM,worst}[j\text{-bit error}] \tag{7-42}$$

where $\Pr_{SCM,worst}[j\text{-bit error}]$ is the probability of j-bit error in m-bit symbol; $1 \le j \le m$.

Assuming that the error bits are independent of one another, the probability of j-bit error in m-bit symbol is given by

$$\Pr_{SCM,worst}[j\text{-bit error}] = \binom{m}{j} BER_{SCM,worst}^{j} \left(1 - BER_{SCM,worst}\right)^{m-j} \tag{7-43}$$

Applying (7-43) to (7-42) the *SER* of the worst channel can be found. As assumed previously the worst channel dominates the *BER* of the recovered data; thus, if the

received symbol from the worst channel is wrong, the recovered symbol is also wrong. That is, the *SER* of the recovered data is identical to the *SER* of the received data from the worst channel and is given by

$$\begin{aligned} SER_{SCM,recovered} &= SER_{SCM,worst} \\ &= \sum_{j=1}^{m} \Pr_{SCM,worst}[j\text{-bit error}] \\ &= \sum_{j=1}^{m} \binom{m}{j} BER_{SCM,worst}^{j} \left(1 - BER_{SCM,worst}\right)^{m-j} \end{aligned} \quad (7\text{-}44)$$

Note that the *SER* of the recovered data in (7-44) is an upper bound to *SER* since it is determined from the *SER* of the received data from the worst channel.

From (7-42) to (7-44), with different values of $BER_{SCM,worst}$, it is seen that if $BER_{SCM,worst}$, is very large (> 0.5), $SER_{SCM,worst}$ will also be very large (close to unity). However, this is not an interesting region since we will not send the signal in this high *BER* region. As $BER_{SCM,worst}$ becomes smaller, the probability of 1-bit error will become large compared to the probabilities of 2-bit error, 3-bit error, and so on. Also, in this case, the probability of 1-bit error is close to $m \times BER_{SCM,worst}$. Thus, with a small $BER_{SCM,worst}$, $SER_{SCM,worst}$ and $SER_{SCM,recovered}$ can be approximated by $m \times BER_{SCM,worst}$.

Using the $SER_{SCM,recovered}$ found previously, the bit-error-rate of the recovered data has to be determined. Assuming that all possible recovered symbols (except the correct symbol since now we are talking about the wrong symbol) are equally likely, then the probability of each wrong recovered symbol is $\frac{1}{2^m - 1}$ since there are 2^m–1 possible

wrong symbols in GF(2^m). Considering the vector-space presentation in GF(2^m), for any correct symbol, the number of possible wrong symbols that lead to i-bit error is given by

$$K\left(i\text{-bit error in } m\text{-bit symbol}\right) = \binom{m}{i} \tag{7-45}$$

Using this information, it is found that

$$\Pr_{SCM,recovered}\left[i\text{-bit error in } m\text{-bit symbol} | d_{recovered} \neq d_{correct}\right] = \frac{\binom{m}{i}}{2^m - 1} \tag{7-46}$$

where $d_{recovered}$ is the recovered symbol for the failure channel

$d_{correct}$ is the correct symbol for the failure channel.

And, the bit-error-rate of the recovered data ($BER_{SCM,recovered}$) is given by

$$BER_{SCM,recovered} = SER_{SCM,recovered} \sum_{i=1}^{m} i \times \Pr\left[i\text{-bit error in } m\text{-bit symbol} | d_{recovered} \neq d_{correct}\right]$$

$$= \left\{\sum_{j=1}^{m} \binom{m}{j} BER_{SCM,worst}^{j} \left(1 - BER_{SCM,worst}\right)^{m-j}\right\} \times \left\{\sum_{i=1}^{m} i \times \frac{\binom{m}{i}}{2^m - 1}\right\} \tag{7-47}$$

Note also that $BER_{SCM,recovered}$ in (7-47) is an upper bound BER since it is determined from an upper bound $SER_{SCM,recovered}$.

If $BER_{SCM,worst}$ is small ($<10^{-2}$), the bit-error-rate of the recovered data ($BER_{SCM,recovered}$) can be approximated by

$$BER_{SCM,recovered} \cong m \times BER_{SCM,worst} \times \left\{ \sum_{i=1}^{m} i \times \frac{\binom{m}{i}}{2^m - 1} \right\} \quad (7\text{-}48)$$

The *BER*s of all recovered carriers are assumed to be identical and given by (7-47). Note that from (7-47) and (7-48), $BER_{SCM,recovered}$ will be larger than $BER_{SCM,worst}$. Using (7-47) and (7-48), the total *BER* of the system using *M* for *N* diversity coding with *n* failure data channels is given by

$$BER = \frac{1}{N}\left(n \times BER_{SCM,recovered} + \sum_{\substack{i=1 \\ i \neq k_1,k_2,\ldots,k_n}}^{N} BER_{SCM,i} \right) \quad (7\text{-}49)$$

where $BER_{SCM,i}$ is the bit-error-rate from i^{th}-channel, which can be determined from the *Q*-parameter (as defined in Chapter 5) corresponding to the i^{th}-channel.

$BER_{SCM,recovered}$ is the bit-error-rate of the recovered channel, which can be determined from (7-47).

From (7-49), it is seen that if all data channels are good (i.e., $n = 0$), there is no need to do the decoding. Thus, in this case, $BER_{SCM,recovered}$ is not included in the calculation of the total *BER* of the system.

Applying the results of this analysis to a 10-subcarrier system as discussed in the previous section, the *BER* of that system can be determined. The number of total subcarriers is 10; 8 of these are for data channels and 2 of these are for parity channels (i.e., $N = 8$ and $M = 2$). 2 parity channels are for recovering 2 data failure channels. The number of bits per symbol in each channel is 4; thus, $m = 4$. Since there are 2 parity

channels, the maximum number of failure channels ($N_{failure}$) is 2. Also, the maximum number of failure data channels (n) is 2. That is, if n = 2, $N_{failure}$ is also 2 and all parity channels (2 parity channels) must be good in order to recover two failure data channels. Applying these parameters to the results of the *BER* analysis (i.e., (7-41) to (7-49)), the total *BER* of the 10-subcarrier SCM system is given by

$$BER = \frac{1}{8}\left(n \times BER_{SCM,\,re\,\mathrm{cov}\,ered} + \sum_{\substack{i=1 \\ i \neq k_l;\,1 \le l \le n}}^{8} BER_{SCM,i} \right) \tag{7-50}$$

$$\begin{aligned} BER_{SCM,\,re\,\mathrm{cov}\,ered} &= SER_{SCM,\,re\,\mathrm{cov}\,ered} \sum_{j=1}^{4} j \times \Pr\left[j\text{-bit error} | d_{re\,\mathrm{cov}\,ered} \neq d_{correct} \right] \\ &= SER_{SCM,\,re\,\mathrm{cov}\,ered} \times \left\{ 1 \times \frac{4}{15} + 2 \times \frac{6}{15} + 3 \times \frac{4}{15} + 4 \times \frac{1}{15} \right\} \\ &= \frac{32}{15} SER_{SCM,\,re\,\mathrm{cov}\,ered} \end{aligned} \tag{7-51}$$

$$SER_{SCM,\,re\,\mathrm{cov}\,ered} = \sum_{j=1}^{4} \binom{4}{j} BER_{SCM,worst}^{j} \left(1 - BER_{SCM,worst} \right)^{4-j} \tag{7-52}$$

$$\begin{aligned} BER_{SCM,worst} = BER\Big[\min\left\{ SNR_{SCM,i} \right\} \;\Big|\; & \text{for } 1 \le i \le 8,\ i \neq k_j,\ 1 \le j \le n; \\ & \text{for } 9 \le i \le 10,\ i = 8 + l_j,\ 1 \le j \le n \Big] \end{aligned} \tag{7-53}$$

where $SNR_{SCM,i}$ is the signal-to-noise ratio from the i^{th}-channel

$BER_{SCM,i}$ is the bit-error-rate from the i^{th}-channel, which can be determined from the Q-parameter corresponding to i^{th}-channel, which is obtained from system simulations as discussed in the following section.

- *BER simulation for the SCM multimode fiber system with diversity coding*

The block diagram of the SCM multimode fiber system with diversity coding is shown Figure 7.1. The total number of subcarriers is $N+M$ (N subcarriers for data symbols and M subcarriers for parity symbols). The number of bits per symbol is m. The input bit rate is R_b. Since there are N data carriers, the bit rate for each subcarrier will be $R_{b,SCM} = R_b/N$. The data symbols from these N subcarriers are sent into the diversity encoder to generate M parity symbols for M parity subcarriers. The parity symbols are generated according to the procedure outlined in the previous section (Section 7.2). The data from these $N+M$ subcarriers is summed forming a bandpass electrical signal. This signal is converted into an optical signal at the laser. This optical signal is then transmitted through a multimode fiber. At the photodetector, the optical signal is detected and converted back to an electrical signal. Thermal noise is added to this electrical signal. The received electrical signal is sent to $N+M$ different paths corresponding to $N+M$ different subcarriers. Each path contains a bandpass filter, a frequency-down converter and a lowpass filter. The output signal of each path is the received signal for a particular subcarrier. The signal-to-noise ratio (*SNR*) of the output signals of these $N+M$ paths is determined by simulation.

These *SNR*s are compared to one another. The signals of the M poorest subcarries (in terms of *SNR*s) is disregarded; that is, $N_{failure} = M$. If these M poorest subcarriers are parity subcarriers, there is no need to do the decoding at the receiver, the received data from all data subcarriers can be sent to the parallel-to-serial block immediately. And, the

total *BER* of the system is just the average *BER* of the *BER*s of these data subcarriers, which can be determined by their *Q*-parameters. However, if at least one of these *M* poorest subcarriers is a data subcarrier, the signals from other good subcarriers (i.e., *N* subcarriers) will be used in the diversity decoder to generate the signals for these *M* poorest subcarriers.

The *Q*-parameter of each subcarrier signal can be determined by evaluating 4 parameters; that is, the averages and standard deviations of bits 0 and 1, as seen in (7-55). These four parameters are determined at the receiver by simulation. Then, the *BER* corresponding to each subcarrier signal can be determined using the *Q*-parameter; that is,

$$BER_{SCM,i} = K\left(\frac{\mu_1 - \mu_0}{\sigma_1 + \sigma_0}\right) = K\left(Q_{SCM,i}\right) \tag{7-54}$$

where $Q_{SCM,i}$ is the *Q*-parameter corresponding to the i^{th}-channel and is given by

$$Q_{SCM,i} = \frac{\mu_1 - \mu_0}{\sigma_1 + \sigma_0} \tag{7-55}$$

$$K\left(x\right) = \frac{1}{\sqrt{2\pi}} \int_x^{\infty} e^{-\frac{u^2}{2}} du \tag{7-56}$$

μ_1 = average value for bit 1

μ_0 = average value for bit 0

σ_1 = standard deviation for bit 1

σ_0 = standard deviation for bit 0.

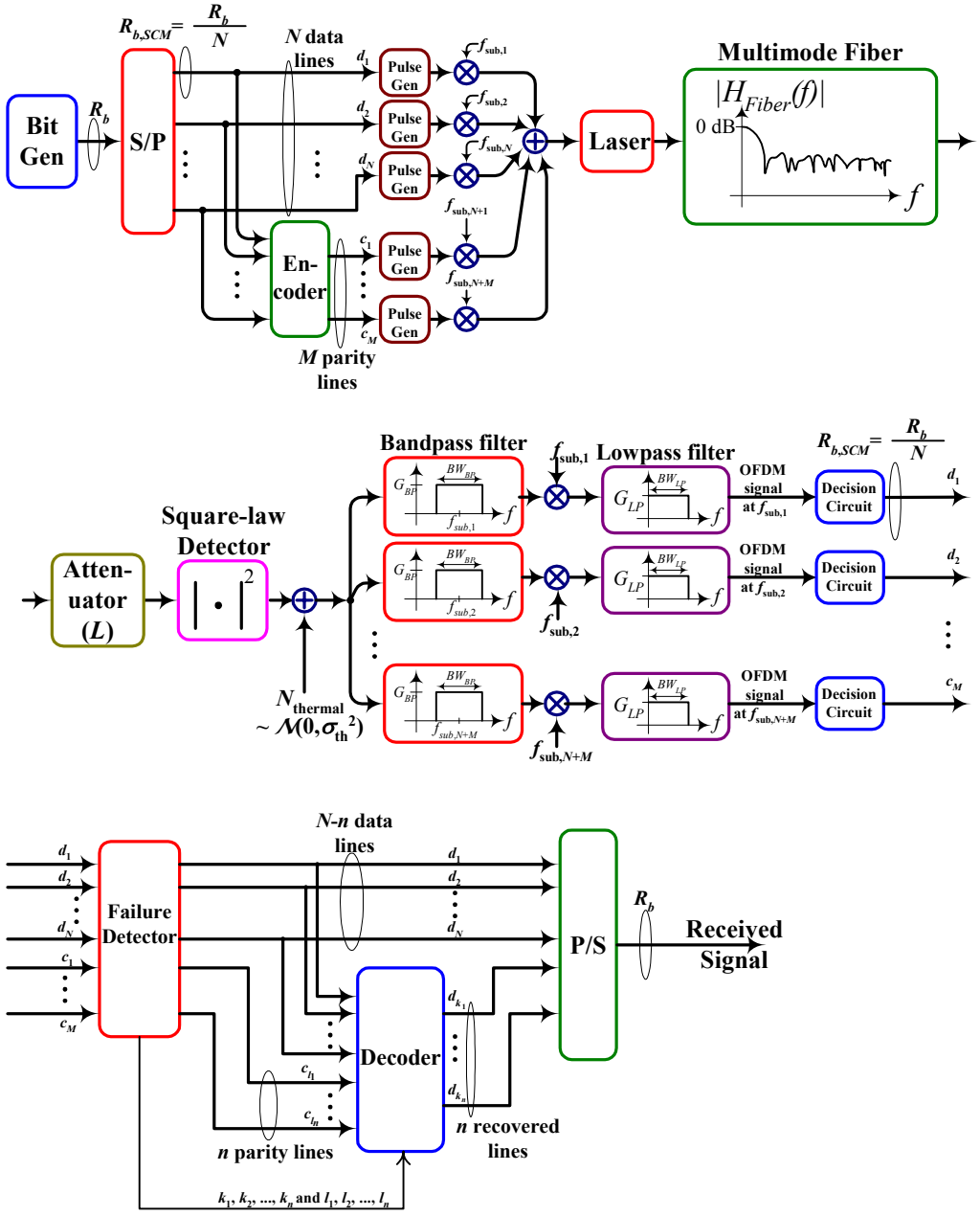

Figure 7.1 Diagram of subcarrier multiplexed multimode fiber system with diversity coding.

As indicated previously the simulation is conducted for a 10-subcarrier system in which eight subcarriers are used for data symbols and two subcarriers are for parity symbols. The total bit rate is 500 Mbps. Since there are 8 data subcarriers, the bit rate for each subcarrier will be 500/8 = 62.5 Mbps. The number of bits per symbol is 4. Other

parameters are the same as used in Chapter 5. The *SNR* of the output signals of the 10 subcarriers is determined, and the two poorest are discarded; that is, $N_{failure} = 2$. If these two poorest subcarriers are parity subcarriers, there is no need to do the decoding at the receiver, and the total *BER* of the system is just the average *BER* of these data subcarriers, which can be determined by their *Q*-parameters. However, if at least one of these two poorest subcarriers is a data subcarrier, the signals from the other good subcarriers are used in the diversity decoder to generate the signals for these two poorest subcarriers. Using the information from the simulation, the *Q*-parameters of these 8 good subcarriers can be determined; thus, the *BER*s for all 8 good subcarriers can be evaluated. The worst *BER* among these 8 *BER*s will be used as $BER_{SCM,worst}$ (see (7-53)). With this $BER_{SCM,worst}$ and the result from the analysis from the previous section, the total *BER* of the system can then be determined.

The *BER* simulations for different sets of multimode fiber and different system modifications are given in Figures 7.2 and 7.3. There are five plots in Figure 7.2 corresponding to the five different sets of multimode fiber as shown in Figure 5.2. In each of these five plots, there are three *BER* curves corresponding to the following three cases: (1) no training and no diversity coding, (2) training with dropping 2 channels, and (3) diversity coding with 2 parity channels

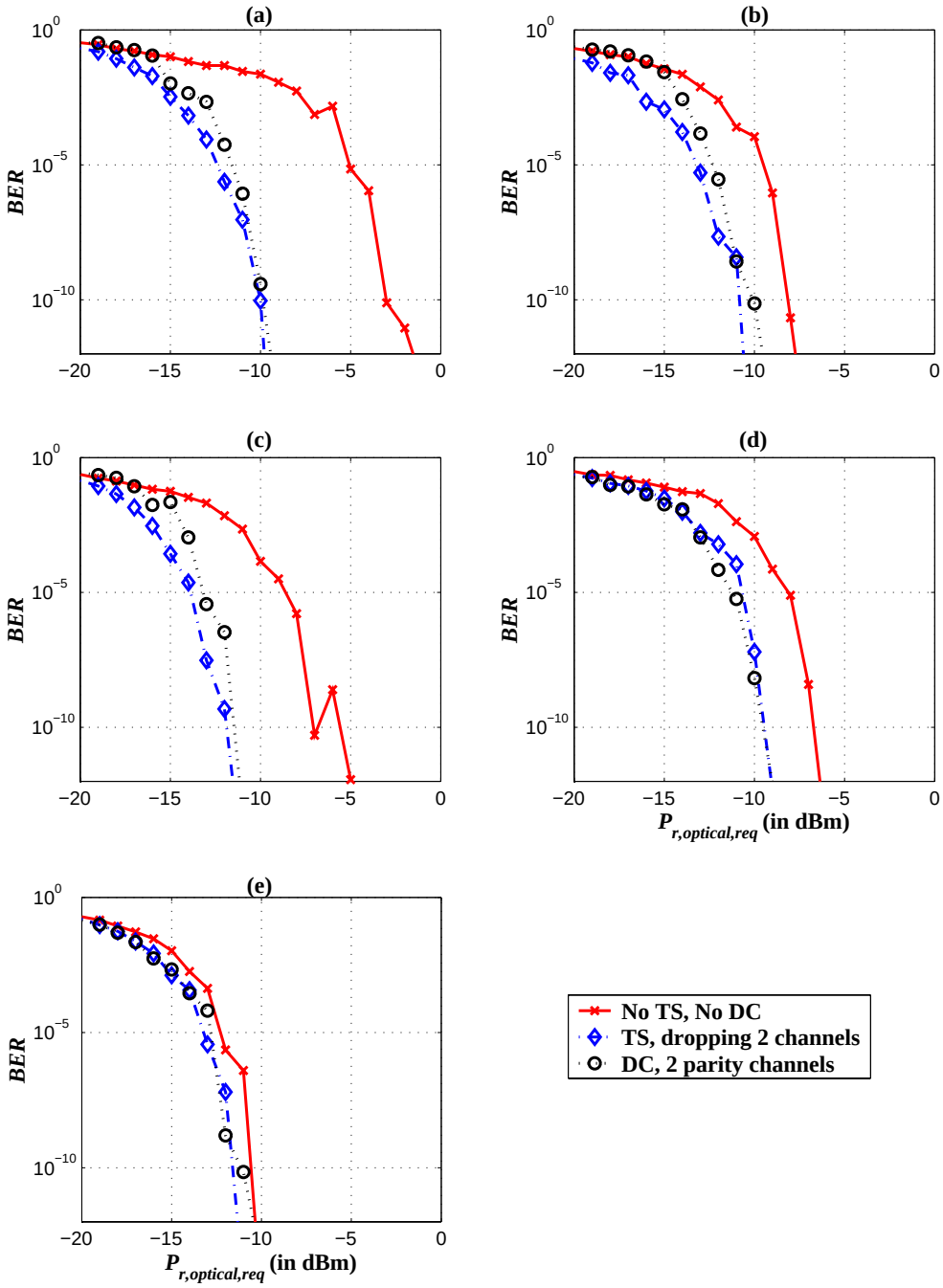

Figure 7.2 Comparison of performance of (1) no training sequence or diversity coding (No TS, No DC), (2) training sequence with two dropped channels, and (3) diversity coding with 2 parity channels. The five plots (a)-(e) correspond to the five different sets of multimode fiber from Figure 5.2

It is seen from Figure 7.2 that the best *BER* is from the system with training sequence since the channels' properties are known in advance. Using diversity coding the system performance can also be improved significantly as seen from Figures 7.2(a) and 7.2(c). It is seen that the achieved *BER*s from using training sequences and using diversity coding are almost identical. This suggests that diversity coding is a very powerful tool for improving the *BER* for SCM multimode fiber system.

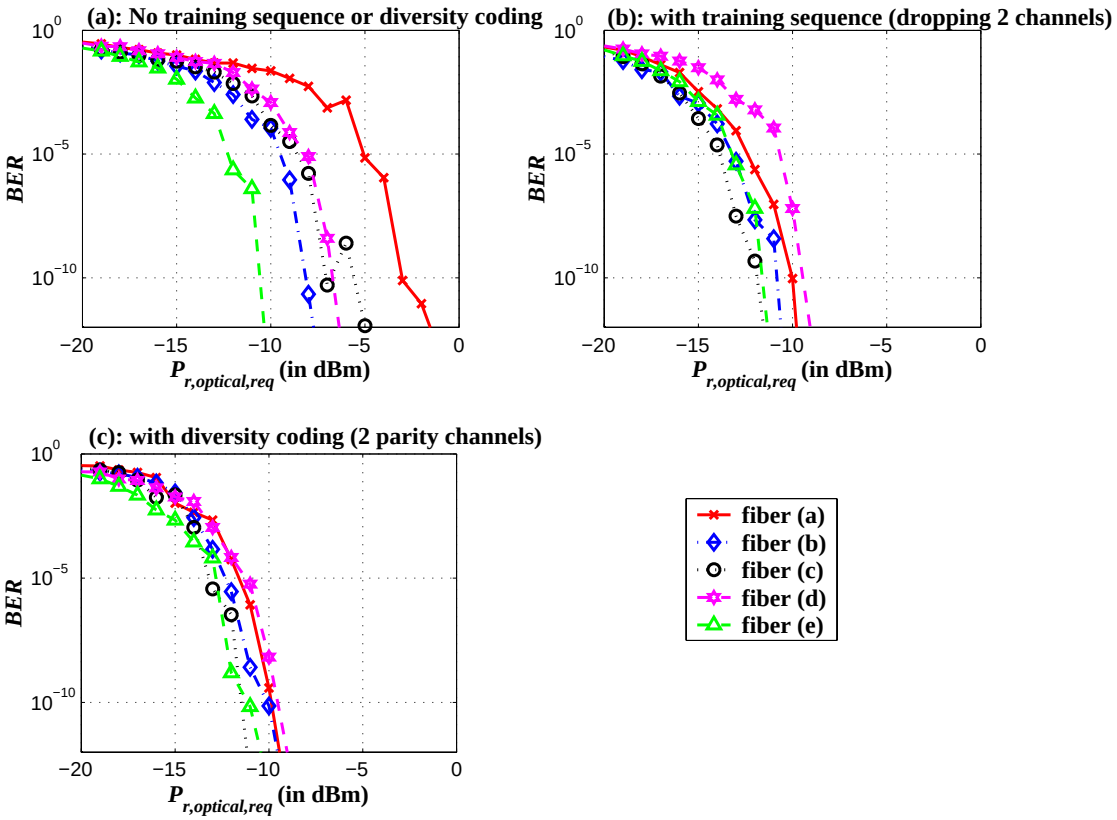

Figure 7.3 Performance of the three system configurations indicating sensitivity to fiber frequency response.

In Figure 7.3, the *BER*s from all five different sets of multimode fiber are shown in the same plot to indicate the sensitivity of the results to variations in the fiber response. There are three plots in this figure; that is, for the three systems described above. For the

case of no training sequence or diversity coding (Figure 7.3(a)), the variation of $P_{r,optical,req}$ is approximately 8 dB at *BER* of 10^{-9}. From Figures 7.3(b) and 7.3(c) this variation is only 2.5 dB when either training sequences or diversity coding is used. Note also that the training sequence and diversity coding cases have essentially the same average $P_{r,optical,req}$ (-11 dBm at *BER* of 10^{-9}).

7.5 Conclusions

The theory of diversity coding, which is normally used in network and data storage applications, is given. In diversity coding, at the transmitter, the symbols from all data channels are used to generate the parity symbols, which are transmitted via parity channels. At the receiver, if there are some failure channels, the received data from those failure channels are discarded. The data from those failure channels can be recovered by the received data from all other good channels. The application of this diversity coding to the SCM multimode fiber system in order to cancel the effects of having some subcarriers located at the deep nulls of multimode fiber has been studied. The *BER* analysis for the SCM multimode fiber system with diversity coding is given. The results from the *BER* simulation for a 10-subcarrier SCM multimode fiber system with diversity coding (2 parity channels) are presented. It is seen that the performance of the system with diversity coding is much better than the performance of the system without coding or training. Comparing the performance between the system with a training sequence (2 channels dropped) and the system with diversity coding (2 parity channels), the performance of

these two systems is almost identical. However, with diversity coding, a training is not required; thus, there is less system complexity. Moreover, if the frequency response of the multimode fiber is slowly time-varying, the system with a training process is required to send the training sequence to update the channel property more frequently. In the system with diversity coding, there is no need to update the channel property since the data from the failure data channels can be recovered at the receiver. This then suggests that diversity coding is a very powerful technique for canceling the effects of having some subcarriers located at the deep nulls of the multimode fiber magnitude response.

Chapter 8

Practical Performance Limits and System Capacity

8.1 Introduction

The performance of the subcarrier multiplexed multimode fiber system with different system modifications has been presented in Chapters 5-7. In the examples considered the bit rate of the transmitted signal is 500 Mbps, which is five times larger than the intermodal bandwidth supported by the multimode fiber. The achieved *BER* at this bit rate depends on many factors; that is, the bandwidth of each subcarrier, the number of subcarriers, and the locations of the subcarriers in the frequency domain relative to the nulls in the frequency response of the multimode fiber. From the results given in Chapter 5, it is seen that using a larger number of subcarriers does not always give a small *BER*. On the other hand, if the number of subcarriers is small, the bandwidth of each subcarrier needs to be large to achieve the given bit rate. These larger bandwidth subcarriers will then be significantly affected by the amplitude variation of the frequency response of the multimode fiber. Thus, the resulting *BER* from a small number of subcarriers can become large, as well. The above considerations apply to the case of a fixed total bit rate. Also, since the results are for a fixed fiber bandwidth, they apply for a fixed transmission

distance. In this chapter we consider the factors affecting the total bit rate, transmission distance and *BER* of a subcarrier multiplexed (SCM) system in multimode fibers.

Assuming that no modifications are made to the system (that is, no training process and no diversity coding), there are two main factors affecting the total *BER* of the SCM multimode fiber system; that is, the total bandpass bandwidth and the number of subcarriers.

1) The total bandpass bandwidth of the fiber

In the model considered in Chapter 2, the results appear to indicate that there is no limit to the bandpass bandwidth of the multimode fiber. However, in Chapter 2, only the effect of modal dispersion was considered. If the transmission bandwidth becomes very large, another type of dispersion, called chromatic dispersion should be taken into account, as well. By considering the effect of chromatic dispersion, the upper limit of the bandpass bandwidth of multimode fiber can be determined. It is of interest to determine how large the bandpass bandwidth of the multimode fiber can be if the chromatic dispersion is considered.

2) The number of subcarriers ($N_{carrier}$) of the SCM multimode fiber system.

From the analysis in Chapter 2, it is seen that the available bandwidth for one frequency band in the high frequency region is comparable to the intermodal bandwidth ($BW_{\text{intermodal}}$) of the multimode fiber. This means that if all subcarriers in the SCM multimode fiber system are located at the middle of each passband region, the bandwidth of each subcarrier signal should be less than the intermodal bandwidth so that the major

portion of frequency response of all subcarrier signals will not be located at the nulls of the fiber frequency response. This will increase the signal power and signal quality at the receiving end, and certainly decrease the system *BER*. Since both side-bands of each subcarrier signal are included in the transmission, the maximum bit rate of each subcarrier signal should be less than one-half of the intermodal bandwidth. From this point of view, it is seen that if the total bit rate is fixed, the number of subcarriers should be large enough to make the bit rate of each subcarrier signal less than one-half of the intermodal bandwidth.

However, as the number of subcarriers increases, it is shown in Chapter 5 that the system performance is not always improved since the effect of deep nulls in the bandpass region of the fiber becomes a major degradation to the system. The possibility that some of subcarriers are located at the deep nulls becomes larger as the number of subcarriers increases. This means that there will be more subcarriers located at the deep nulls. Hence, the performance of the system with a large number of subcarriers can be degraded significantly.

From this discussion, it is seen that the number of subcarriers is an important parameter. For a fixed total bit rate, if the number of subcarriers is too small, the bandwidth of each subcarrier signal may be larger than one-half of the intermodal bandwidth of the fiber; thus, the amplitude variation within the bandpass region can degrade the system performance. On the other hand, if the number of subcarriers is large, there will be more subcarriers located at the deep nulls; thus, the achieved bit-error-rate

(*BER*) becomes high. The available bandwidth of each possible passband region has been analyzed in Chapter 2. Hence, the lower limit of the number of subcarriers can be determined by using the intermodal bandwidth of multimode fiber if the total transmission bit rate is fixed. However, the number of subcarriers located at the nulls of the fiber in the high frequency range has not been considered. It is important then to determine the number of subcarriers located at the nulls as a function of the number of subcarriers used in the SCM system.

In the following sections, the effect of chromatic dispersion on the bandpass bandwidth of multimode fiber is discussed. The number of subcarriers located at the nulls of multimode fiber at high frequencies is then analyzed. Finally, the bit rate and distance limitations of the SCM multimode fiber system are presented.

8.2 Effect of chromatic dispersion on the available bandpass bandwidth of multimode fiber

It appears from the analysis in Chapter 2 that the bandpass bandwidth of the multimode fiber is unlimited. However, in multimode fibers, another type of dispersion, namely chromatic dispersion, becomes a limiting factor at high frequency. In this section, the effect of chromatic dispersion on the bandpass bandwidth of multimode fibers is discussed.

Chromatic dispersion can be divided into two types; that is, waveguide dispersion and material dispersion. Waveguide dispersion is very important in singlemode fibers since the optical signal launched into the fiber travels to the end of the fiber via core and cladding. The major portion of the signal travels within the core, and the rest within the cladding. Because of the difference between the refractive indexes in the core and cladding, the optical signal travels through the core and cladding with different velocities, resulting in the pulse spreading at the receiving end. This type of chromatic dispersion is negligible in multimode fiber transmission since the size of the core in multimode fibers is very large; thus, most of the optical signal is confined in the core. On the other hand, material dispersion, which is caused by the wavelength dependence of the refractive index of the fiber core, can become a limiting factor in the multimode fiber transmission if the operating wavelength is far from the zero-dispersion wavelength and/or the spectral width of the optical source is large. The pulse spreading per unit length caused by material dispersion is given by

$$\Delta\tau_{material} = D_{material}(\lambda) \times \Delta\lambda \tag{8-1}$$

where $D_{material}(\lambda)$ is the material dispersion parameter depending on operating wavelength, λ.

$\Delta\lambda$ is the spectral width of the optical source.

From (8-1), the approximate bandwidth-distance product due to material dispersion is given by [39]

$$BL_{material} = \frac{1}{4\left|\Delta\tau_{material}\right|} \tag{8-2}$$

To consider the material dispersion parameter, the operating wavelength, λ, has to be considered. There are three important operating wavelength regions in fiber optic transmission; that is, at 850, 1300, and 1550 nm. The 850-nm operating wavelength was the first wavelength used in practical fiber optic transmission in the 1970s. Even though this wavelength does not offer either the lowest material dispersion or fiber attenuation, in the 1970s, good sources and detectors were only available at this wavelength. The next operating wavelength is located at 1300 nm. At this wavelength, the fiber attenuation is very small compared to the fiber attenuation at the wavelength of 850 nm. However, the most attractive property of the wavelength at 1300 nm is that at this wavelength, the material dispersion is very small, close to zero-dispersion for silica based fibers. For the wavelength of 1550 nm, the material dispersion is larger than the material dispersion at 1300 nm. However, what makes this wavelength interesting is that the fiber attenuation at 1550 nm is even lower; it can be as low as 0.2 dB/km [1]. So from this discussion, it is seen that the smallest material dispersion is achieved at the 1300-nm operation wavelength. However, it is of interest to consider some numerical examples of this material dispersion parameter so that we can compare the bandwidth-distance product limited by the material dispersion.

Using the three-term Sellmeier equation, the material dispersion parameter is approximated by [1]

$$D_{material}(\lambda) = \frac{\lambda S_0}{4}\left[1 - \left(\frac{\lambda_0}{\lambda}\right)^4\right] \tag{8-3}$$

where S_0 is the zero-dispersion slope and λ_0 is the zero-dispersion wavelength.

From [40], for 50/125 graded-index multimode fibers, λ_0 is 1305 nm and S_0 is 0.096 ps/(nm^2·km). Applying these parameters to (8-3) for different operating wavelengths, we get that

- for λ = 850 nm, $D_{material}(\lambda) = -92.94$ ps/(nm·km) (8-4)
- for λ = 1300 nm, $D_{material}(\lambda) = -0.48$ ps/(nm·km) (8-5)
- for λ = 1550 nm, $D_{material}(\lambda) = 18.50$ ps/(nm·km) (8-6)

From (8-4) to (8-6), it is seen that the smallest material dispersion parameter is from the operating wavelength of 1300 nm. However, to determine the bandwidth-distance product due to the material dispersion, the spectral width of the optical source has to be considered. Because of the low power coupled into a fiber, the small modulation bandwidth, and very large spectral width offered by LEDs, LEDs are not suitable for high bit-rate transmission using subcarrier multiplexing on multimode fibers. An alternative choice is vertical cavity surface-emitting lasers (VCSELs), which have been used in many research experiments for data transmission using subcarrier multiplexing on multimode fibers. Thus, in this discussion, it is assumed that the VCSEL is used as the

optical source in the transmitter. The spectral width of a VCSEL is very small. A spectral width of 0.5 nm is available in commercial devices [40]. Assuming $\Delta\lambda = 0.5$ nm; using (8-1), (8-2) and (8-4) to (8-6), the bandwidth-distance products due to the material dispersion for different operating wavelengths are given as follows

- for $\lambda = 850$ nm, $BL_{material}(\lambda) = 2.7$ GHz·km (8-7)
- for $\lambda = 1300$ nm, $BL_{material}(\lambda) = 517.8$ GHz·km (8-8)
- for $\lambda = 1550$ nm, $BL_{material}(\lambda) = 13.5$ GHz·km (8-9)

From (8-7) to (8-9), it is seen that if the data is transmitted within the intermodal bandwidth of the multimode fiber, the effect of material dispersion can be neglected since the bandwidth-distance product (approximately 400 MHz·km) of the intermodal bandwidth from modal dispersion is much less than the bandwidth-distance product due to the material dispersion. However, in data transmission using the passband region of the multimode fiber, the effect of material dispersion can become a limiting factor if the subcarrier frequencies are larger than the material dispersion bandwidth. This can also be explained graphically by using Figure 8.1.

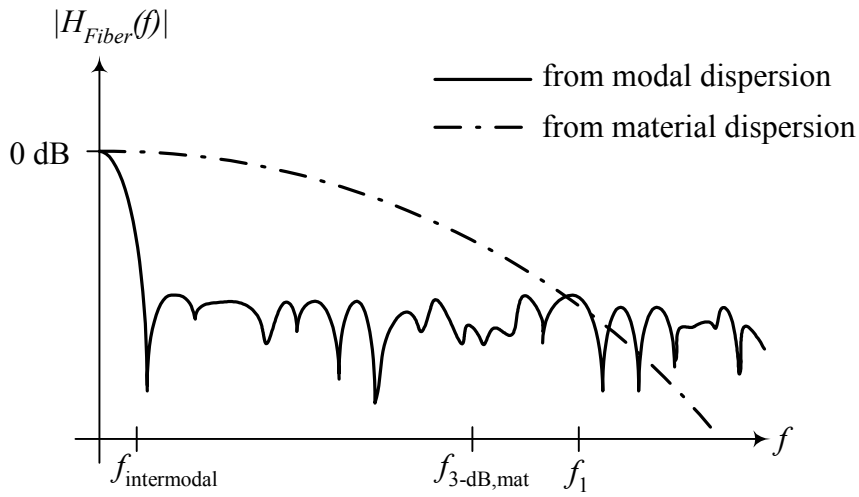

Figure 8.1 Illustration of frequency response of multimode fiber due to modal and material dispersion.

An illustration of the frequency response of the multimode fiber resulting from modal dispersion and material dispersion is shown in Figure 8.1. It is seen that if the transmission bandwidth is very small; that is, within the intermodal bandwidth, the effect of material dispersion is negligible. For transmission using subcarrier multiplexing on multimode fibers, the bandpass region of multimode fibers has to be used. If the modal dispersion is the only dispersion taken into account, it is seen that the available bandpass bandwidth is unlimited. However, this is not true since at this high frequency region, the effect of material dispersion is significant and limits the available bandpass bandwidth to be less than the frequency f_1, as shown in Figure 8.1.

Applying the effect of material dispersion to the transmission bandwidth used in the simulations of subcarrier multiplexing on multimode fibers in Chapter 5 to 7, it is seen that since the maximum transmission frequency is approximately 8 GHz, the operating wavelengths suitable for this transmission are at 1300 nm and 1550 nm. However, to

guarantee that there will be no limitation on the bandpass bandwidth (at least up to 500 GHz), the operating wavelength at 1300 nm is chosen.

From the discussion in this section, it is seen that the material dispersion is very important for bandpass transmission using multimode fibers. This dispersion can limit the available bandpass bandwidth, which seems to be unlimited if only modal dispersion is considered. The maximum bandpass bandwidth due to material dispersion depends on two parameters; that is, the operating wavelength and the spectral width of the optical source. The appropriate operating wavelength is at 1300 nm since at this wavelength the material dispersion parameter is nearly minimized. For subcarrier multiplexing on multimode fibers, a vertical cavity surface-emitting laser (VCSEL) is used as an optical source in the transmitter. The spectral width of a VCSEL is very small; that is, approximately 0.5 nm can be achieved. Using the 1300-nm operating wavelength with a VCSEL with a spectral width of 0.5 nm, the maximum bandpass bandwidth-distance product can be up to 500 GHz·km, which is very large compared to the transmission bandwidth required by the simulations in Chapter 5 to 7. Operating at a wavelength of 1300 nm, the maximum bandwidth will be limited by practical microwave circuit considerations rather than by material dispersion.

8.3 Number of subcarriers located at deep nulls

8.3.1 Probability of having k subcarriers (from an N-subcarrier system) located at the nulls

From the simulation results in Chapter 5, it is seen that using a large number of subcarriers does not guarantee that the achieved bit-error-rate (*BER*) will always be low, though the bit rate per subcarrier is low. On the other hand, the achieved *BER* of the system using a small number of high bit rate subcarriers is generally not high. Moreover, in some cases, the *BER* from the system with a small number of subcarriers is lower than that from the system with a large number of subcarriers. The reason for this, as discussed qualitatively in Chapter 5, is mainly from the locations of the subcarriers relative to the nulls in the transmission bandwidth. If there are many subcarriers located at the nulls of the magnitude response of the multimode fiber, the *BER* for those subcarrier signals will then be high; thus, resulting in a high system *BER*. The possibility of having some subcarriers located at the nulls depends on the number of subcarriers in the system. In this section, the probability of having k subcarriers (from an N-subcarrier system) located at the nulls of multimode fibers is studied. The results from the analysis in Chapter 2 are used.

Assumptions:

- The maximum subcarrier frequency is less than the passband bandwidth limited by chromatic dispersion. The passband bandwidth limited by chromatic dispersion is very large. If the operating wavelength is at 1300 nm, the maximum bandwidth-distance product is 500 GHz ·km. It is assumed that 10% of this bandwidth-distance product is

used; that is, the maximum bandwidth-distance product limited by chromatic dispersion is 50 GHz ·km.

- The frequency spacing between two adjacent subcarriers is greater than the intermodal bandwidth of the multimode fiber. With this assumption, the amplitudes of the magnitude response of the multimode fiber from two subcarriers are essentially independent of one another. This was shown in Chapter 2 by the correlation function of the frequency response of the multimode fiber in the high frequency region. This correlation function is approximately zero if the separation between two subcarriers is greater than the intermodal bandwidth.

- The amplitude (A_{null}) of a null is defined by a ratio (ε) compared to the average amplitude ($m_{|H_{fiber}(f)|}$) of the magnitude response of the multimode fiber; that is,

$$A_{null} = \varepsilon m_{|H_{fiber}(f)|} \tag{8-10}$$

Note: ε should be much smaller than unity for the signal to be considered to be at a null. The amplitude of the null is said to be $10\log_{10}|\varepsilon|$ dB below the average amplitude.

From the above assumptions, the probability of having k subcarriers (from an N-subcarrier system) located at nulls (with at least $10\log_{10}|\varepsilon|$ dB below the average amplitude) has a Binomial distribution and is given by

$$P(k,N,\varepsilon)=\binom{N}{k}F^{k}\left(\varepsilon m_{|H_{fiber}(f)|}\right)\cdot\left[1-F\left(\varepsilon m_{|H_{fiber}(f)|}\right)\right]^{N-k} \tag{8-11}$$

where $\binom{N}{k}=\frac{N!}{k!(N-k)!}$

$F\left(\varepsilon m_{|H_{fiber}(f)|}\right)$ is the probability that the amplitude of the frequency response in the passband region is less than A_{null} (or $\varepsilon m_{|H_{fiber}(f)|}$).

It is seen that to determine the probability in (8-11), $F\left(\varepsilon m_{|H_{fiber}(f)|}\right)$ has to be determined. It is found from Chapter 2 that the magnitude response of multimode fibers at high frequencies is Rayleigh distributed. Letting $X=\left|H_{fiber}(f)\right|$, the probability density function ($f_X(x)$) of X and its expected value (m_X) are given by

$$f_X(x)=\frac{x}{\sigma^2}e^{-\frac{x^2}{2\sigma^2}}U(x) \tag{8-12}$$

$$m_X=m_{|H_{fiber}(f)|}=\sqrt{\frac{\pi}{2}}\sigma \tag{8-13}$$

where $U(x)$ is the unit-step function.

From (8-12), the probability that the amplitude of the frequency response of multimode fibers in the passband region is less than x is given by

$$F(x)=\int_0^x f_X(u)\,du=\int_0^x\frac{u}{\sigma^2}e^{\frac{-u^2}{2\sigma^2}}du=1-e^{\frac{-x^2}{2\sigma^2}} \tag{8-14}$$

Substituting $\varepsilon m_{|H_{fiber}(f)|}$ for x into (8-14), we get

$$F\left(\varepsilon m_{|H_{fiber}(f)|}\right) = F\left(\varepsilon m_X\right) = 1 - e^{\frac{-\varepsilon^2 m_X^2}{2\sigma^2}} \tag{8-15}$$

Substituting m_X from (8-13) into (8-15), we get

$$F\left(\varepsilon m_{|H_{fiber}(f)|}\right) = F\left(\varepsilon m_X\right) = 1 - e^{\frac{-\pi}{4}\varepsilon^2} \tag{8-16}$$

From (8-11) and (8-16), the probability of having k subcarriers (from an N-subcarrier system) located at nulls (with at least $10\log_{10}|\varepsilon|$ dB below the average amplitude) is given by

$$P(k,N,\varepsilon) = \binom{N}{k}\left(1 - e^{\frac{-\pi}{4}\varepsilon^2}\right)^k \cdot \left(e^{\frac{-\pi}{4}\varepsilon^2}\right)^{N-k} \tag{8-17}$$

Applying different values of k, N and ε to (8-17), the probability of having k subcarriers (from an N-subcarrier system) located at the nulls is plotted and shown in Figure 8.2 for four values of N; that is, 10, 20, 30, and 40. Three values of ε are used; that is, 0.5, 0.316, and 0.1 corresponding to -3, -5, and -10 dB below the average amplitude, respectively. The probability is shown as a function of k, for k ranging from 1 to 10.

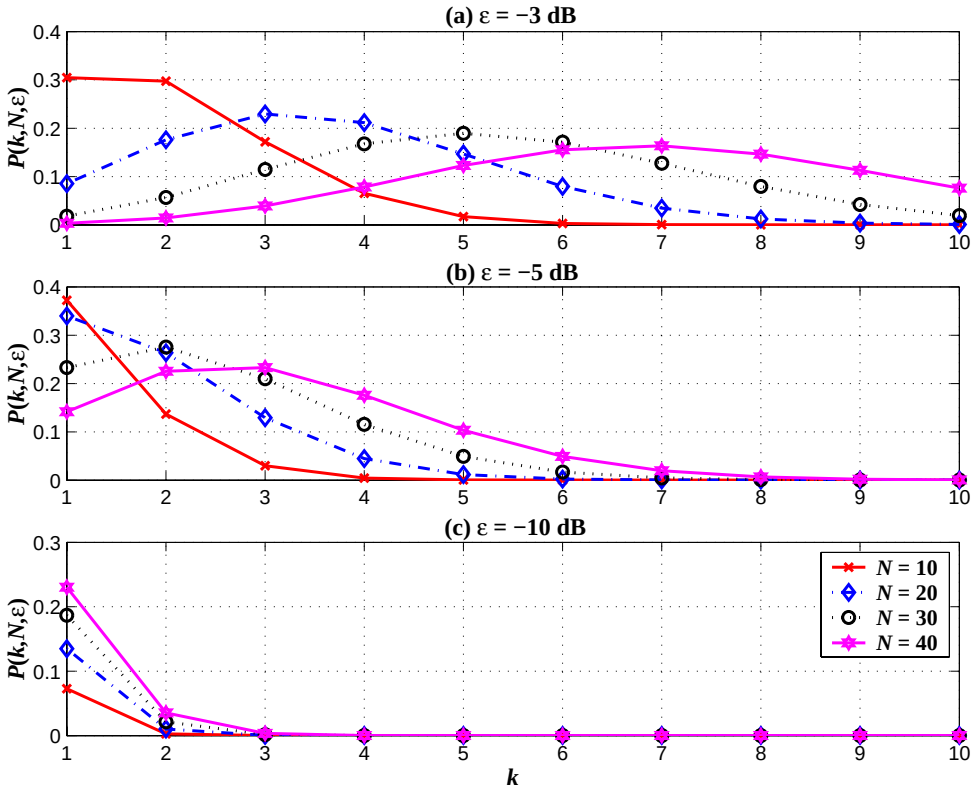

Figure 8.2 Probability of having k subcarriers (from an N-subcarrier system) located at nulls: for different values of N and ε.

From Figure 8.2(a), with ε = -3 dB, the amplitude of the null is not very small compared to the average amplitude; that is, $A_{null} = \frac{1}{2} m_{|H_{fiber}(f)|}$. If a subcarrier is located at this null, the signal of such subcarrier will be attenuated by one-half. This might not lead to a large total *BER* if there are just one or two subcarriers located at these nulls. However if the number of subcarriers located at these nulls increases, the total *BER* can then become larger. It is seen that for N = 10, the probability of having 1 or 2 nulls is largest; that is, approximately 0.3. And, the probability decreases as k increases. However, as N increases, the maximum probability is shifted to higher k; for example, for N = 10, 20, and 30, the maximum probabilities are at k = 1, 3, and 5, respectively. That is,

for large N, it is more likely to have large number of subcarriers located at the nulls; thus, resulting in a large total *BER*. For Figure 8.2(b), ε = -5 dB or the amplitude of the null is approximately $0.316 m_{|H_{fiber}(f)|}$. The probability for different values of k and N can also be explained in the same fashion as explained for Figure 8.2(a). It is seen that from these two figures, the amplitude of the null is just 3 or 5 dB below the average amplitude. These nulls may not degrade the system performance significantly if there are one or two subcarriers located at these nulls.

In Figure 8.2(c), the amplitude of the null is very small; that is, one tenth of the average amplitude. If there are just a few subcarriers located at these deep nulls, the system performance can be degraded considerably. It is seen that in this case the probability of having k subcarriers located at the nulls decreases as k increases. And, for any k, the minimum and maximum probabilities are from the system with N = 10 and 40, respectively. This may not be easily seen when k is large; for example, at $k \geq 3$. From the calculation, the probabilities of having 3 subcarriers located at the nulls from the systems with N = 20, 30, and 40 are approximately 9, 29, and 65 times larger than the probability of having 3 subcarriers located at the nulls from a 10-subcarrier system. And, these ratios become larger as k increases. Since from the simulation results in Chapter 6 and 7, only 2 bad subcarriers are discarded by using a training process or diversity coding, if there are more than 2 subcarriers located at deep nulls, the signal performance at the receiving end will be degraded by the bad subcarriers (which are not ignored); thus, a high total *BER* results. Using this point of view with the result shown in Figure 8.2(c), it is seen that using a larger number of subcarriers is not a good choice to transmit the signal using the

bandpass region of multimode fibers since the probability of having k subcarriers located at deep nulls increases as N increases.

From this section, for both shallow (ε = -3 or -5 dB) and deep (ε = -10 dB) nulls, it is shown from the analysis that using a large number of subcarriers will increase the probability of having a large number of subcarriers located at nulls. This is not good for the system since it will degrade the signal at the receiving end causing a large total *BER*. Using a small number of subcarriers is preferable. This analysis can be used to explain the previous simulation results; that is, why the system with larger number of subcarriers, which has a small bit rate per subcarrier, does not always give the best *BER*.

8.3.2 Number of subcarriers located at deep nulls

In the previous section, the probability of having k subcarriers (from an N-subcarrier system) located at the nulls has been discussed. Three levels of nulls have been used; that is, 3, 5, and 10 dB below the average amplitude. Since the first two levels are not very small compared to the average amplitude, they might not affect the system performance significantly. For the deep nulls (10 dB below the average amplitude), the signal performance can be degraded significantly if some subcarriers are located at these nulls. However, in the previous section, the plot of the probability of having k subcarriers located at the deep nulls did not clearly show the probability for k larger than 2 since it

was plotted on a linear scale. In this section, this probability is presented on a logarithmic scale so that the probability for large k can be easily seen. Also, setting the probability to a fixed value, the number (k) of subcarriers located at the deep nulls for different N is shown and studied. Note that the assumptions used in the previous section are also used in this section.

From (8-17), the probability of having k subcarriers (from an N-subcarrier system) located at the deep nulls (at least 10 dB below the average amplitude or $\varepsilon = 0.1$) is given by

$$P(k, N, \varepsilon = 0.1) = \binom{N}{k}\left(1 - e^{\frac{-\pi}{4}\varepsilon^2}\right)^k \cdot \left(e^{\frac{-\pi}{4}\varepsilon^2}\right)^{N-k}$$

$$= \binom{N}{k}\left(1 - e^{\frac{-0.01\pi}{4}}\right)^k \cdot \left(e^{\frac{-0.01\pi}{4}}\right)^{N-k}$$

$$= \binom{N}{k} 0.0078^k 0.9922^{N-k} \qquad (8\text{-}18)$$

From (8-18), the probability of having k subcarriers located at the deep nulls can be determined. The plot of this probability is shown in Figure 8.3 on a logarithmic scale as a function of k. The total number of subcarriers is varied from 10 to 100.

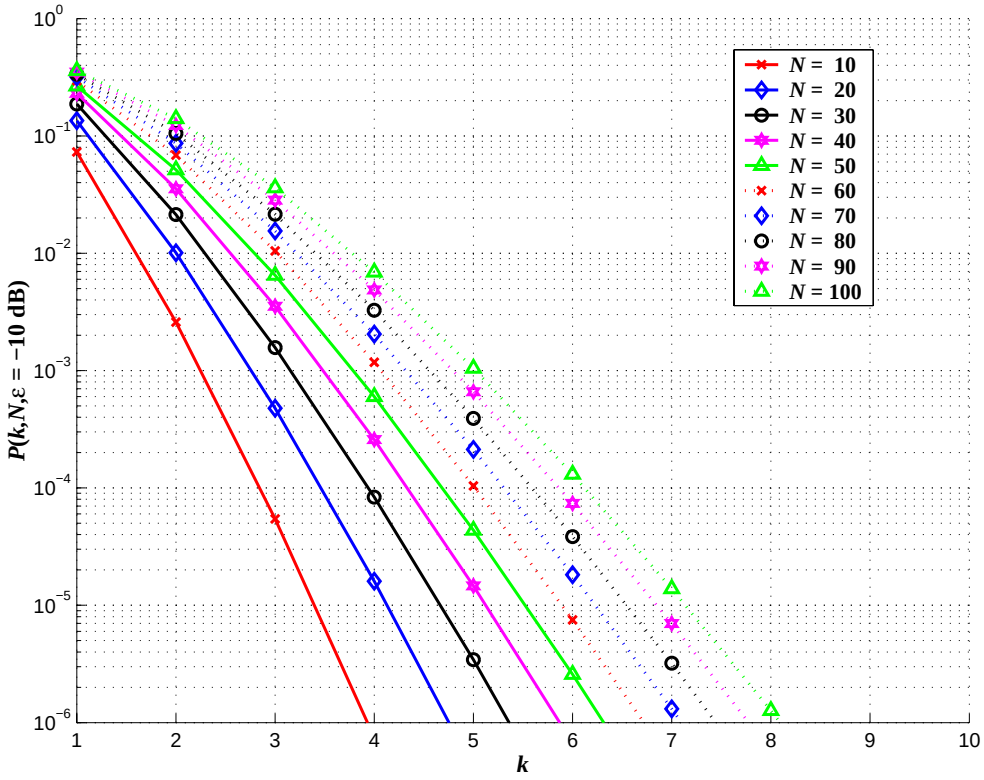

Figure 8.3 Probability of having k subcarriers (from an N-subcarrier system) located at deep nulls (at least 10 dB below the average amplitude).

From Figure 8.3, it is seen that for a fixed N, the probability of having k deep nulls decreases as k increases. This means that it is more likely to have a small number of deep nulls than to have a large number of deep nulls. Considering the probability of having a fixed k for different values of N, it is seen that as N increases, the probability of having k subcarriers located at deep nulls increases. For example, at k = 3, the probabilities of having 3 subcarriers located at the deep nulls for N = 10, 20, 30, and 40 are 5.4×10^{-5}, 4.8×10^{-4}, 1.6×10^{-3}, and 3.5×10^{-3}, respectively. This result shows that using larger number of subcarriers will increase the probability of having k subcarriers located at deep nulls. From this figure, it is interesting to see the relationship between the number of deep nulls

and the total number of subcarriers for a fixed probability. Using the plot from Figure 8.3, the plot of number of subcarriers located at deep nulls as a function of total number of subcarriers is shown in Figure 8.4. There are 4 curves corresponding to 4 different values of the probability; that is, 10^{-2}, 10^{-3}, 10^{-4}, and 10^{-5}. Note that the values of k shown in this figure are not all integers since they are determined from the point where the curves in Figure 8.2 cross the probability of interest.

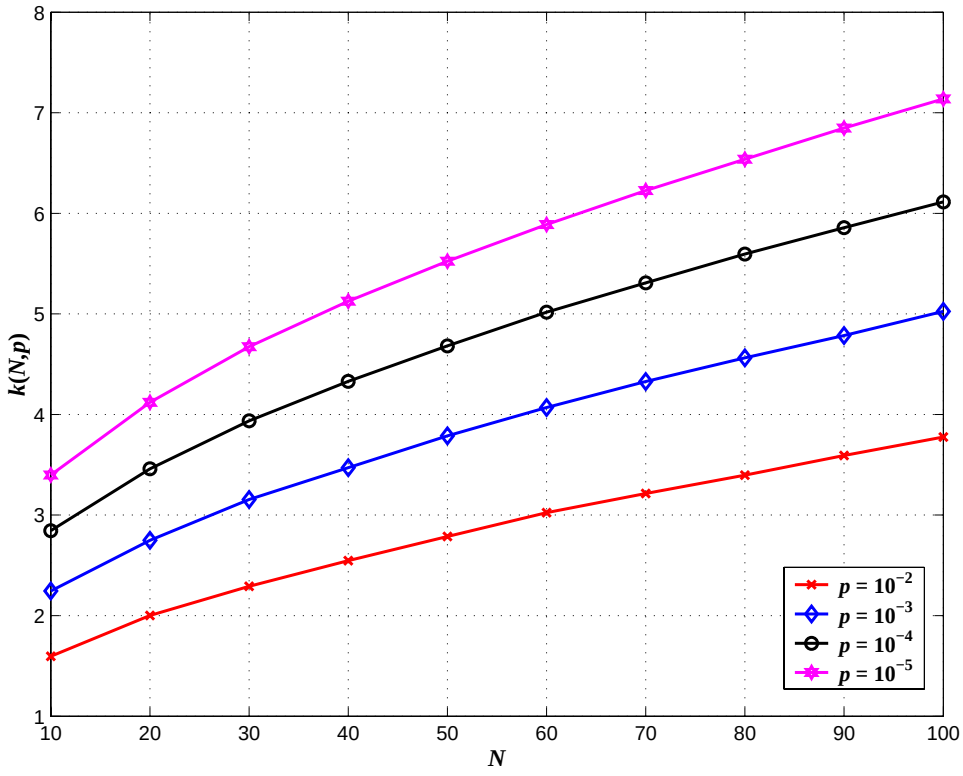

Figure 8.4 The number (k) of subcarriers located at deep nulls as a function of the total number (N) of subcarriers, for different values of probabilities.

From Figure 8.4, it is seen that for all four values of probability, the number of subcarriers located at deep nulls increases almost linearly as a function of the total number of subcarriers. The number of subcarriers located at deep nulls becomes larger as

the probability of interest decreases. It should be noted that the probabilities used in this figure are chosen arbitrarily so some probabilities may not be useful for system design. It is of interest to determine which of these probabilities is really useful.

From the simulation results in Chapter 6, it is seen that the system performance (in terms of bit-error-rate (*BER*)) for a 10-subcarrier system using a training process (dropping 2 channels) is good for all five sets of multimode fiber. This implies that for a 10-subcarrier system the maximum number of subcarriers located at deep nulls is not greater than 2. And, the *BER*s for the system with a larger number of subcarriers using a training process (dropping 2 channels) are not low for all five sets of multimode fiber. This means that with a larger number of subcarriers, the number of subcarriers located at deep nulls can be larger than 2 subcarriers. Using this information with the curves shown in Figure 8.4, it is seen that the curves from using probabilities of 10^{-4} and 10^{-5} are pessimistic since the number of subcarriers located at deep nulls from these two curves for $N = 10$ are 2.8 and 3.4, which is larger than 2. And, the curve from the probability of 10^{-2} is slightly optimistic since for $N = 20$ and 30, the numbers of subcarriers located at deep nulls are 2 and 2.3, which are close to 2. Considering the curve from the probability of 10^{-3}, it is seen that for $N = 10$, the number of subcarriers located at deep nulls is 2.2, and for $N = 20$, 30, and 40, the numbers of subcarriers located at deep nulls are 2.8, 3.2, and 3.5. The information from the curve with a probability of 10^{-3} agrees with the simulation results. Note that the simulation results were done with 5 different fiber responses, which were chosen to have generally poor response. This means that even though only 5 fiber responses were studied, the curve from the probability of 10^{-3} can be

reasonably used for approximating the number of subcarriers that are located at deep nulls for a given N.

Another important conclusion that can be drawn from this figure is the total bit rate that can be used in the system. It is seen that if the system complexity and the bandwidth limited by chromatic dispersion are not taken into account, the total bit rate can be as high as we want just by increasing the number of subcarriers since it is assumed that each subcarrier signal carries a fixed bit rate; that is, one-half of the intermodal bandwidth. However, a high bit rate may not be feasible since when the number of subcarriers increases, the number of subcarriers located at deep nulls also increases. To get good system performance with a large number of subcarriers located at deep nulls, system complexity becomes an important factor since the system will certainly need more channels to be dropped for a training process or more complex diversity coding in order to recover the data from all good channels. Moreover, with a larger number of subcarriers, the bandwidth required for transmitting the signal becomes larger. This large bandwidth may exceed the bandwidth limited by chromatic dispersion, or it may be larger than that achievable with practical electronics. Therefore, it is seen that the total bit rate is not unlimited. It is limited by the system complexity and the available bandwidth limited by chromatic dispersion and practical circuit considerations. For example, if it is assumed that the bandwidth required by the total bit rate does not exceed the bandwidth limited by chromatic dispersion, and the system can recover the data if up to 5 subcarriers are located at deep nulls (this is determined from the curve with the probability of 10^{-3} in

Figure 8.4), then the total number of subcarriers can be up to 100, resulting in a total bit rate of 5 Gbps (i.e., $100\times0.5\times BW_{\text{intermodal}} = 100\times0.5\times100$ MHz = 5 Gbps).

In summary, the probability of having k subcarriers (from an N-subcarrier system) located at deep nulls has been discussed in this section. The probability has been shown for different numbers of k and N. It has been seen that for a fixed N, the probability decreases as k increases. And, for a fixed k, the probability increases as N increases. Plots relating the number of deep nulls and the total number of subcarriers for different values of probabilities have also been shown. It is found that the relationship between k and N using a fixed probability of 10^{-3} is suitable for system consideration since the information from this curve agrees with the simulation results done previously. The total bit rate of the system can also be determined from this curve if other factors (i.e., system complexity and bandwidth limitation from chromatic dispersion) are not considered.

8.3.3 Number of subcarriers located at the deep nulls from Poisson distribution

The probability of having k subcarriers (from an N-subcarrier system) located at deep nulls (10 dB below the average amplitude) has been discussed in the previous section. The number of subcarriers located at deep nulls for different values of probability has been shown. It was shown that the curve between k and N with the probability of 10^{-3} agrees with the simulation results in Chapter 5 to 7. Also, using the probability of 10^{-3} is reasonable since it can then be interpreted that only 0.1% of multimode fibers might be

expected to give unsatisfactory performance. The data used in Figure 8.4 is from the numerical calculation using the binomial distribution. It is seen that for large N the number k is very small compared to the value of N. And, the probability that the amplitude of the response of the multimode fiber at a particular frequency is less than 10 dB below the average amplitude is very small (i.e., 0.0078) as N gets larger. Hence, the probability of having k subcarriers (from an N-subcarrier system) located at deep nulls can then be approximated by the Poisson distribution. In this section, the analytic result for the probability of having k subcarriers (from an N-subcarrier system) located at deep nulls using the Poisson distribution is studied.

From (8-18), it is seen that as N gets larger, the probability of having k subcarriers (from an N-subcarrier system) located at deep nulls, which is a Binomial distribution, can be approximated by a Poisson distribution. For a particular N, the probability of having k subcarriers (from an N-subcarrier system) located at deep nulls is then given by

$$P(k) = e^{-\lambda} \frac{\lambda^k}{k!} \tag{8-19}$$

where $\lambda = F\left(\varepsilon m_{|H_{fiber}(f)|}\right) \times N = 0.0078 \times N.$

Using (8-19) with different values of k and N, the probability of having k subcarriers (from an N-subcarrier system) located at deep nulls can be determined. The plot of this probability is shown in Figure 8.5 on a logarithmic scale as a function of k. The total number of subcarriers is varied from 10 to 100.

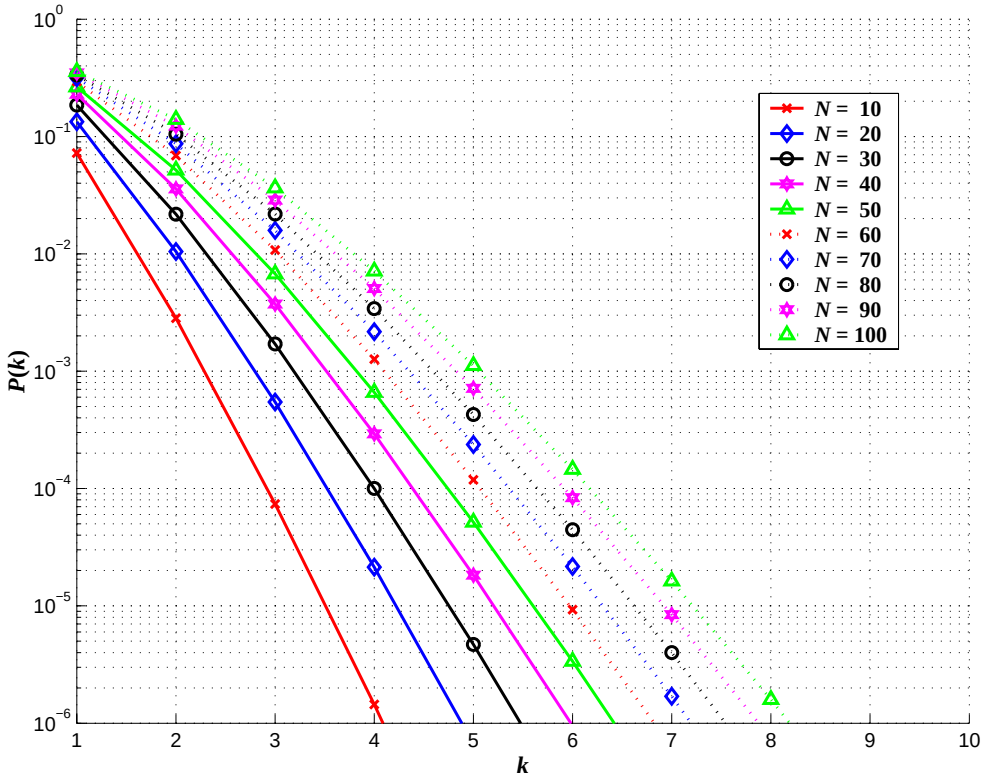

Figure 8.5 Probability of having k subcarriers (from an N-subcarrier system) located at deep nulls (at least 10 dB below the average amplitude) determined from Poisson distribution in (8-19).

Comparing the curves in Figure 8.5 to the curves shown in Figure 8.3 (which is from the Binomial distribution), it is seen that these curves are almost identical. The difference becomes smaller as N gets larger. From Figure 8.5, the relationship between the number of deep nulls and the total number of subcarriers for a fixed probability can be determined. Setting the probability of interest to be 10^{-3}, the number of subcarriers located at deep nulls can be plotted as a function of N, as shown in Figure 8.6.

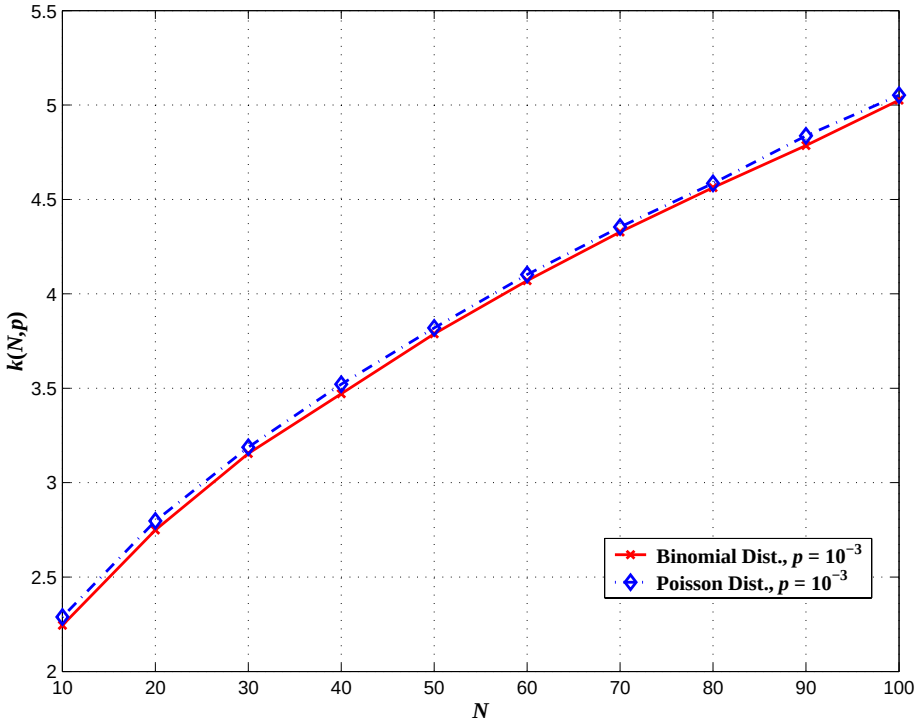

Figure 8.6 The number (k) of subcarriers located at deep nulls as a function of the total number (N) subcarriers: from Binomial and Poisson distributions, $p = 10^{-3}$.

From Figure 8.6, it is seen that there are two curves corresponding to Binomial distribution and Poisson distribution. The number of subcarriers located at deep nulls increases as the number of total subcarriers increases. For a large N, the number of subcarriers located at deep nulls increases almost linearly as a function of the total number of subcarriers. Comparing these two curves, it is clearly seen that they are almost identical. The gap between these two curves is very small, approximately 0.05. This then shows that instead of using a Binomial distribution, the probability of having k subcarriers (from an N-subcarrier system) located at deep nulls can also be determined by using the Poisson distribution, which requires less calculation.

To show how the number of subcarriers located at deep nulls increases as a function of N, the ratio between k and N has to be determined. This ratio, as determined from the results in Figure 8.6, is plotted as a function of N in Figure 8.7.

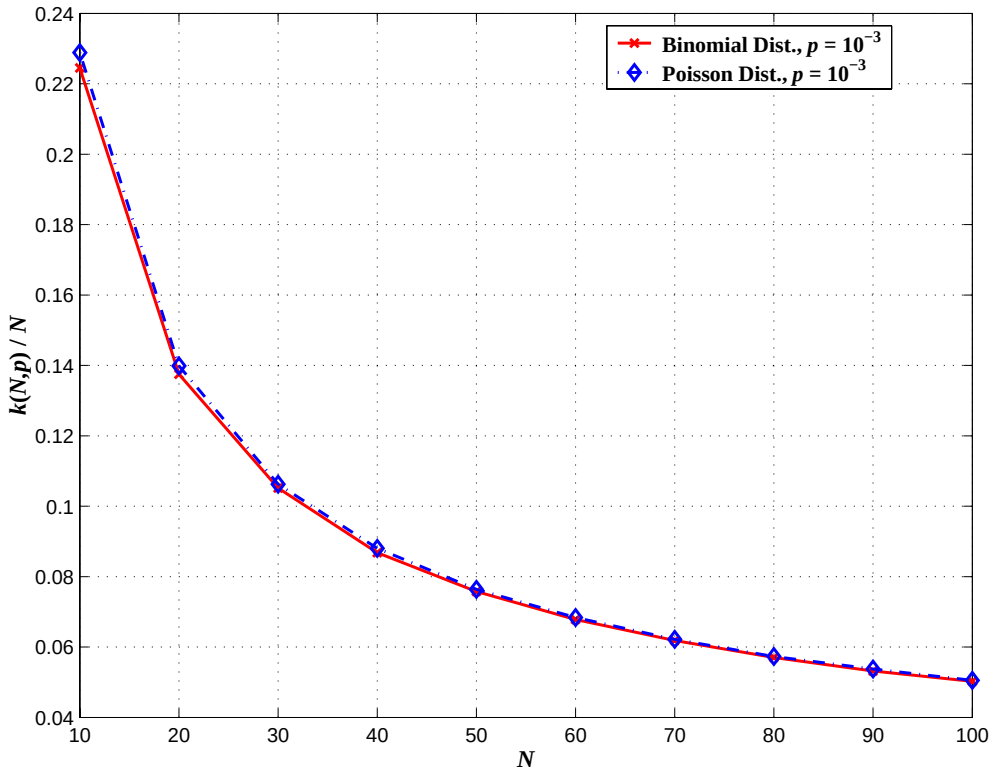

Figure 8.7 The ratio between the number (k) of subcarriers located at deep nulls and the total number (N) of subcarriers as a function of the total number subcarriers: from Binomial and Poisson distributions, $p = 10^{-3}$.

Two curves are shown in Figure 8.7. These two curves are for the Binomial distribution and Poisson distribution and they are almost the same. It is seen that for small N, the parameter k/N is high. And, when N increases, k/N becomes smaller and reaches 0.05 at $N = 100$. This means that as N increases, the number of subcarriers located at deep nulls increases almost linearly as a function of N since k/N approaches a constant. Hence,

the number of subcarriers located at deep nulls can be estimated easily if the total number of subcarriers is known.

An analytic result, approximating the probability of having k subcarriers (from an N-subcarrier system) located at deep nulls, using a Poisson distribution has been given in this section. Plots of k and k/N as a function of N have been shown. It has been seen that as N gets larger, k increases almost linearly as a function of N. This is very useful since the number of subcarriers located at deep nulls can then be easily approximated if the total number of subcarriers is known.

8.4 System Capacity

The available bandpass bandwidth limited by chromatic dispersion and the probability of having k subcarriers (from an N-subcarrier system) located at deep nulls (which have an amplitude less than 10 dB below the average amplitude of the frequency response of multimode fiber) has been analyzed. The result of this analysis shows that the bandpass bandwidth, which seems to be unlimited if only modal dispersion is taken into account, is limited by chromatic dispersion. From the analysis of the probability of having k subcarriers (from an N-subcarrier system) located at deep nulls, it is seen that the number of subcarriers located at deep nulls increases as the total number of subcarriers increases. Also, the probability of having k subcarriers (from an N-subcarrier

system) located at deep nulls can be determined approximately by the Poisson distribution. However, a major system question still remains. What is the total bit rate that may be achieved, and how does this depend on transmitter power and fiber length? In this section, these questions are considered, and a plot relating total bit rate and fiber length will be obtained, making use of the results from previous sections of this chapter.

For optical fiber transmission, the electrical transmitted signal must be converted into an optical format using an optical source. As has been discussed in the previous section, vertical cavity surface-emitting lasers (VCSELs) are suitable for SCM multimode fiber systems. To operate the laser in the stimulated emission region, the laser must be driven by a bias current (I_B), which must be higher than the threshold current (I_{th}). This bias current results in a DC component at the output optical signal of the laser. The fluctuation (ΔI) in the drive current about the bias point is caused by the transmitted signal. This fluctuation in the drive current then results in an AC component of the output optical signal of the laser. For an N-subcarrier system, the transmit optical power in the DC and AC components are given by

$$P_{T,Optical,DC} = \frac{P_{T,Optical}}{1 + m\sqrt{\frac{N_{carrier}}{2}}} \tag{8-20}$$

and,

$$P_{T,Optical,AC} = \frac{P_{T,Optical} m\sqrt{\frac{N_{carrier}}{2}}}{1 + m\sqrt{\frac{N_{carrier}}{2}}} \tag{8-21}$$

where $P_{T,Optical}$ is the total transmit optical power.

$P_{T,Optical,DC}$ is transmit optical power in DC component

$P_{T,Optical,AC}$ is transmit optical power in AC component (i.e., all subcarrier signals)

$N_{carrier}$ is the total number of subcarriers

m is the modulation index for each subcarrier signal, which is assumed to be identical for all subcarriers. Note that the definition of the modulation index was given in Chapter 5. From [34], m is given by

$$m = \mu\sqrt{\frac{2}{N_{carrier}}} \tag{8-22}$$

μ is the total rms modulation index.

From (8-22), the maximum subcarrier modulation index (m) depends on the allowable μ and the number of subcarriers $N_{carrier}$. If μ is fixed as a constant, m will depend only on $N_{carrier}$. $N_{carrier}$ depends on many parameters; that is, the available bandpass bandwidth (B_{BP}), the bit rate per subcarrier ($R_{b,sub}$), and the spacing between two successive subcarriers (Δf_{sub}). $N_{carrier}$ is given by

$$N_{carrier} = \frac{B_{BP}}{\Delta f_{sub} R_{b,sub}} \tag{8-23}$$

It was shown in Chapter 2 that the bit rate for each subcarrier should be less than one-half of the 3-dB modal bandwidth ($B_{3\text{-}dB,modal}$) of the multimode fiber in order to reduce the effect of signal variation caused by the frequency response of the multimode fiber in the bandpass region. Hence, in this section, the bit rate per subcarrier will be assumed to be equal to one-half of $B_{3\text{-}dB,modal}$; that is,

$$R_{b,sub} = \frac{B_{3-dB,\mathrm{modal}}}{2} \tag{8-24}$$

where $$B_{3-dB,\mathrm{modal}} = \frac{BWL_{Fiber}}{L} \tag{8-25}$$

BWL_{Fiber} is the 3-dB modal bandwidth–distance product of the multimode fiber

L is the fiber length.

Note that in (8-25), it is assumed that bandwidth scales inversely with length; i.e., there is no mode mixing.

From (8-23) and (8-24), the total bit rate (R_b) is given by

$$R_b = R_{b,sub} N_{carrier} \tag{8-26}$$

Passing this subcarrier multiplexed signal through the multimode fiber, the signal power in the DC and AC components will be attenuated by the fiber attenuation and attenuation from the passband region of the multimode fiber. The received optical power at the end of the multimode fiber is then given by

$$P_{R,Optical,DC} = \frac{P_{T,Optical}}{1 + m\sqrt{\frac{N_{carrier}}{2}}} \times Loss_{Fiber} \tag{8-27}$$

$$P_{R,Optical,AC} = \frac{P_{T,Optical} m\sqrt{\frac{N_{carrier}}{2}}}{1 + m\sqrt{\frac{N_{carrier}}{2}}} \times Loss_{Fiber} \times Loss_{BP} \tag{8-28}$$

$$Loss_{Fiber} = \alpha_{Fiber} \times L \tag{8-29}$$

$$Loss_{BP} = \sqrt{\frac{\pi}{4N_{\mathrm{mode}}}} \tag{8-30}$$

where $P_{R,Optical,DC}$ is received optical power in the DC component

$P_{R,Optical,AC}$ is received optical power in the AC component (i.e., all subcarrier signals)

$Loss_{Fiber}$ is the attenuation of the multimode fiber

$Loss_{BP}$ is the attenuation from transmitting signal in bandpass region

α_{Fiber} is the multimode fiber attenuation coefficient

N_{mode} is the number of guided modes supported by the multimode fiber.

From (8-27) and (8-28), it is seen that the power of the DC component is only affected by the attenuation from the multimode fiber while the power of AC component is affected by the attenuations from the multimode fiber and the bandpass region since the AC component is transmitted over the bandpass region of the fiber. Hence, the AC component is attenuated significantly. Note that $Loss_{BP}$ given in (8-30) is the average attenuation caused by the high frequency region of the fiber. Hence, the power of the AC component shown in (8-28) is the average power. The received optical signal is sent to the photodetector, in which the received optical signal will be converted to an electrical signal as a photocurrent. The photocurrent for DC and AC components (i.e., $I_{R,DC}$ and $I_{R,AC}$) are given by

$$I_{R,DC} = \mathcal{R} P_{R,Optical,DC} \tag{8-31}$$

and

$$I_{R,AC} = \mathcal{R} P_{R,Optical,AC} \tag{8-32}$$

where $\mathcal{R}$ is the responsitivity of the photodetector.

From (8-32), it is seen that the average electrical power of all received subcarrier signals ($P_{R,Elec,AC}$) and the average electrical power of each received subcarrier signal ($P_{R,Elec,sub}$) are given by

$$P_{R,Elec,AC} = I_{R,AC}^2 = \left(\mathcal{R} P_{R,Optical,AC} \right)^2 \tag{8-33}$$

$$P_{R,Elec,sub} = \frac{P_{R,Elec,AC}}{N_{carrier}} = \frac{\left(\mathcal{R}P_{R,Optical,AC}\right)^2}{N_{carrier}} \tag{8-34}$$

To calculate the signal-to-noise ratio of the received subcarrier signal, the noise power has to be determined. It is assumed that thermal noise is dominant and the receiver's optical front end is transimpedance design with an effective noise capacitance of C_e [41]. The total noise power (P_{Noise}), the noise power in AC portion ($P_{Noise,AC}$), and the noise power per subcarrier ($P_{Noise,sub}$) are given by

$$P_{Noise} = 8\pi q V_T C_e B_e^2 \tag{8-35}$$

$$P_{Noise,AC} = 8\pi q V_T C_e B_e^2 \times \frac{B_{BP}}{B_e} \tag{8-36}$$

$$P_{Noise,sub} = 8\pi q V_T C_e B_e^2 \times \frac{B_{BP}}{B_e} \times \frac{1}{N_{carrier}} \tag{8-37}$$

where q is the electron charge (= 1.6×10^{-19} C), $V_T = \frac{k_B T}{q} = 0.025$ V at $T = 290$ K, k_B is the Boltzmann constant (= 1.38×10^{-23} J/K), T is the absolute temperature, and B_e is the effective noise bandwidth of the receiver.

From (8-34) and (8-37), the signal-to-noise ratio for each subcarrier is given by

$$SNR = \frac{P_{R,Elec,sub}}{P_{Noise,sub}} = \frac{\left(\mathcal{R}P_{R,Optical,AC}\right)^2}{8\pi q V_T C_e B_e B_{BP}} \tag{8-38}$$

For digital signal transmission, the minimum signal-to-noise ratio of the received signal should be greater than 15 dB in order to get good performance. If the signal-to-

noise ratio in (8-38) is less than SNR_{req} = 15 dB, the quality of the received signal is not acceptable and some system parameters have to be modified. If the number of subcarriers decreases, the power in each subcarrier signal will increase. Consequently, the achieved *SNR* will increase. Note that the bit rate per subcarrier is still the same since the fiber length does not change. Thus, the total bit rate will decrease if the number of subcarriers decreases.

Another important factor affecting the total bit rate is the number of subcarriers located at deep nulls. Using the probability of 10^{-3}, the number of subcarriers (from an *N*-subcarrier system) located at deep nulls can be determined by solving the following equation, which was found previously in (8-19); that is,

$$P(k) = e^{-\lambda} \frac{\lambda^k}{k!} \tag{8-39}$$

where $P(k)$ is the probability of having k subcarriers located at deep nulls in $N_{carrier}$ subcarriers and $\lambda = 0.0078 \times N_{carrier}$ for deep nulls.

The number of subcarriers that can successfully transmit the signal to the receiver is determined by subtracting the number of subcarriers located at deep nulls (determined from (8-39)) from the total number of subcarriers. Hence, the total bit rate that can be transmitted to the receiver successfully can be determined.

Next, the results from the discussion above will be used to determine the signal-to-noise ratio, the number of subcarriers and the total bit rate for given system parameters. The following system parameters are assumed. The transmit optical power ($P_{T,Optical}$) is 1 mW. The number of guided modes (N_{mode}) supported by the multimode fiber is 100 modes. The maximum available bandpass bandwidth (B_{BP}) is 4 GHz. The 3-dB modal bandwidth–distance product (BWL_{Fiber}) of the multimode fiber is 500 MHz-km. The total rms modulation index (μ) is 0.5. The value of μ seems to be large; however, it was shown in [34 - 36], using $\mu = 0.5$ is sufficient for a digital system since the carrier to nonlinear distortion ratio from this μ is greater than 25 dB. The spacing between two successive subcarriers (Δf_{sub}) is 2.5 times the bit rate per subcarrier ($R_{b,sub}$). The fiber attenuation coefficient (α_{Fiber}) is 1 dB/km. The responsitivity ($\mathcal{R}$) of the photodetector is 0.9 A/W. The effective noise capacitance (C_e) is 1 pF. The rms thermal noise current (referred to the output of the photodtector) is 2.5 μA. And, the minimum required signal-to-noise ratio (SNR_{req}) for each received subcarrier signal is 15 dB. The fiber length (L) is varied from 0.4 to 6 km. Note that as the fiber length changes, the intermodal bandwidth of the fiber and hence the bit rate per subcarrier also changes. The plots of received optical powers, received signal-to-noise ratio as a function of the fiber length will be shown. Also, the plots of total number of subcarriers and total bit rate as a function of the fiber length will be given.

From (8-20) to (8-22) the transmit DC and AC powers are given by

$$P_{T,Optical,DC} = \frac{P_{T,Optical}}{1+\mu} \tag{8-40}$$

$$P_{T,Optical,AC} = \frac{\mu P_{T,Optical}}{1+\mu} \tag{8-41}$$

From (8-40) and (8-41), it is seen that if the transmit optical power ($P_{T,Optical}$) and the total rms modulation index (μ) are fixed, the DC and AC powers are also fixed. Since in this section, $P_{T,Optical}$ and μ are constant, the DC and AC optical powers do not depend on the fiber length. Applying $P_{T,Optical}$ = 1 mW and μ = 0.5 to (8-40) and (8-41), the DC and AC optical powers are 0.67 and 0.33 mW (or -1.76 and -4.77 dBm), respectively.

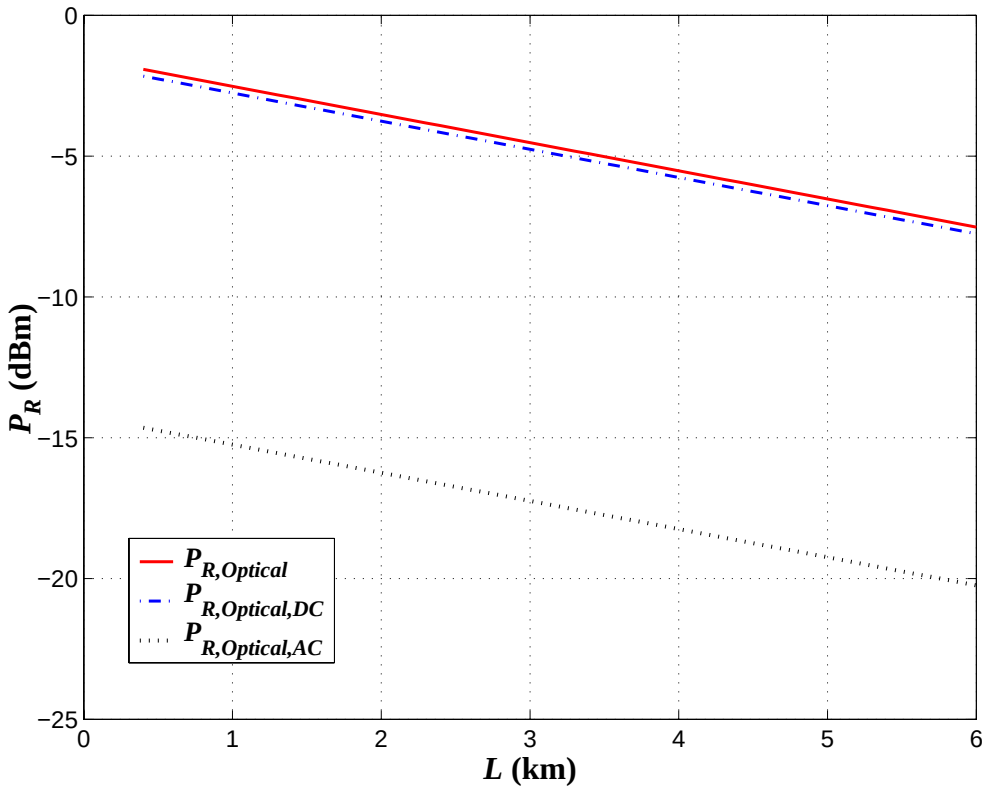

Figure 8.8 Total received optical power, received optical DC power, and received optical AC power as a function of the fiber length, L.

The total received optical power, received optical DC power, and received optical AC power are shown in Figure 8.8. These received optical powers decrease as the fiber length

increases since the fiber attenuation increases. From the figure, it is seen that the received optical DC power is always larger than the received optical AC power. At the receiver, the difference between the DC and AC powers is approximately 12 dB while at the transmitter this difference is just 3 dB. The additional decrease in the optical AC power at the receiver is caused by the attenuation in the bandpass region of the multimode fiber. This attenuation will affect only the AC portion of the transmit signal; hence, the received optical AC power becomes much less than the received optical DC power. Note that from the given system parameters, the number of guided modes supported by the multimode fiber is 100 modes; thus, the attenuation from sending a signal in the passband region is 9.5 dB independent of the fiber length.

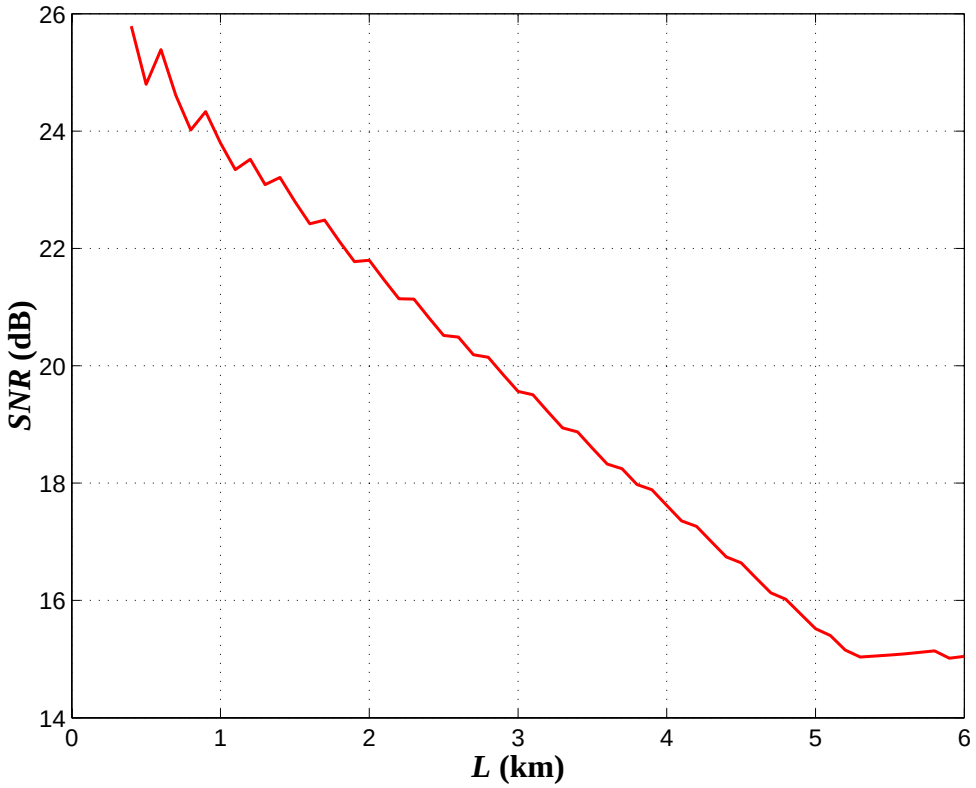

Figure 8.9 The signal-to-noise ratio of the received subcarrier signal as a function of the fiber length, *L*.

In Figure 8.9, the signal-to-noise ratio of the received subcarrier signal is plotted as a function of the fiber length. It is seen that for the fiber length less than 5.2 km, the signal-to-noise ratio decreases as the fiber length increases. This is the effect of the fiber attenuation, which increases as a function of the fiber length. However, for the fiber length greater than 5.2 km, the number of subcarriers has to be decreased in order to keep the signal-to-noise ratio above the minimum required signal-to-noise ratio, which is 15 dB. Therefore, for the fiber length greater than 5.2 km, the signal-to-noise ratio is slightly above 15 dB. The effect of keeping signal-to-noise ratio above 15 dB will be shown by the number of subcarriers and the total bit rate shown in Figure 8.10 and 8.11.

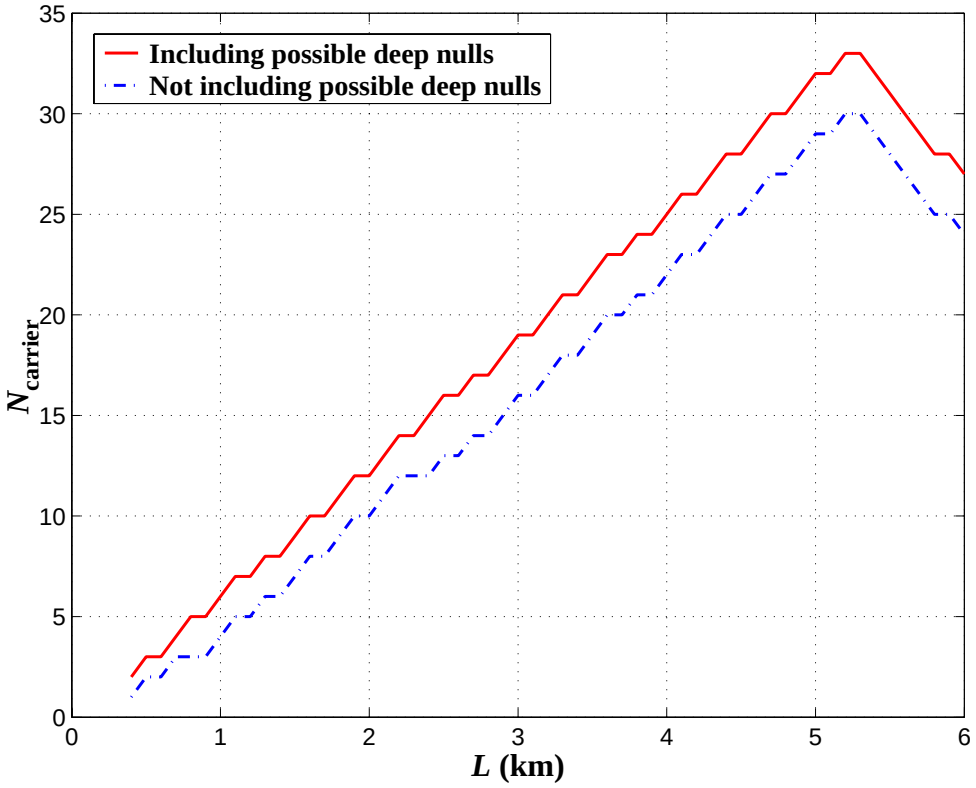

Figure 8.10 The number of subcarriers as a function of the fiber length.

The number of subcarriers for different fiber lengths is shown in Figure 8.10. There are two curves in this figure; that is, the number of subcarriers calculated from (8-23) and the number of subcarriers calculated from (8-23) subtracted by the number of possible deep nulls. For the fiber length below 5.2 km, the number of subcarriers from these two curves increases as the fiber length increases. This is because as distance increases, fiber bandwidth decreases, and the bit rate per subcarrier decreases. The difference of number of subcarriers between these two curves increases as the fiber length increases since the number of possible subcarriers located at deep nulls increases as the total number of subcarriers increases. For a fiber length greater than 5.2 km, the number of subcarriers from these two curves decreases. This is the effect from keeping the signal-to-noise ratio of the received subcarrier signal above the minimum required signal-to-noise ratio by decreasing the number of subcarriers. The decrease of the number of subcarriers will certainly affect the total bit rate. This is shown in Figure 8.11.

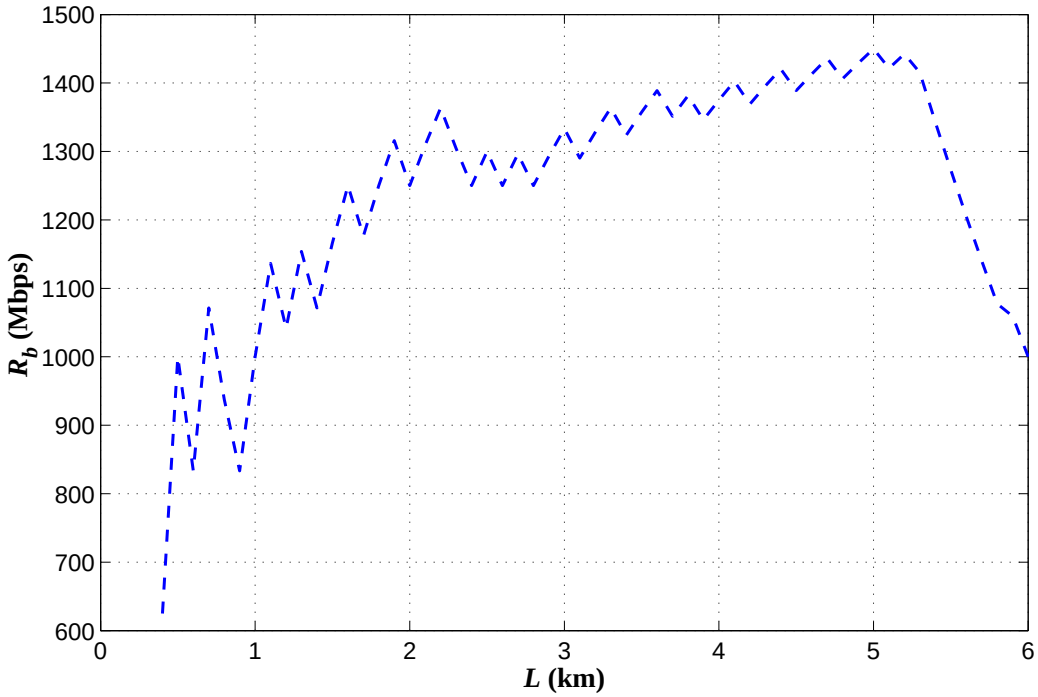

Figure 8.11 The total bit rate as a function of the fiber length.

The total bit rate as a function of the fiber length is shown in Figure 8.11. The curve shown in Figure 8.11 corresponds to the total bit rate from subcarriers that are not located at deep nulls. That is, it is assumed that the effects of having some subcarriers located at the deep nulls are overcome by some system modifications; for example, training process or diversity coding. Note that the reasons for the fluctuation of this curve will be discussed later. It is seen that for the fiber length below 5.2 km, the total bit rate increases as the fiber length increases. At a fiber length less than 2.2 km, the total bit rate strongly increases as a function of the fiber length. This can be explained as follows. For a short fiber length, the bit rate per subcarrier is large because the intermodal bandwidth is large, and the total number of subcarriers ($N_{carrier}$) is then small. Discarding only one or two

subcarriers located at deep nulls will significantly decrease the total bit rate. And, as the fiber length increases; the bit rate per subcarrier decreases, $N_{carrier}$ increases, and the number (k) of subcarriers located at deep nulls increases. However, the increase of k is much less than the increase of $N_{carrier}$. For example, for $N_{carrier}$ = 10, k = 2 while for $N_{carrier}$ = 20, k = 3. And, since the bit rate per subcarrier is small, discarding a small number of subcarriers (which are located at deep nulls) from a large $N_{carrier}$ will not significantly decrease the total bit rate of the system. Hence, as the fiber length increases, the total bit rate increases.

It is seen that for a fiber length below 2 km the total bit rate is low compared to the total bit rate at longer distances. Generally, it is expected that the total bit rate should be high at a short distance. It is not true in this system as seen from Figure 8.11. This is because the total number of subcarriers is determined by the bit rate per subcarrier, which is assumed to be one-half of the 3-dB modal bandwidth ($B_{3\text{-}dB,modal}$) for a particular fiber length (see (8-23) and (8-24)). For a short fiber length, the 3-dB modal bandwidth is large (e.g., at L = 1.0 km, $B_{3\text{-}dB,modal}$ = 500 MHz), the bit rate per subcarrier is then high; hence, the total number of subcarriers is small. This small number of subcarriers is the minimum number of subcarriers to be used so that each subcarrier signal will not experience large amplitude variation from the frequency response of the fiber. However, with a small number of subcarriers, the total bit rate is then considerably reduced if only one or two subcarriers are ignored. To increase the total bit rate for the system at such short distance, it is possible to decrease the bit rate per subcarrier; that is, there will be many subcarriers in one passband region. Hence, the total number of subcarriers used in the system will

increase. This will then lessen the effect of discarding some subcarriers located at deep nulls. From Chapters 5-7, it is seen that a 10-subcarrier system gives good system performance. Also, the number of subcarriers in a 10-subcarrier system is not too large; that is, the system complexity is not a problem. Therefore, if the minimum number of subcarriers of the system is set to be 10, the total bit rate at short distances should increase. For example, at L = 0.9 km, with $N_{carrier}$ = 10, the total bit rate is 1,280 Mbps. Note that, with $N_{carrier}$ = 10, the bit rate per subcarriers is 160 Mbps and the number of subcarriers located at deep nulls is 2. Comparing this total bit rate to the total bit rate (which is 830 Mbps) at L = 0.9 km shown in Figure 8.11, it is seen that limiting the total number of subcarriers to be at least 10 subcarriers can increase the total bit rate.

From Figure 8.11 there are some fluctuations in the total bit rate as the fiber length increases. This can be explained as follows. In Figure 8.10, it is seen that the number of subcarriers does not always increase as the fiber length increases. There is a situation where the numbers of subcarriers from two fiber lengths are identical. To determine the total bit rate, this number of subcarriers has to be multiplied by the bit rate per subcarrier. Since the bit rate per subcarrier from the longer fiber is less than the bit rate per subcarrier from the shorter fiber, the total bit rate from the longer fiber is then less than the total bit rate from the shorter fiber. Considering the total bit rate curve in Figure 8.11, there are two points where the decrease of total bit rate is significant; that is, at L = 0.9 and 2.4 km. At these two fiber lengths, the number of subcarriers located at deep nulls increases from 1 to 2 and from 2 to 3, respectively. This results in a smaller number of subcarriers that are not located at deep nulls; thus, the lower total bit rate. For the fiber

length greater than 5.2 km, the total bit rate decreases rapidly as the fiber length increases. The reason for this was explained previously as a consequence of keeping the signal-to-noise ratio of the subcarrier signal above the minimum required signal-to-noise ratio. Note that the maximum total bit rate is approximately 1,450 Mbps, which is at L = 5.2 km. This bit rate is approximately 15 times larger than the bit rate of the signal transmitted over the 3-dB modal bandwidth of the same fiber length. From this figure, it is seen that the system is not bandwidth-limited but noise-limited. If the transmit optical power increases, the higher total bit rate can then be achieved.

In this section, the relationships between many system parameters (e.g., signal-to-noise ratio, number of subcarriers, total bit rate, and fiber length) are discussed. The DC and AC optical powers at the transmitter are assumed constant since the transmitter power and the total rms modulation index are fixed. The DC and AC optical powers at the receiver decreases as the fiber length increases. This is the effect of the fiber attenuation. As the fiber length increases, the 3-dB modal bandwidth of the fiber decreases and the bit rate per subcarrier decreases. This then leads to an increase in the total number of subcarriers since the maximum available bandpass bandwidth of the fiber is fixed. As the total number of subcarriers increases, the signal power per sucarrier decreases; hence, the signal-to-noise ratio of the received subcarrier signal decreases. That is, the signal-to-noise ratio of the received subcarrier signal decreases as the fiber length increases. However, the signal-to-noise ratio should not be below the minimum required signal-to-noise ratio since if it is below the minimum required signal-to-noise ratio, the received signal performance will be poor; thus, large bit-error rate will be

achieved. To keep the signal-to-noise ratio above the minimum level, the number of subcarriers must decrease. This then increases the power in each subcarrier signal. However, the total bit rate will decrease because the number of subcarriers decreases. There is a maximum fiber length that can give a high total bit rate. If the fiber length is longer than this maximum length, the total bit rate will not further increase but decrease rapidly. It is seen that the multimode fiber system using subcarrier multiplexing is not bandwidth-limited but noise-limited. A higher bit rate can be achieved if the transmit optical power increases.

8.5 Conclusions

The performance limits and system capacity of the SCM multimode fiber system have been analyzed in this chapter. The effect of the chromatic dispersion on the available bandpass bandwidth has been discussed. It is seen that the available bandpass bandwidth of a multimode fiber is limited by the chromatic dispersion. It is shown that the maximum bandpass bandwidth-distance product up to 500 GHz·km can be achieved if the 1300-nm operating wavelength and a VCSEL with a spectral width of 0.5 nm are used. The effects of having some subcarriers located at the nulls of multimode fiber were also analyzed. It was found that as the total number of subcarriers increases, the number of subcarriers located at the nulls of multimode fiber increases. Three levels of nulls were considered; that is, 3, 5, and 10 dB below the average amplitude of the magnitude response of the multimode fiber at high frequencies. Having some subcarriers located at the shallow

nulls, which are 3 or 5 dB below the average amplitude, does not significantly degrade the received signal quality since the received signal is not strongly attenuated by the nulls. Hence, the effect of these nulls on the received signal should be small. On the other hand, for the case of deep nulls (whose amplitude is lower than 10 dB below the average amplitude), having some subcarriers located at these nulls will certainly degrade the quality of the received signal. It has been shown that the probability of having some subcarriers located at the nulls of multimode fiber can be described by the Binomial distribution, as shown in (8-17). And, for the case of deep nulls, this probability can also be approximated by the Poisson distribution, as shown in (8-19). Curves relating the number of subcarriers located at deep nulls, and the total number of subcarriers for different values of probability, have been presented. Comparing these curves to the results found in Chapter 6 and 7, it is seen that the curve with a probability of 10^{-3} is the most suitable for predicting the relationship between the number of subcarriers located at deep nulls and the total number of subcarriers in the system. Using the information from this curve, the system capacity of the SCM multimode fiber system has been discussed. The total bit rate up to 1.45 Gbps can be achieved for the fiber length of 5.2 km. The high total bit rate cannot be achieved at shorter distances (with the assumptions made in the analysis) since the bit rate per subcarrier is large and the total number of subcarriers is small. To increase the total bit rate at the fiber length below 2 km, a minimum total number of subcarriers should be set. That is, if the total number of subcarriers determined from (8-23) is smaller than the minimum, it will be set to be identical to the minimum and the bit rate per subcarrier will be decreased. It has been shown that the total bit rate at short distances increases if the minimum total number of subcarriers is set to be 10. For

the fiber length greater than 5.2 km, the total bit rate decreases rapidly. This is the consequence of having the achieved *SNR* below the minimum required *SNR*. It is seen that the system is not bandwidth-limited but noise-limited. If the transmit optical power increases, the higher total bit rate can then be achieved. The maximum fiber length, the maximum bit rate, and the number of subcarriers for different transmit optical powers are shown in Table 8.1.

Table 8.1 List of the maximum fiber length, the maximum bit rate, and the number of subcarriers for different values of transmit optical power

P_T (mW)	$L_{\max}$ (km)	$R_{b,\max}$ (Gbps)	$N_{carrier}$
0.5	2.2	1.36	14
1	5.2	1.45	33
2	8.3	1.47	52
5	12.1	1.5	78
10	15.2	1.52	97

From Table 8.1, it is seen that the maximum bit rate increases only slightly as the transmit optical power increases, but the maximum distance increases significantly. One disadvantage of the system with higher power and longer distance is that the number of subcarriers is very large as seen from the table. Since the higher maximum bit rate is achieved from the system with a longer fiber length, the bit rate per subcarrier of such system is very small. Hence, more subcarriers are needed in order to cover all available passband bandwidth. This then means that to get longer distance and higher maximum bit rate, more system complexity is needed.

Chapter 9

Summary and Conclusions

In this dissertation, the frequency response of multimode fiber at high frequencies is analyzed. Different transmission approaches for sending the signal via this high frequency region and the resulting system performance are studied. To improve the performance of the SCM multimode fiber system, two types of system modifications are studied; that is, a training process and diversity coding. The practical limits and capacity of the SCM multimode fiber system are presented.

From the analysis of the passband region of multimode fiber, the impulse response of the complex envelope of the fiber is modeled as the combination of delta functions corresponding to different delays. With this model, the probability density function of the magnitude response of the fiber at high frequencies is a Rayleigh density function. The magnitude response of the fiber at high frequencies does not fall off monotonically as the frequency increases, but becomes relatively flat with many nulls. The average amplitude of this flat region does not depend on the frequency but depends on the number of guided modes supported by the fiber. Also, the available bandwidth of each passband region is comparable to the intermodal bandwidth of the fiber.

To transmit a signal over the high frequency region of multimode fiber, many transmission approaches are studied in this dissertation. It has been shown that adding an electrical equalizer at the receiver in order to compensate the attenuation caused by the amplitude variation in the passband region of the fiber is not a good approach since the noise can be significantly amplified. The effect of using direct sequence spread spectrum is also studied. It has been shown that the standard deviation of the signal-to-noise ratio of the received signal decreases as the code length increases. However, the average signal-to-noise ratio of the received signal also decreases as the code length increases. This is because the phase information of the received optical signal is totally discarded by the non-coherent receiver. As a result, the power of the received decoded signal is not improved. However, as the code length increases, the required bandpass bandwidth increases, and consequently the noise power increases. Therefore, using direct sequence spread spectrum with passband transmission on multimode fiber is not a good choice.

The system performance of the multimode fiber system using subcarrier multiplexing has been studied. A high bit rate signal is divided into many low bit rate signals. These low bit rate signals are then modulated onto different subcarrier frequencies. With this approach, the frequency response of multimode fiber, which is a wideband frequency-selective channel, is transformed into a series of many narrowband frequency-nonselective channels. It has been shown that a 500-Mbps signal can be transmitted over the passband region of multimode fiber. The effect of the number of subcarriers has also been studied. For a fixed total bit rate, with a large number of subcarriers, the bit rate per subcarrier becomes small resulting in less signal variation caused by the fiber. However,

with this large number of subcarriers, the probability that some subcarriers are located at deep nulls of the fiber becomes high. And, these subcarriers located at deep nulls can significantly degrade the system performance.

To improve the system performance of the SCM multimode fiber system; that is, to cancel the effect of having some subcarriers located at deep nulls, a training process and diversity coding are studied. It has been shown that both techniques can improve the system performance. However, diversity coding requires less system complexity since the extra circuit for sending information about the channels' property back to the transmitter and extra subcarriers are not needed. Hence, diversity coding is a very powerful technique for canceling the effects of having some subcarriers located at the deep nulls of the magnitude response of multimode fiber.

The practical limits and capacity of the SCM multimode fiber system are studied. For the available passband bandwidth of the fiber, it has been shown that the passband bandwidth is limited by chromatic dispersion. The probability of having some subcarriers located at deep nulls of the fiber is studied. This probability is a Binomial distribution and, for the case of deep nulls, can be approximated by the Poisson distribution. It has been shown analytically for a given probability the number of subcarriers located at deep nulls for the case of a large number of subcarriers is large. Making reasonable assumptions, it has been shown that a 1.45-Gbps signal can be transmitted over a 5-km multimode fiber. It is found that the SCM multimode fiber system is not bandwidth-limited but noise-limited.

9.1 Summary of Contributions

The following contributions to the field of multimode fiber transmission systems have been made as an outcome of the research in this dissertation: (1) the statistical properties of the frequency response of multimode fiber at high frequencies are analyzed [18, 42], (2) the performance of the SCM multimode fiber system for different number of subcarriers is presented [42], (3) the system performance of the SCM multimode fiber system with a training process, which is used for canceling the effect of having some subcarriers located at deep nulls, is studied [42, 43], (4) diversity coding, which requires less system complexity than the training process, is proposed and shown to be a powerful technique for canceling the effect of the deep nulls in SCM multimode fiber system [42, 43], and (5) the practical limits and system capacity of the SCM multimode fiber system are analyzed [43].

9.2 Suggestions for Future Research

In this dissertation, it is assumed that the optical carrier is a perfect sinusoid. However, practical sources have finite linewidth (phase noise) and the effect of this noise on the response of the fiber should be investigated. This type of noise can also degrade the system performance. It should be useful to understand the effect of the laser phase noise on the SCM multimode fiber system. Hence, the study about the laser phase noise on the SCM multimode fiber could be an interesting future research topic. Another

interesting topic is to include the modal effects and chromatic dispersion to the response of the fiber. That is, a more precise model of the multimode fiber should be studied. Measurement of frequency response of the fiber is another topic that can be done. The analytical model can be compared to the results from the measurement and determine how well it agrees with the measurement.

Appendix A

Effect of bandwidth of bandpass filter (or the bandwidth of electrical equalizer) on the received signal-to-noise ratio

The effect of the bandwidth of bandpass filter (or the bandwidth of electrical equalizer) on the signal-to-noise ratio of the received signal studied in Chapter 3 is presented here. Varying the bandwidth of the bandpass filter and/or the bandwidth of the electrical equalizer from $1.5R_b$ to $4R_b$, SNR_{out} and $SNR_{out,Eq}$ at different $f_{subcarrier}$ are determined. The plots of SNR_{out} and $SNR_{out,Eq}$ are given in Figure A.1 and A.2.

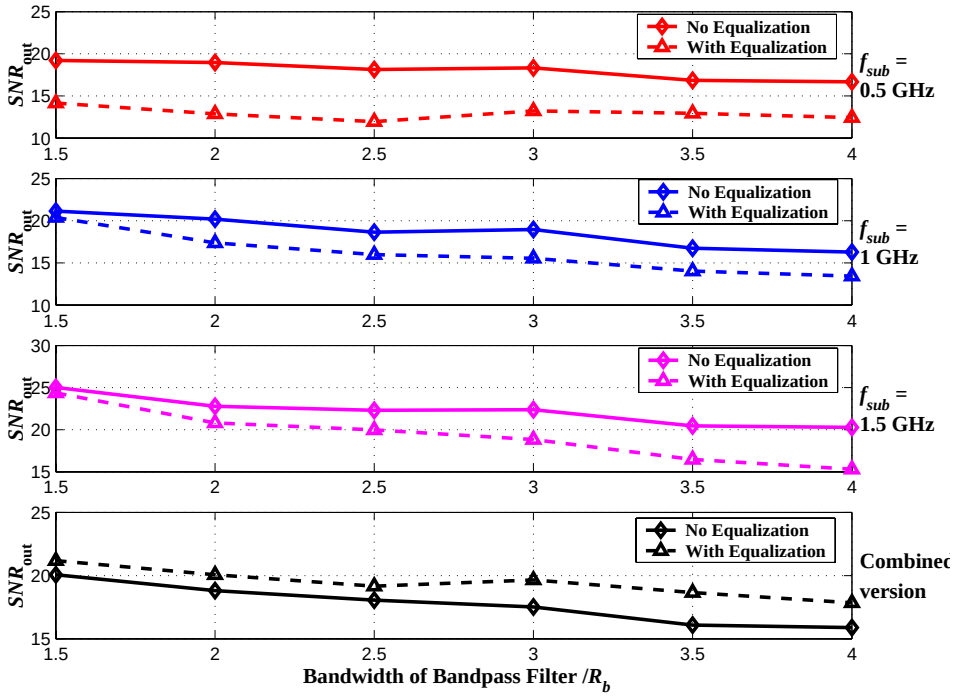

Figure A.1 Signal-to-noise ratio as a function of the bandwidth of bandpass filter: for different subcarriers.

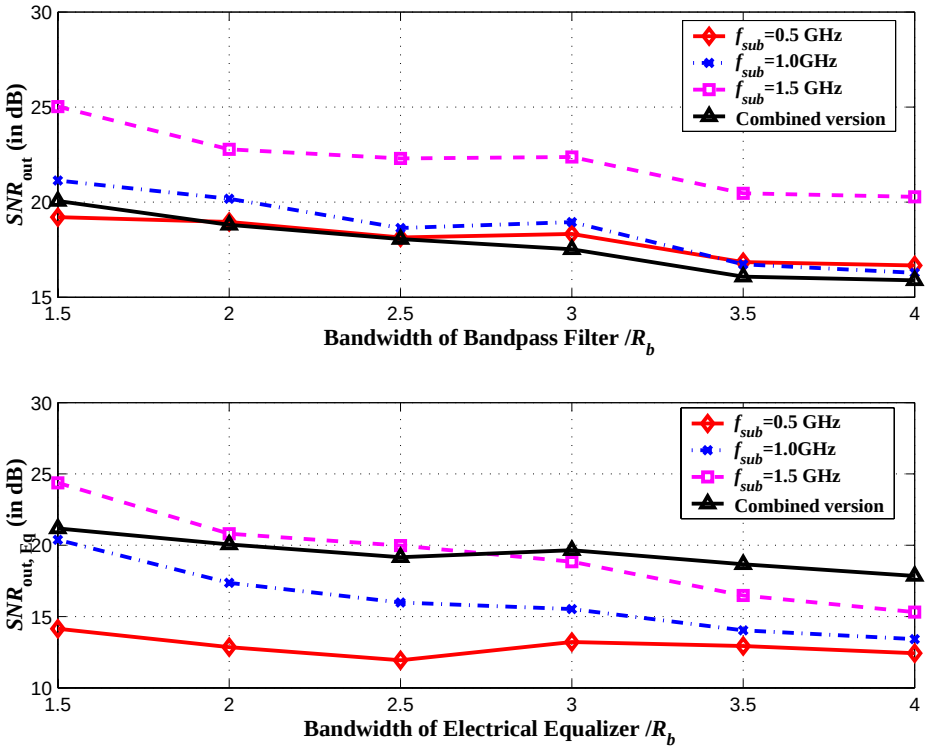

Figure A.2 Signal-to-noise ratio as a function of the bandwidth of bandpass filter (or the bandwidth of electrical equalizer): without and with electrical equalization.

In Figure A.1, the plots of SNR_{out} and $SNR_{out,Eq}$ for different subcarriers are presented. For each subcarrier signal, it is seen that equalization results in a reduction in the output signal-to-noise ratio. This reduction depends on the subcarrier frequency (i.e., the frequency response of the multimode fiber) and the bandwidth of the equalizer. For example, at $f_{subcarrier}$ = 0.5 GHz, a large *SNR* reduction is from the case of small BW_{BP} (e.g., $1.5R_b$) while a smaller *SNR* reduction is from the case of large BW_{BP} (e.g., $4R_b$). This can be explained by using the plot of the magnitude response of the multimode fiber. It is seen from Figure 3.2 that there is a large attenuation at the frequency at 0.52 GHz. And, at this frequency the signal power is not large compared to those at $f_{subcarrier}$ and $f_{subcarrier} \pm R_b$. It means that there will be a large gain from the electrical equalizer at this

frequency. With a small BW_{BP} (e.g., at $1.5R_b$), the large signal components at $f_{subcarrier} \pm R_b$ will be rejected while the thermal noise at the frequency of 0.52 GHz will be strongly amplified. This then results in a small $SNR_{out,Eq}$. On the other hand, if the bandwidth of the equalizer increases (e.g., at $4R_b$), the large signal components at $f_{subcarrier} \pm R_b$ will be included and these two large signal components will increase the signal power; thus, a larger $SNR_{out,Eq}$. Note that the larger bandwidth of the electrical equalizer, the more thermal noise introduced to the output signal. However, for the case of combined version, $SNR_{out,Eq}$ is better than SNR_{out} as seen from the plot.

In Figure A.2, the signal-to-noise ratios are also plotted as a function of the bandwidth of the bandpass filter (or the bandwidth of the equalizer). The signal-to-noise ratio from the system without equalization is shown in the upper plot and the signal-to-noise ratio from the system with equalization is shown in the lower plot. It is seen that for the system without equalization, SNR_{out} of the combined signal is less than SNR_{out} from individual subcarrier signal. While, for the system with equalization, $SNR_{out,Eq}$ of the combined signal is greater than $SNR_{out,Eq}$ from individual subcarrier signal. The improvement of the combined signal for the system with equalization and the degradation of the combined signal for the system without equalization can be explained as follows.

For the case of using equalization, considering only the signal component (not considering the noise), the signal at each $f_{subcarrier}$ is equalized and has a shape that is close to the shape of the input signal. Also, the equalized signals are almost in-phase to one another; thus, when these three signals are combined, the signal strength of the combined signal can be three times larger than the signal strength from one subcarrier

signal. And, the total power of the combined signal is approximately increased by 9.5 dB maximum (from $10\log_{10}[3^2]$); however, this maximum increase rarely happens since the equalized signals are not totally in-phase. Considering the noise component of each equalized signal, it is seen that thermal noise in this case is strongly amplified since the frequency response of the equalizer is not flat. When the noise from three subcarrier signals is combined, the total noise power is just the linear sum of the noise powers from three signals. Comparing the total signal power to the total noise power for the case of using equalization, it is clearly seen that $SNR_{out,Eq}$ of the combined signal can be larger than $SNR_{out,Eq}$ of the individual subcarrier signal as seen from the lower plot of $SNR_{out,Eq}$ for different cases in Figure A.2.

For the case of without equalization, considering only the signal component (not considering the noise), depending of the frequency response of the multimode fiber, the shape of the individual subcarrier signal can be almost like the shape of input signal. However, since the signal at each $f_{subcarrier}$ is not equalized, the phases of these subcarrier signals are not in-phase. When three different subcarrier signals are combined, there is no guarantee that these signals will increase the signal strength of the combined signal. They may also cancel one another and lead to a small increase in signal strength or smaller signal strength. As a result, the power of the combined signal cannot be dramatically increased as discussed for the case of using equalization. Considering the noise component of each subcarrier signal, it is seen that thermal noise powers from these signals are the same since there is no equalization in the system. When the noise from three subcarrier signals is combined, the total noise power is just the linear sum of the

noise powers from three signals; thus, the total noise power is three times larger than the noise power from individual subcarrier signal. Comparing the total signal power to the total noise power for the case of without equalization, it is clearly seen that SNR_{out} of the combined signal cannot be larger than SNR_{out} of the individual subcarrier signal as seen in Figure A.2. Therefore, from the above explanation, it is seen that SNR_{out} of the combined equalized signal can be larger than SNR_{out} of the combined signal without equalization.

Appendix B

Effect of Δ*G* on the received signal-to-noise ratio of the system with limited-gain equalization

In this section the signal-to-noise ratio of the system with limited-gain electrical equalization as a function of Δ*G* studied in Chapter 3 is presented. Also, the signal-to-noise ratios from two types of electrical equalization; that is, ideal and limited-gain electrical equalizations, are compared. The plots of output *SNR*s as a function of Δ*G* are presented in Figure B.1 and B.2.

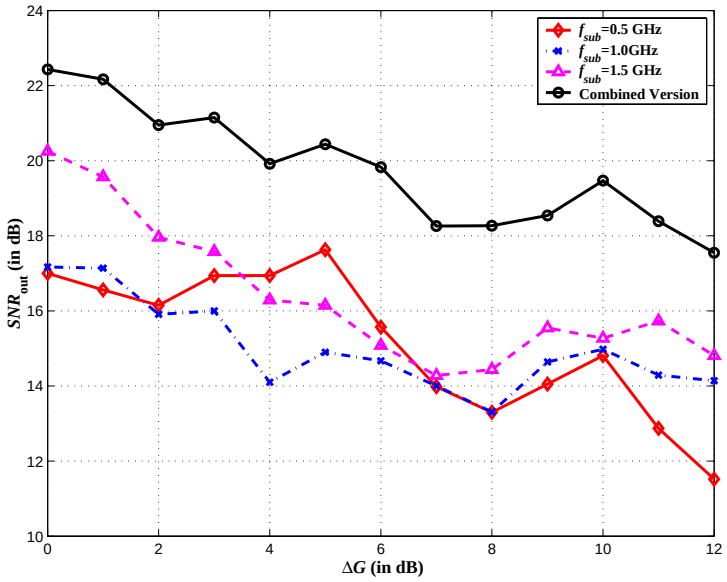

Figure B.1 Output signal-to-noise ratio as a function of Δ*G*: for limited-gain equalization with $BW_{Eq} = 4R_b$.

Figure B.1 shows the output *SNR* as a function of Δ*G* for the limited-gain equalization. It is seen that as Δ*G* increases the achieved output *SNR* decreases and becomes nearly constant as Δ*G* further increases. As Δ*G* becomes larger than 0 dB, more thermal noise is introduced to the signal; thus, a smaller output *SNR*. As Δ*G* further increases and becomes larger than the gain difference between the minimum and maximum gains of the ideal equalizer, the magnitude responses of the limited-gain and ideal equalizers are identical; thus, the output *SNR* becomes constant; that is, not a function of Δ*G*. It should be pointed out that the improvement of combining all three subcarrier signals in terms of signal-to-noise ratio is approximately 3 dB for all values of Δ*G*.

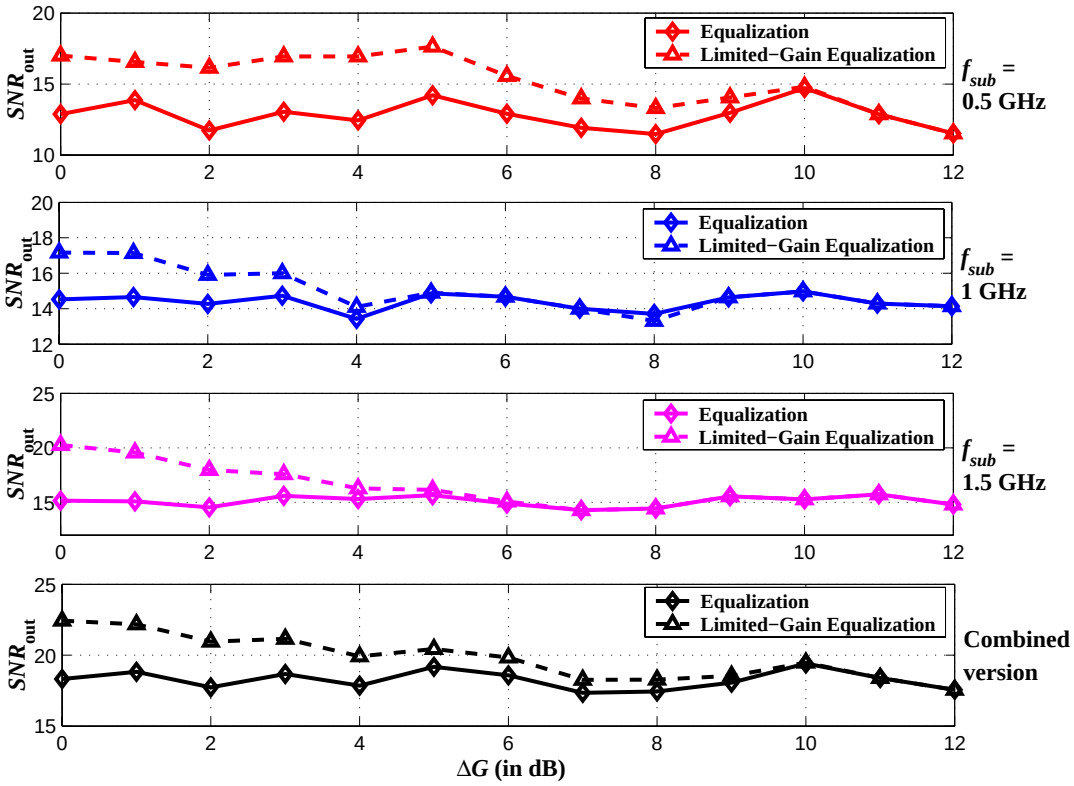

Figure B.2 Output signal-to-noise ratio (in dB) as a function of Δ*G*: for different subcarriers, $BW_{Eq} = 4R_b$.

In Figure B.2, the output *SNR* from different subcarrier frequencies and the combined signal is shown. The output *SNR* from the case of using ideal equalizer does not depend on ΔG; however, it is given for comparison purposes. It is seen that as the output *SNR* for the case of using limited-gain equalization is better that the output *SNR* for the case of using ideal equalization. However, as ΔG increases, the difference between these two output *SNR*s becomes smaller and smaller; and, finally these two output *SNR*s becomes identical. The reason for this behavior was given previously. That is, as ΔG increases and becomes larger than the gain difference between the minimum and maximum gains of the ideal equalizer, the magnitude responses of the limited-gain and ideal equalizers are identical; thus, the output *SNR*s for these two cases becomes identical.

LIST OF ACRONYMS

AC	Alternating Current
BER	Bit Error Rate
bps	bits per second
CDF	Cumulative Distribution Function
DC	Diversity Coding or Direct Current
DEMUX	De-multiplexer
DFT	Discrete-Fourier Transform
DS	Direct Sequence
GF	Galois Field
IM/DD	Intensity Modulation with Direct Detection
LAN	Local Area Network
LED	Light-Emitting Diode
MUX	Multiplexer
OFDM	Orthogonal Frequency Division Multiplexing
pdf	probability density function
PMD	Polarization-mode Dispersion
P/S	Parallel-to-Serial
rms	root mean square
Rx	Receiver
SCM	Subcarrier Multiplexing
SER	Symbol Error Rate

SNR	Signal-to-Noise Ratio
S/P	Serial-to-Parallel
SQAM	Staggered Quadrature Amplitude Modulation
SS	Spread Spectrum
TS	Training Sequence
Tx	Transmitter
VCSEL	Vertical-Cavity Surface-Emitting Laser

REFERENCES

[1] G. Keiser, *Optical fiber communications*, 2nd ed., McGraw-Hill, Inc., 1991.

[2] L. Raddatz, I. H. White, D. G. Cunningham, and M. C. Nowell, "Influence of restricted mode excitation on bandwidth of multimode fiber links," *IEEE Photonics Technology Letters*, vol. 10, no. 4, pp. 534-536, April 1998.

[3] L. J. Sargent, M. Webster, I. H. White, P. J. Heard, R. V. Penty, M. R. Tan, and D. G. Cunningham, "High performance multimode fibre link using ring-lasing vertical cavity surface emitting lasers," *24th European Conference on Optical Communication*, 1998, vol. 1, pp. 20-24, September 1998.

[4] M. Webster et al, "Mode-Controlled Vertical Cavity Surface Emitting Lasers for Bandwidth Enhancement of Multimode Fibre Links," *Conference on Laser and Electro-Optics*, 1998, pp. 33.

[5] L.J. Sargent et al, "Spatial Emission Control of Vertical Cavity Surface Emitting Lasers to Provide Bandwidth Gain in Multimode Fibre Links Using a Simple Alignment Technique," *Semiconductor Laser Conference 1998*, pp. 241-242.

[6] M. Webster, L. Raddatz, I. H. White, and D. G. Cunningham, "A statistical analysis of conditioned launch for Gigabit Ethernet links using multimode fiber," *Journal of Lightwave Technology*, vol. 17, no. 9, pp. 1532-1541, September 1999.

[7] I. H. White, M. Webster, and R. V. Penty, "High bandwidth optical links over multimode fibre," *IEEE Lasers and Electro-Optics Society*, 12th Annual Meeting, Vol. 2, page 695-96, November 1999.

[8] R. V. Penty, M. Webster, A. B. Massara, and I. H. White, "Physical layer strategies for 10 Gigabit Ethernet," in *Electronic Components and Technology Conference 2000*, pp. 487-490.

[9] G. Giaretta, R. Michalzik, and A. J. Ritger, "Long distance (2.8 km), short wavelength (0.85 mm) data transmission at 10 Gb/sec over new generation high bandwidth multimode fiber," in *Conference on Lasers and Electro-Optics 2000 (CLE0 2000)*, pp. 683-684.

[10] M. Webster, E. J. Tyler, I. H. White, R.V. Penty, "A multi-level subcarrier modulation technique for 10 Gb/s installed base multimode fibre links," *Conference on Lasers and Electro-Optics 2001 (CLE0 2001)*, pp. 416-417.

[11] L. Raddatz and et al., "High bandwidth multimode fiber links using subcarrier multiplexing in vertical-cavity surface-emitting lasers," in *Optical Fiber Communication Conference and Exhibit, 1998 (OFC'98)*, pp 358-9.

[12] C. C. Lee and S. Chi, "Three-wavelength-division-multiplexed multichannel subcarrier-multiplexing transmission over multimode fiber with potential capacity of 12 Gb/s," *IEEE Photonics Technology Letters*, vol. 11, no. 8, pp. 1066-1068, August 1999.

[13] L. Raddatz and I. H. White, "Overcoming the modal bandwidth limitation of multimode fiber by using passband modulation," *IEEE Photonics Technology Letters*, vol. 11, no. 2, pp. 266-268, February 1999.

[14] T. K. Woodward, S. Hunsche, A. J. Riger, and J. B. Stark, "1-Gb/s BPSK Transmission at 850 nm Over 1 km of 62.5-μm-Core Multimode Fiber Using a Single 2.5-GHz Subcarrier," *IEEE Photonics Technology Letters*, vol. 11, no. 3, pp. 382-384, March 1999.

[15] T. K. Woodward, S. Hunsche, A. J. Riger, and J. B. Stark, "1.6 Gb/s transmission over 1 km of 62.5 micron-core multimode fiber by subcarrier modulation of 850 nm VCSELs," *Optical Fiber Communication Conference, 1999*, pp. 80-82.

[16] E. J. Tyler, M. Webster, A. Wonfor, R. V. Penty, and I. H. White, "Transmission of a single 2.5 Gb/s subcarrier modulated channel over 300m of 62.5μm multimode fibre," *IEEE Lasers and Electro-Optics Society*, 13th Annual Meeting, vol. 2, pp. 354-5, November 2000.

[17] E. J. Tyler, M. Webster, R. V. Penty, and I. H. White, "Penalty Free Subcarrier Modulated Multimode Fiber Links for Datacomm Applications Beyond the Bandwidth Limit," *IEEE Photonics Technology Letters*, vol. 14, no. 1, pp. 110-112, January 2002.

[18] Surachet Kanprachar and Ira Jacobs, "Bandpass Transmission Characteristics of Multimode Fiber," presented at Optics in the Southeast Meeting 2001, Clemson University, South Carolina, October 2001.

[19] John A. C. Bingham, "Multicarrier Modulation for Data Transmission: An Idea Whose Time Has Come," *IEEE Communications Magazine*, vol. 28, pp 5-14, May 1990.

[20] William Y. Zou and Yiyan Wu, "COFDM: An Overview," *IEEE Transactions on Broadcasting*, vol. 41, no. 1, pp. 1-8, March 1995.

[21] William Y. Zou and Yiyan Wu, "Orthogonal Frequency Division multiplexing: A Multi-Carrier Modulation Scheme," *IEEE Transactions on Consumer Electronics*, vol. 41, no. 3, pp. 392-399, August 1995.

[22] S. B. Weinstein and Paul M. Ebert, "Data Transmission by Frequency-division Multiplexing Using the Discrete Fourier Transform," *IEEE Transactions on Communication Technology*, vol. COM-19, no. 5, pp. 628-634, October 1971.

[23] Botaro Hirosaki, "An Orthogonally Multiplexed QAM System Using the Discrete Fourier Transform," *IEEE Transactions on Communications*, vol. COM-29, no. 7, pp. 982-989, July 1981.

[24] Qun Shi, "Error Performance of OFDM-QAM in Subcarrier Multiplexed Fiber-Optic Transmission," *IEEE Photonics Technology Letters*, vol. 9, no. 6, pp. 845-847, June 1997.

[25] Bryn J. Dixon, Roger D. Pollard, and Stavros Iezekiel, "Orthogonal Frequency-Division Multiplexing in Wireless Communication Systems with Multimode Fiber Feeds," *IEEE Transactions on Microwave Theory and Techniques*, vol. 49, no. 8, pp 1404-1409, August 2001.

[26] Hideki Ochiai and Hideki Imai, "Block Codes for Frequency Diversity and Peak Power Reduction in Multicarrier Systems," *Information Theory, 1998*, pp. 192, August 1998.

[27] Mohammad G. Rahman, R. M. Rajatheva, and Kazi M. Ahmed, "Performance of Serial Concatenated Convolutional Code in Rayleigh Multipath Fading Channel," in *Vehicular Technology Conference 1999*, vol. 5, pp. 2510-2514.

[28] Klaus Witrisal, Yong-Ho Kim, and Ramjee Prasad, "A Novel Approach for Performance Evaluation of OFDM with Error Correction Coding and Interleaving," in *Vehicular Technology Conference 1999*, pp. 294-299.

[29] J. F. Helard and B. Le Floch, "Trellis Coded Orthogonal Frequency Division Multiplexing for Digital Video Transmission," in *Global Telecommunications Conference 1991*, pp. 785-791.

[30] A. D. Jayalath, R. M. Rajatheva, and K. M. Ahmed, "Coded Orthogonal Frequency Division Multiplexing for Wireless ATM," in *Vehicular Technology Conference 1999*, pp. 2049-2053.

[31] Ender Ayanoglu, Chih-Lin I., R. D. Gitlin, and J. E. Mazo, "Diversity Coding for Transparent Self-Healing and Fault-Tolerant Communication Networks," *IEEE Transactions on Communications*, vol. 41, no. 11, pp. 1677-1685, November 1993.

[32] Stephen B. Wicker, *Error Control Systems for Digital Communication and Storage*, Prentice Hall, Upper Saddle River, New Jersey 1995.

[33] Govind P. Agrawal, *Fiber-Optic Communication Systems*, 2nd ed., John Wiley & Sons, Inc., 1997.

[34] Chul-Jong Chung and Ira Jacobs, "Practical TV Channel Capacity of Lightwave Multichannel AM SCM Systems Limited by the Threshold Nonlinearity of Laser Diodes," *IEEE Photonics Technology Letters*, vol. 4, no. 3, pp. 289-292, March 1992.

[35] A.A.M. Saleh, "Fundamental limit on number of channels in SCM lightwave CATV system", *Electronics Letters*, vol. 25, pp. 776-777, 1989.

[36] K. Alameh and R.A. Minasian, "Ultimate limits of subcarrier multiplexed lightwave transmission," *Electronics Letters*, vol. 27, pp. 1260-1262, 1991.

[37] Leon W. Couch, *Digital and Analog Communication Systems*, 5th ed., Prentice-Hall, Inc., 1993.

[38] Theodore S. Rappaport, *Wireless Communications: Principles and Practice*, Prentice-Hall, Inc., 1996.

[39] John G. Proakis, *Digital Communications*, 3rd ed., McGraw Hill, Inc., 1995.

[40] D. K. Mynbaev and L. L. Scheiner, *Fiber-Optic Communications Technology*, Prentice Hall, 2001.

[41] Ira Jacobs, *Handbook of Optics: Fiber Optics and Non-linear Optics*, Chapter 2, Volume IV, 2nd Edition, Mc-Graw Hill, Inc., 2000.

[42] Surachet Kanprachar and Ira Jacobs, "Diversity coding for subcarrier multiplexing on multimode fibers," submitted to *IEEE Transactions on Communications.*

[43] Surachet Kanprachar and Ira Jacobs, "Bit-rate and distance limitations of subcarrier multiplexing on multimode fiber," submitted to *Conference of Lasers and Electro Optics 2003 (CLEO 2003).*

VITA

Surachet Kanprachar was born on May 9, 1974, in Hadyai, Thailand. He attended Chulalongkorn University in Bangkok (1992-1996) and received a B.Eng. degree (1st class honors) in Electrical Engineering. In 1996, he spent one year as a lecturer at the Faculty of Engineering, Naresuan University in Phitsanuloke; then was awarded a scholarship from the Royal Thai Government (1997) to further his studies in Electrical Engineering. Surachet attended the Bradley Department of Electrical and Computer Engineering, Virginia Tech in 1997 and received his M.Sc. in Electrical Engineering in 1999. He is currently a Ph.D. student at Virginia Tech, working toward his Ph.D. degree in the area of fiber optic communications. During 1998 to 2003, he served the Bradley Department of Electrical and Computer Engineering at Virginia Tech as a graduate teaching assistant for many classes in the communications area.